NSTX-CALC-11-06

Structural Analysis of NSTX Passive Plates and Support Structures

Prepared by : B. Nelson (ORNL) 6/15/98

Reviewed by P. Goranson (ORNL) 6/15/98

Rev. 0

June 8, 1998

Structural Analysis of NSTX Passive Plates and Supports

Introduction and summary

The passive stability structures experience thermal and electromagnetic loads during bakeout and normal operation. The thermal loads tend to put the plates in hoop compression, while the electromagnetic loads act in all directions. The plates are supported through flexible ribs to the vacuum vessel.

The stresses in the plates are moderate for disruption loads, with a Von Mises stress in the copper plates of about 15 ksi and a similiar stress in the support brackets. This compares to an allowable limit for bending and membrane of 1.5 Sm or 20 ksi for chrome zirconium copper at 150C and 21 ksi for 304L stainless steel.

The stresses are higher for the bakeout condition, where the passive structure is assumed to be 350C, or 200C hotter than the vacuum vessel. Several design iterations were necessary to reduce the bakeout stress to allowable limits. In the final case, the maximum stress in the copper flex jumpers is ~25 ksi, but the allowable limit is 3 Sm, or 40 ksi at 350C. The stress in the primary passive plate is not as high, peaking at around 16 ksi.

Description of passive stability structure

The outer passive stabilizers consist of a series of conically shaped, 0.5 inch thick copper plates arranged in upper and lower rings on the outboard side of the plasma, as shown in Figure 1. Each stabilizer is segmented into two poloidal and twelve toroidal plates. The secondary passive plates, which are located away from the midplane, extend from an elevation of about +/-43 inches to about +/-53 inches and are inclined at a 54.75 degree angle. The primary passive plates, which are located toward the midplane, extend from an elevation of +/- 22 inches to +/-40 inches. The dimensions are shown in Figure 2.

The plates are electrically connected in the toroidal direction except at one location which contains a toroidal electrical break. At this location there is a saddle connection between the upper and lower sets of plates. such that current flowing clockwise in the upper set of plates are constrained to flow counterclockwise in the lower set of plates. At each of the other connections there is a flexible jumper extending in the radial direction that provides a gap through the plates for diagnostic access and provides for thermal expansion of the plates relative to the vacuum vessel. A typical jumper is shown in Figure 3. In addition to the toroidal and saddle jumpers are a set of flexible jumpers that tie the primary and secondary plates together at each end of each passive plate. The connection scheme is shown schematically in Figures 4 and 5.

The jumpers are formed from .250 inch thick copper plate, and welded to contact lugs. Stainless steel tubing is brazed around the perimeter of the jumpers for heating and

cooling of the jumper during bakeout and operation. The passive plates will be conductively cooled to the jumpers. In this way, the plates can be demounted for access and modification without disturbing the cooling circuit.

The individual plates are bolted to radial support brackets which are supported from the vessel wall. One bracket at each location is free to move in the toroidal direction to allow thermal expansion of the passive plates, while the other is fixed to provide toroidal rigidity. [Note...The original design used flexible brackets instead of sliding bracket to accommodate thermal expansioin, but in the process of design evolution the brackets became too short for this approach to be feasible. Figure 6 illustrates the relationship between bracket length and stress.] The support backetss are fastened to the vessel domes and central cylinder in a two-step process. First a pattern of vertical and horizontal channels are welded into position every 30 degrees, centered on the radial planes through the ports. The support brackets are then temporarily clamped to these ribs and the bolting surfaces are carefully aligned to global machine reference system. This is critical to establish a very accurate mounting datum for the passive plates. Once the bolting surfaces are aligned, inserts in the brackets are match-marked to holes in the supporting channels. After the support bracket inserts are marked, they are accurately drilled, reassembled into the support brackets, and bolted back into position. The inserts are designed to allow vertical growth of the brackets during bakeout, while maintaining a high degree of rigidity in the radial direction to resist disruption loads. After the brackets are installed, the surfaces are re-measured and any errors are compensated by custom machining of the shims provided on the front face of each bracket. Once the shims are machined, the flexible jumpers are installed and the cooling lines are routed and leak checked. Finally, the passive plates are bolted into position. The bolts go through the plates, toroidal flex jumpers, poloidal jumpers, shims and brackets and clamp the entire stack. The brackets are threaded to receive the bolts. There is no electrical insulation between the supports and the plates.

Loading conditions

The loads on the passive plate structure consist of electromagnetic loads from the plasma disruptions and thermal expansion loads during bakeout. Seismic, gravity, and other operational loads are approximately two orders of magnitude lower and are ignored.

The electromagnetic loads are documented in references 1 through 5. The loads result from the interaction of inductive and conductive (halo) currents in the plates during a plasma disruption. These loads occur at separate times during the disruption and are generally not additive. The results of the force calculations are summarized in Tables 1 and 2.

Table 1 Electromagnetic load summary, induced toroidal currents (including uncertainty multiplier of 1.5)

	Unit	Primary Passive Plate	Secondary Passive Plate
Radial Force	lbs per plate	-15000	-5350
Vertical Force	lbs per plate	-3930	-2800
Normal Force	lbs per plate	-15500	-6000
(Normal Pressure)	psi	28 (inward)	15 (inward)
Poloidal Force	lbs per plate	970	800
Toroidal Force	lbs per plate	0	0
Vertical load on flex jumpers	lbs per side	+/-770 [6]*	+/-383 [6]*
Normal pressure on flex jumpers	psi	~5 (spreading force)	~5 (spreading force)

*adjusted for shortened radial dimension of jumpers compared to reference memo

Table 2 Electromagnetic load summary, poloidal (halo) currents

	Unit	Primary Passive Plate	Secondary Passive Plate
Radial Force	lbs per plate	600	500
Vertical Force	lbs per plate	200	350
Normal Force	lbs per plate	640	615
(Normal Pressure)	psi	1.2	1.6
Poloidal Force	lbs per plate	0	0
Toroidal Force	lbs per plate	670	1005
Vertical load on flex jumpers	lbs per side	0	0

The thermal loads are due to the relative expansion of the passive plates compared to the vacuum vessel during bakeout. It is assumed that the passive plates are at 350C and the vacuum vessel is at 150 C. Table 3 summarizes the expansion information. The toroidal force is derived from the information shown in Appendix xx.

Table 3 Thermal expansion of passive plates

	Unit	Primary Passive Plate	Secondary Passive Plate
Material		CuCrZr	CuCrZr
Average radius	inches	56.48	48.3
ΔL/L, 150C to 350 C [2]	in/in	.0035	.0035
Toroidal expansion of plate	inches	.11	.09
Toroidal load in flex jumper	pounds	830	470

Material Properties

There are two types of structural materials in the passive plate system. Stainless steel type 304 L is used for the support hardware and shims, while copper-chrome-zirconium alloy type 18150 is used for the passive plates and flex jumper. Standard OFHC copper was originally proposed for these applications, but due to the reduction in thickness of the passive plates from .75 inches to .5 inches and the outward shift in the plates (that shortened the flex jumper by over 2 inches), the stresses quickly exceeded the allowable limits for OFHC (Sm of 5 ksi [5] at operating temperature of < 150C). In addition, OFHC has practically no strength at the bakeout temperature of 350C (662F), so even small thermal stresses could result in permanent deformation. Cu-Cr-Zr properties are summariized in Appendix 2 [6].

The properties assumed for the analysis are listed in Table 4.

Table 4 Material properties assumed for analysis

Property	units	304L sst [7]		Cu-Cr-Zr, (18150) Solution annealed and aged [6]	
		150 C (302 F)	350 C (662 F)	150 C (302 F)	350 C (662 F)
Young's modulus (temp effect < 5%)	psi	28 E6	28 E6	17 E6	17 E6
Min Tensile strength	psi	70,000 (RT)	--	49,000	38,000
Min. Yield Strength	psi	25,000 (RT)	--	40,000	34,000
Sm		15, 300	13,700	16,500	13,000
Coeff of therm expansion	in/in-F	0.96 E-5	0.96 E-5	0.98 E-5	0.98 E-5
Thermal Conductivity	BTU/ hr-ft-F	9.4	9.4	208	202

Analysis approach and models

The passive plates and structure can be analyzed as individual parts using standard formulas for beams, plates and arches, but the end constraints are complicated enough that a finite element approach was taken. The model geometry was obtained directly from the Pro-Engineer files, and simplified by taking out the bolt holes. For both the primary and secondary plate systems, the model consisted of two passive plates, the flexible jumper assembly, two shims, a flexible support bracket, a rigid support bracket and the various brackets that are welded to the vacuum vessel. The models for the primary and secondary passive plate systems are shown in Figures 7 and 8.

The loads were applied as uniform pressure loads to the surfaces and edges of the plates. Three load cases were run, including bakeout, generic disruption and halo disruption, as described above. The analysis package used is PTC Mechanica, which employs solid P-elements. The order of the elements is changed iteratively until the strain energy converges to a prescribed value (10%). In this way the mesh is optimized for each loading condition. The analysis also picks up stress concentrations at discontinuities, which must be filtered by the observer.

Results

The results are summarized in Tables 5 and 6 for the various components. Table 5 lists the Von Mises stress and Table 6 lists the maximum displacement. The stresses are highest for the primary plates, since the loads are higher, the plates are wider, and there is no stiffening rib. The secondary passive plates have a greater span, and may or may not have a stiffening rib.

Figures are arranged in the Appendices under S1 through S3 for the secondary plates and P1 through P4 for the primary plates. As is apparent from the stress and deformation plots, the peak stress values are similar during bakeout and disruption loading, and are smallest for the halo loads. Some of the stresse around the inserts are artificially high due to a discontinuity in the temperature of the constraint. The figures in section P1 show the results for a single plate, fixed on one end and allowed to slide toroidally on the other end. Appendix 3 shows the bearing stress assumptions and results.

The disruption pressure on the plates causes the highest primary stresses, and this is partially due to the reduction in thickness of the plates from 0.75 to 0.5 inches. Figure 9 illustrates the effect of thickness on stress for the primary and secondary plates.

Table 5 Stress results

	Von Mises stress (ksi)*		
Load Case	**Disruption loads**	**Halo loads**	**Bakeout at 350C**
Structure Location:			
Primary Passive Plate			
Passive plate	~ 15	< 1	~16
Flex jumper	~ 5	< 1	~25
Support bracket	~ 15	< 1	~14
Inserts*	11	< 1	**
Weld channels on vessel*	11	< 1	**
Secondary Passive Plate			
Passive plate	~ 7	< 2	~ 14
Flex jumper	< 4	< 2	~22
Support bracket	~12	< 3	~ 14
Inserts *	5	~ 3	**
Weld channels on vessel*	5	~ 3	**

**Bearing stress around insert and bolts*

*** Very little stress unless there is significant friction, binding*

Table 6 Displacement results

	Maximum Displacement (inches)*		
Load Case	**Disruption loads**	**Halo loads**	**Bakeout at 350C**
Structure Location:			
Primary Passive Plate			
Passive plate	.055	~ .002	.13
Flex jumper	.020	< .001	.13
Support bracket	.020	< .001	.13
Inserts	< .002	< .001	< .002
Weld channels on vessel	< .002	< .001	< .002
Secondary Passive Plate			
Passive plate	.024	.006	.11
Flex jumper	.020	.006	.11
Support bracket	.020	.008	.11
Inserts	< .002	< .001	< .002
Weld channels on vessel	< .002	< .001	< .002

Conclusion

Several conclusions can be drawn from this analysis:

1. The disruption and bakeout conditions produce similar stress magnitudes for the passive plates and support brackets, but the bakeout condition is much worse for the flex jumper. The primary passive plate brackets experience higher stresses than the secondary due to the higher loading. The boundary conditions are conservative, since it is unlikely that the holes in the brackets will be completely restrained by the inserts.

2. It is not possible to use OFHC copper due to the high bakeout temperature and the possibility of permanent deformation during bakeout.

3. The passive plates experience some deflection during a disruption load, but this should not be a problem unless there is significant springback. If the springback is a large fraction of the statically calculated displacement, then the bellville washers may flatten out and the tiles could be pinched. This problem would require a local curvature of more than.005 inches across the width of the tile, which would appear to require a spring back of almost 100%.

4. Halo loading produces relatively small stresses. The lateral deflection in the secondary plates is due to the longer radial dimension of the support brackets and the flexibility of the support brackets in the vicinity of the lateral stops.

References:

[1] 11-971215-CLN-01, "Forces on Passive Plates"
[2] 13-970217-AWB-02, "Loads on CS Due to Plasma Disruption"
[3] "Disruption Forces Due to Halo Currents", S Kaye 2/2/98
[4] 11-980223-CLN, "Forces On Internal Hardware"
[5] "Forces on NSTX Tiles and Structure", B. Nelson, revised 3/98
[6] ITER Structural Design Criteria, Appendix A
[7] ASME Boiler and Pressure Vessel Code, Section VIII, Table UHA-23

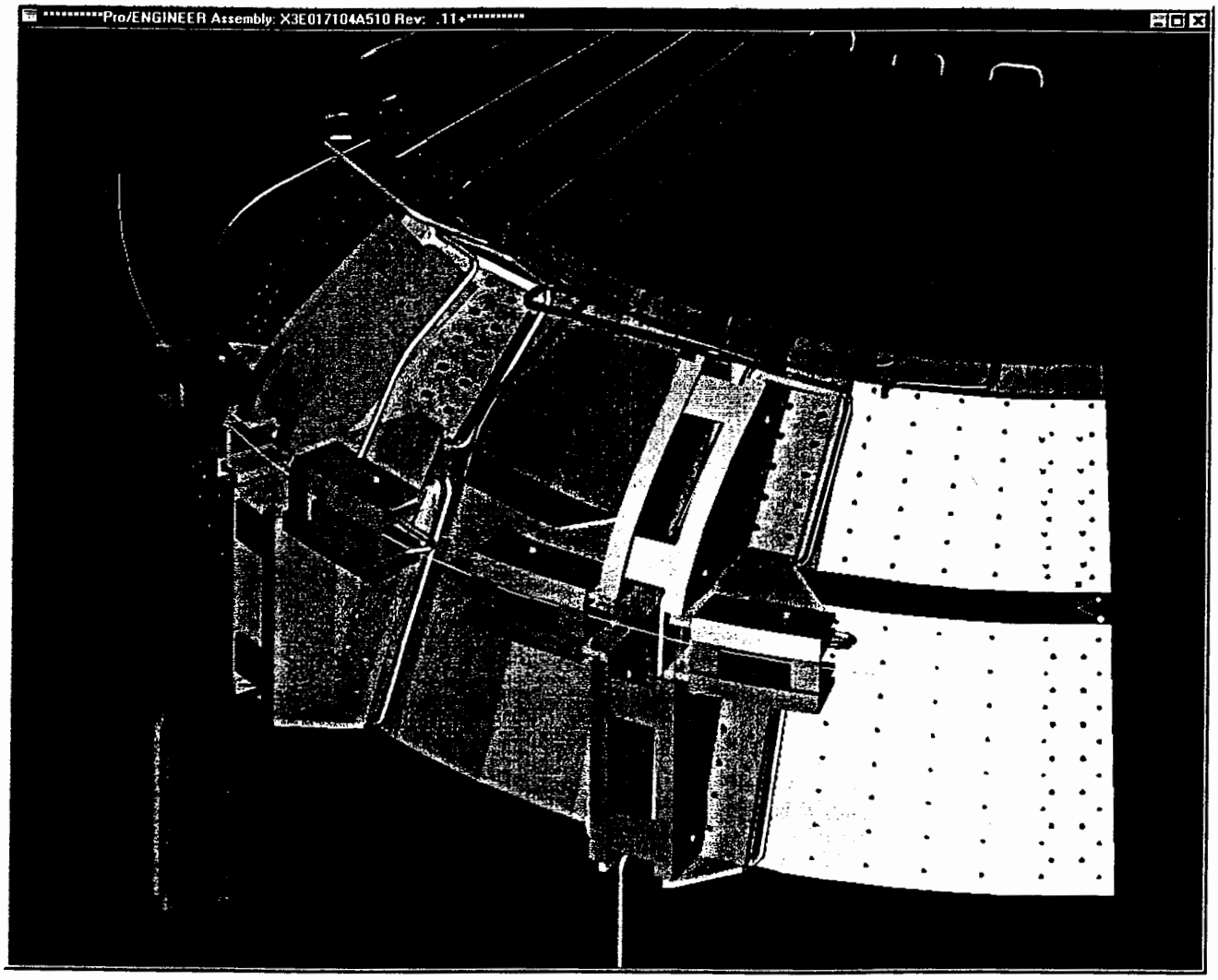

Figure 1 General arrangement of the passive plates and structure

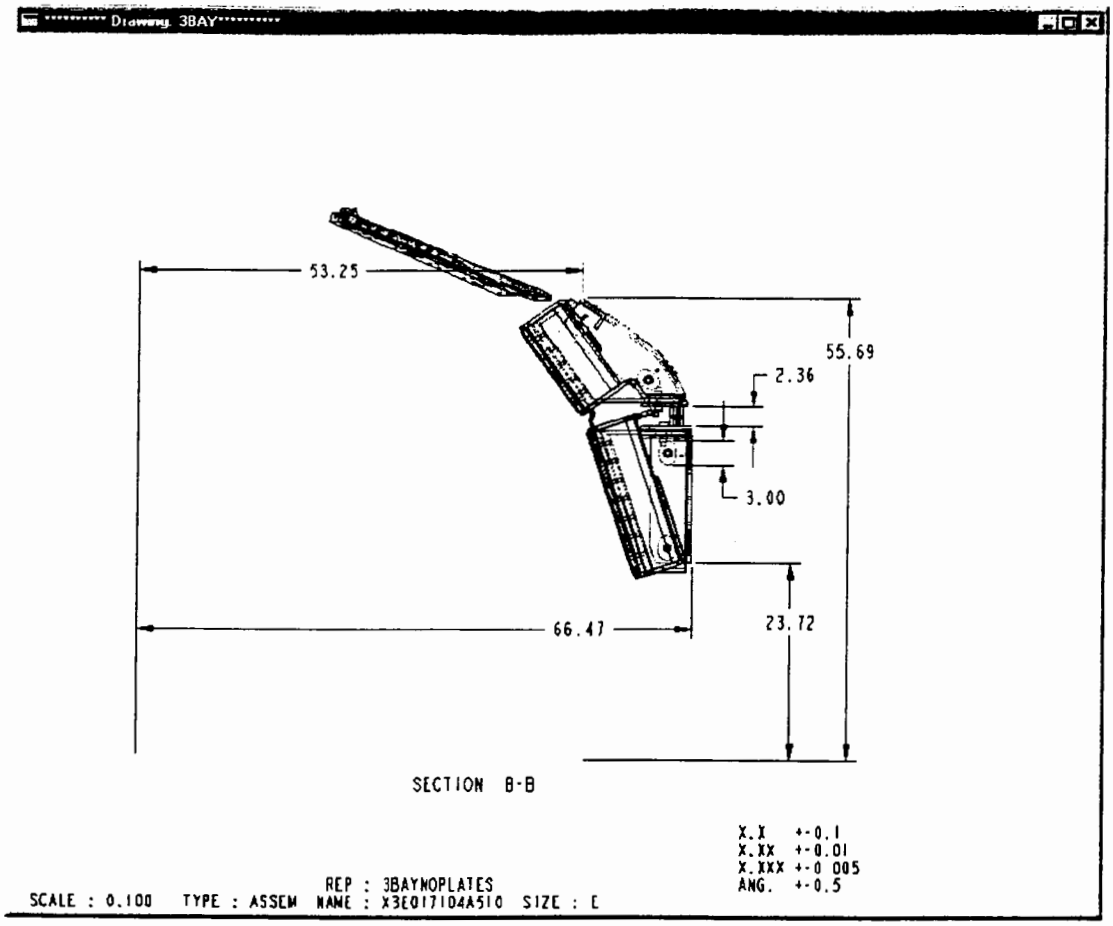

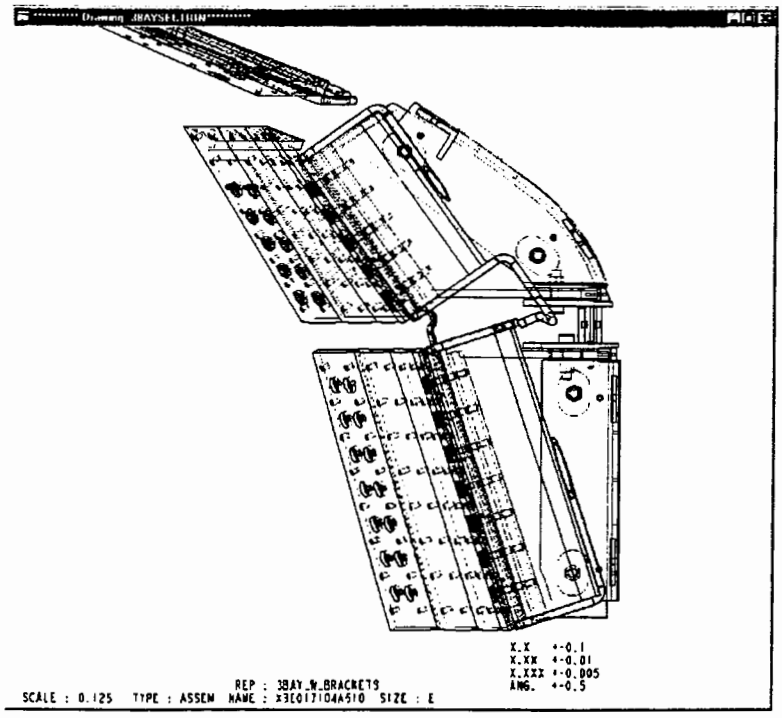

Figure 2 Passive plate / support dimensions

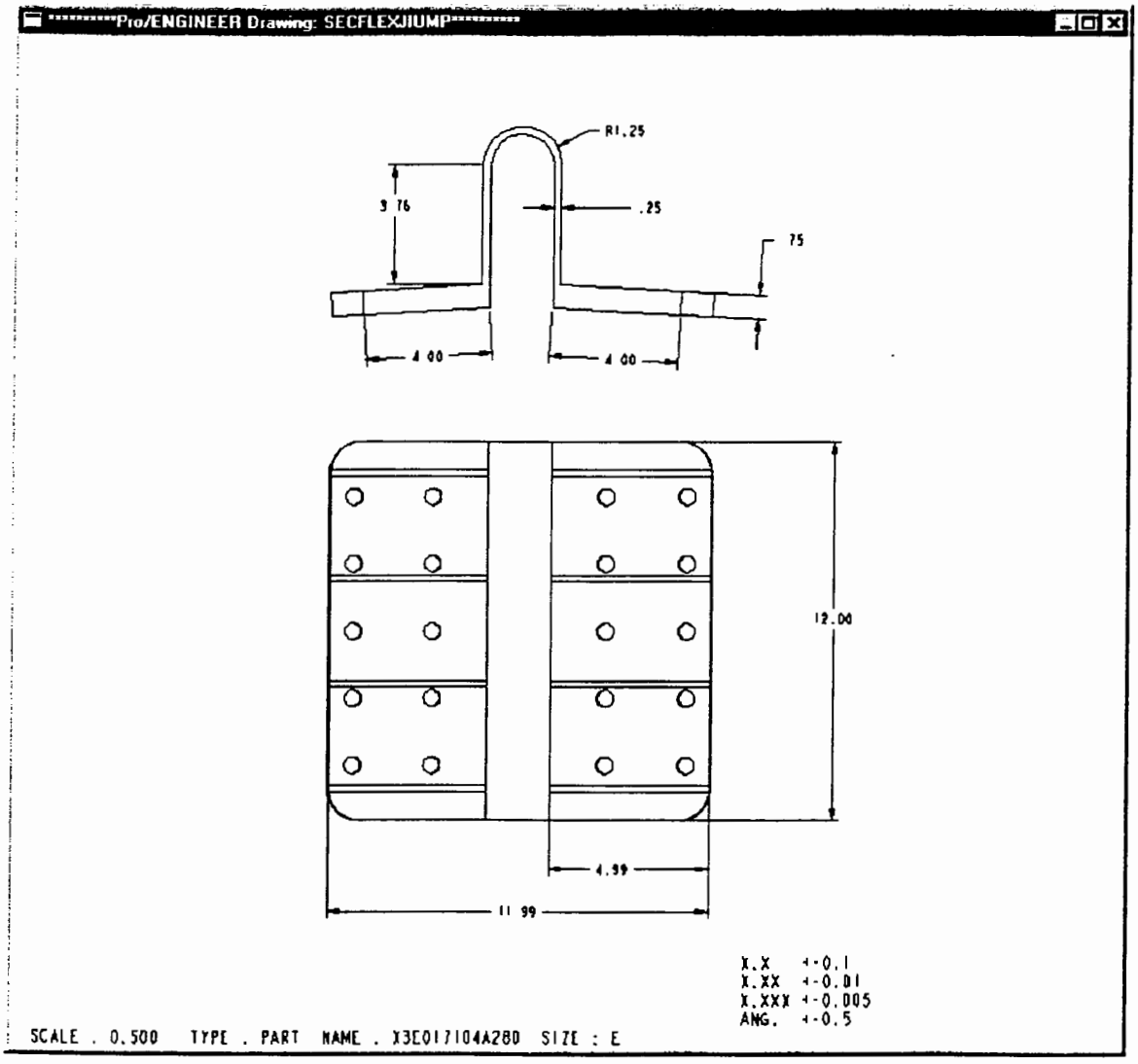

Figure 3 Typical flex jumper and dimensions

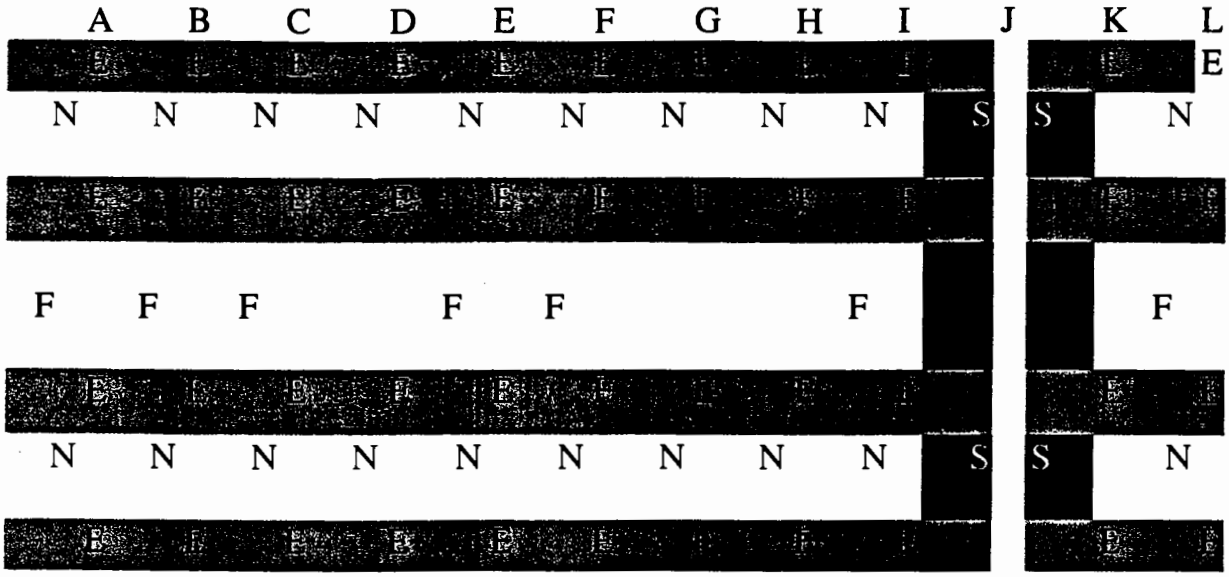

	=passive plate
E	=existing jumper
N	=new jumper
F	=future jumper
S	=saddle connection

Figure 4 Passive Plate Electrical Connection Schematic*

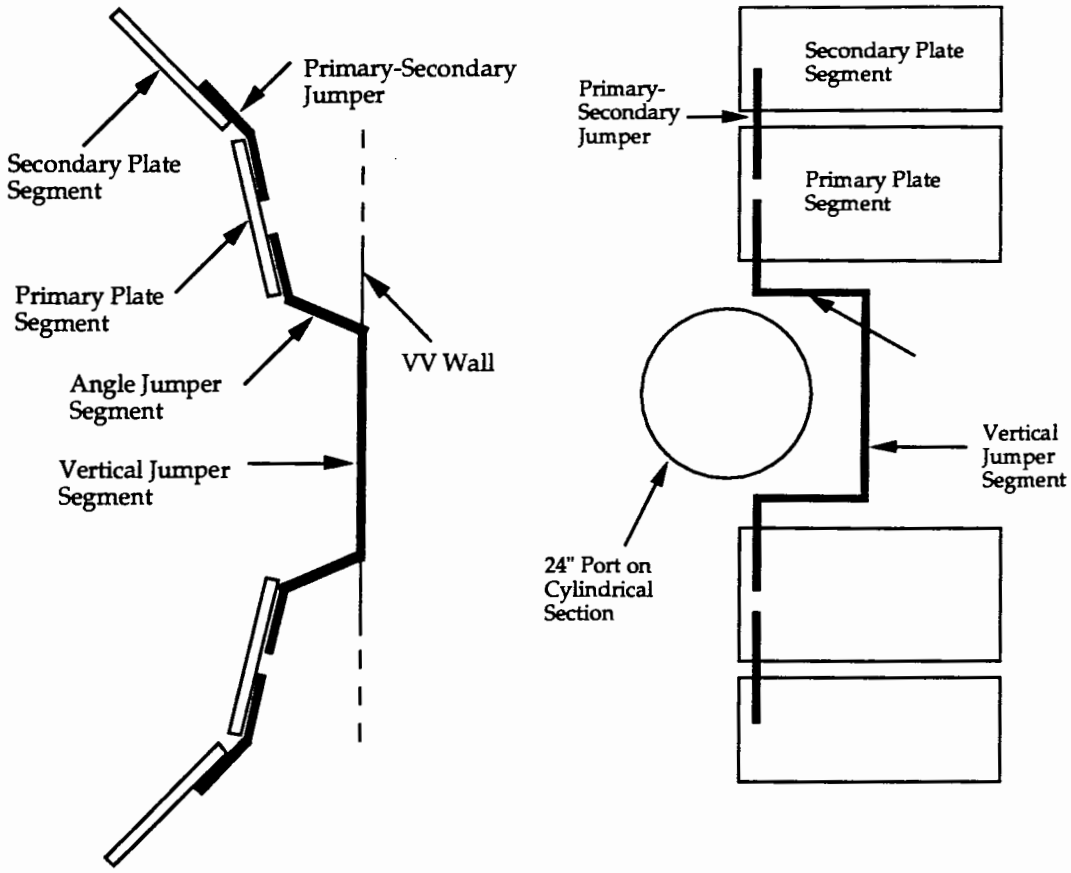

Figure 5 Passive Plate Electrical Connection Schematic

* reference PPPL memo by C. Neumeyer, 11-971029-CLN-01

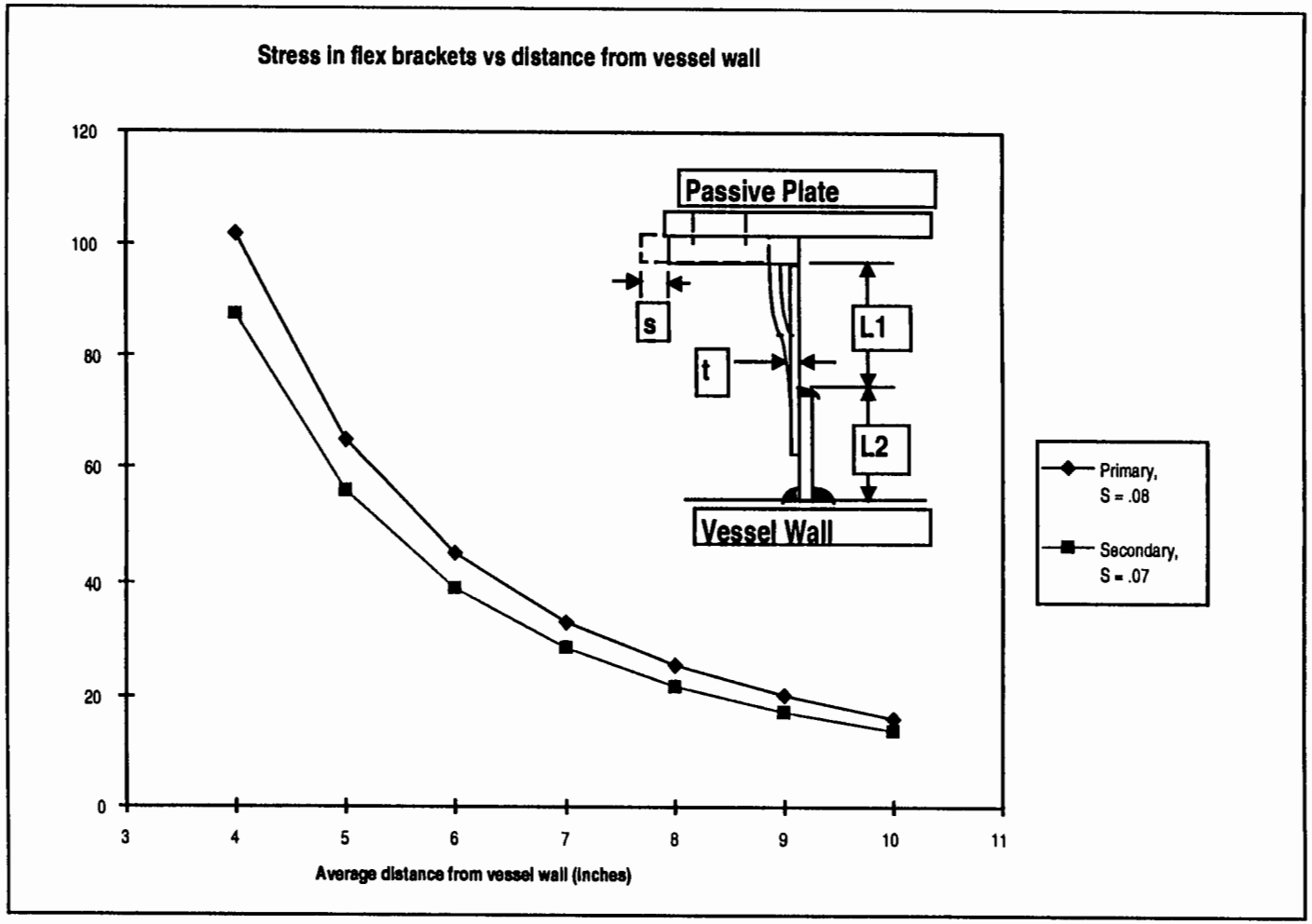

Figure 6 Stress in flexible bracket versus distance from wall for primary passive plate during bakeout conditions

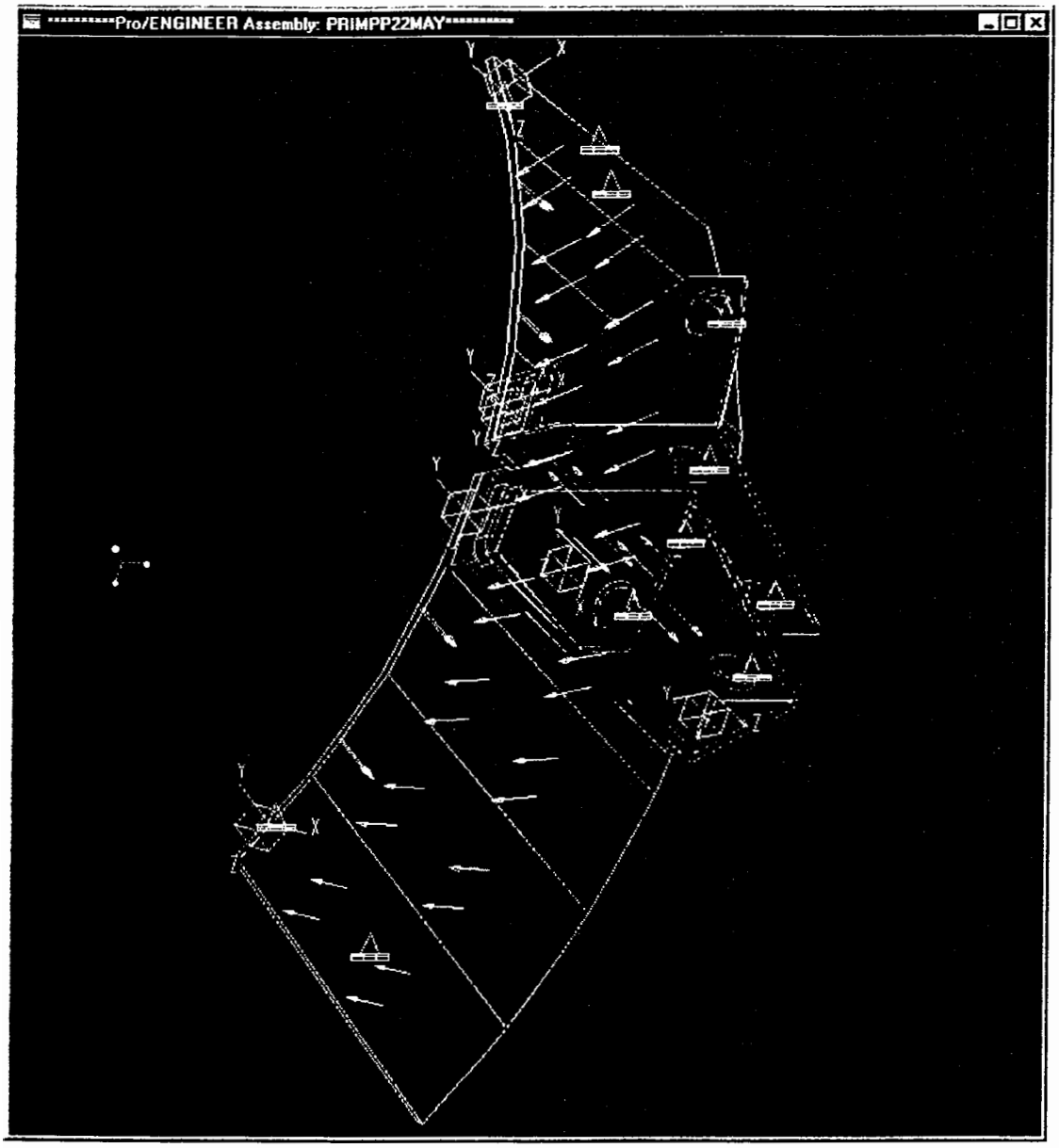

Figure 7 Model of Primary passive plates shown with disruption loads

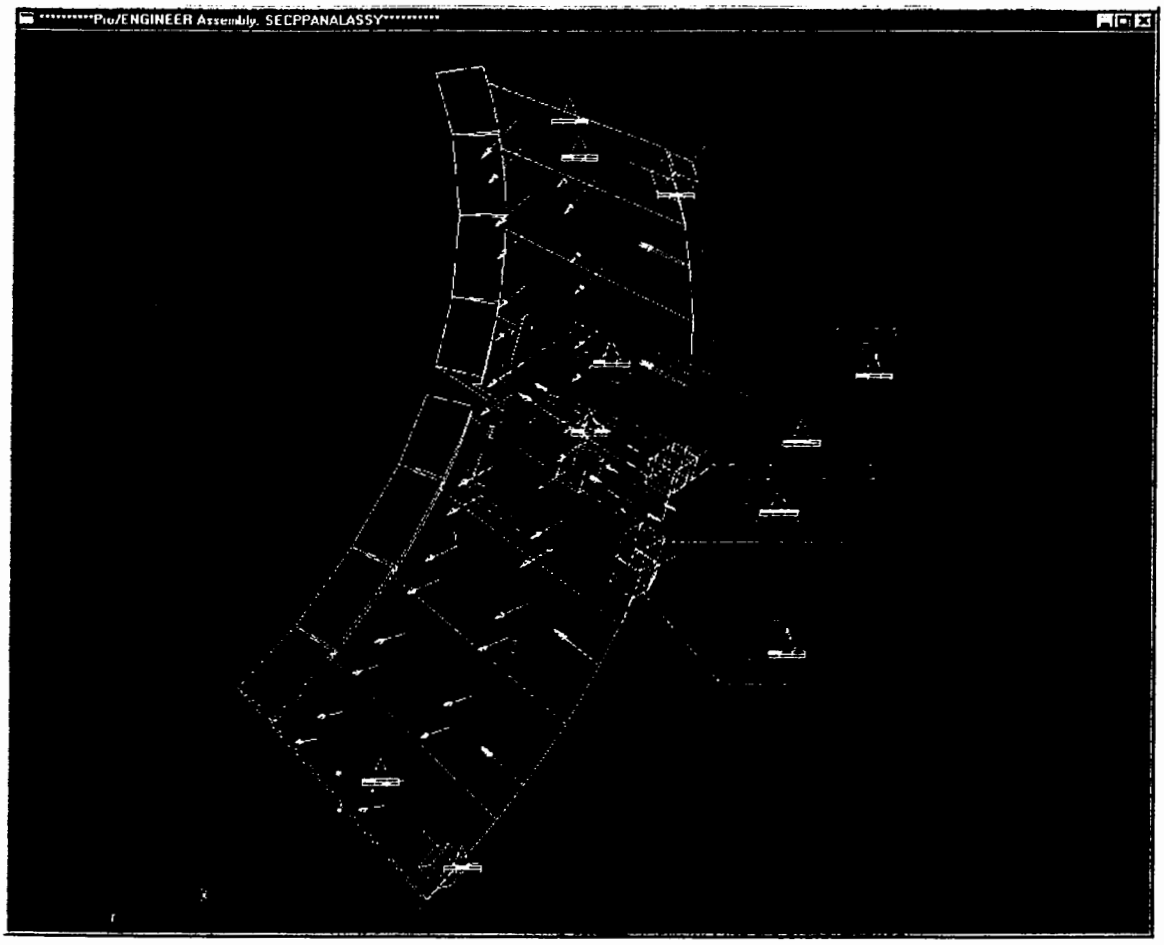

Figure 8 Model of Secondary passive plates shown with disruption loads

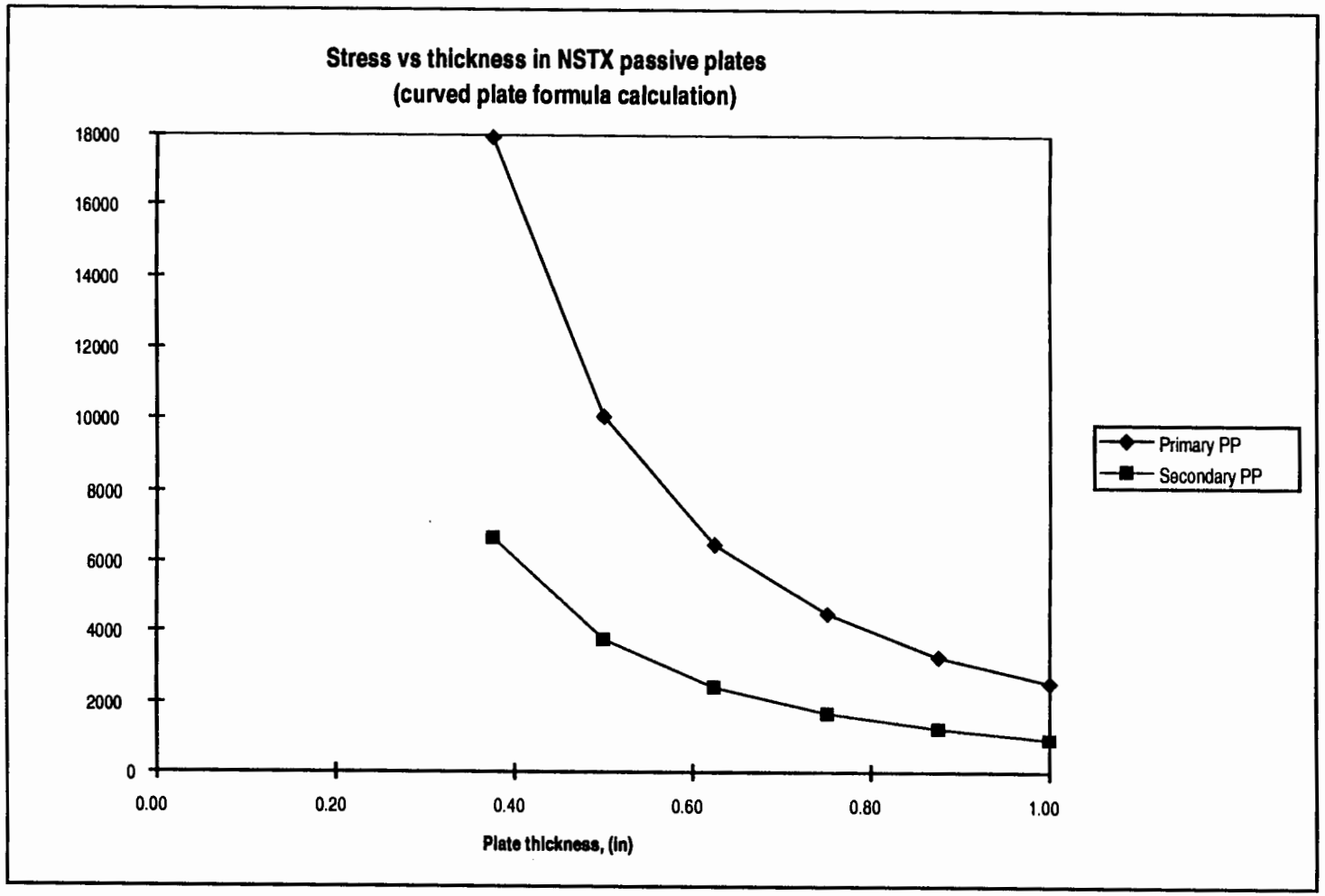

Figure 9 Stress in curved plate subject to pressure load for secondary and primary passive plates relative to thickness

APPENDIX 1

Reaction loads from flex jumpers

From Shigley, pages 130-131
(free end)

Let:	Primary PP	Secondary PP	
L =	3.75	3.75	in
r =	1.13	1.13	in
thickness, t =	0.25	0.25	in
E =	1.70E+07	1.70E+07	psi
height (h) =	18	12	in
I =	2.34E-02	1.56E-02	in^4
F =	380	217	lbs
y deflection/lb =	2.66E-04	3.99E-04	in
x deflection =	3.26E-03	2.79E-03	in
moment =	1852	1056	in-lbs
stress =	9877	8447	psi
R pass plate =	1.43	1.23	m
	56.48	48.30	in
delta T =	200	200	C
	360	360	F
COE =	9.50E-06	9.50E-06	per F
delta plate =	1.01E-01	8.65E-02	in

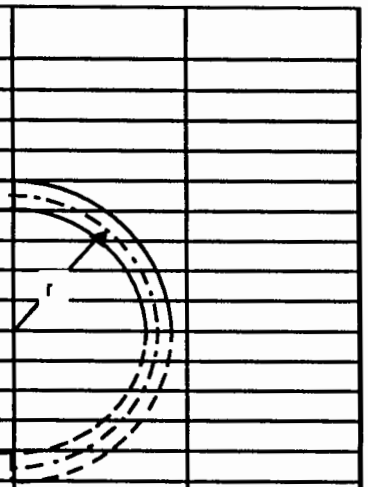

APPENDIX 2

Material Property data for Cu-Cr-Zr [3]

Table A.S2.3.1-1: Minimum Yield Stress

T (°C)	20	25	50	75	100	125	150	175	200	225	250
S_y (MPa)	297	297	293	289	285	281	277	272	267	262	257
S_y (min) (MPa)	264	264	260	256	252	248	244	239	235	230	224

T (°C)	275	300	325	350	375	400	425	450	475	500
S_y (MPa)	252	246	240	234	228	222	215	208	201	194
S_y (min) (MPa)	219	213	208	201	195	189	182	175	168	161

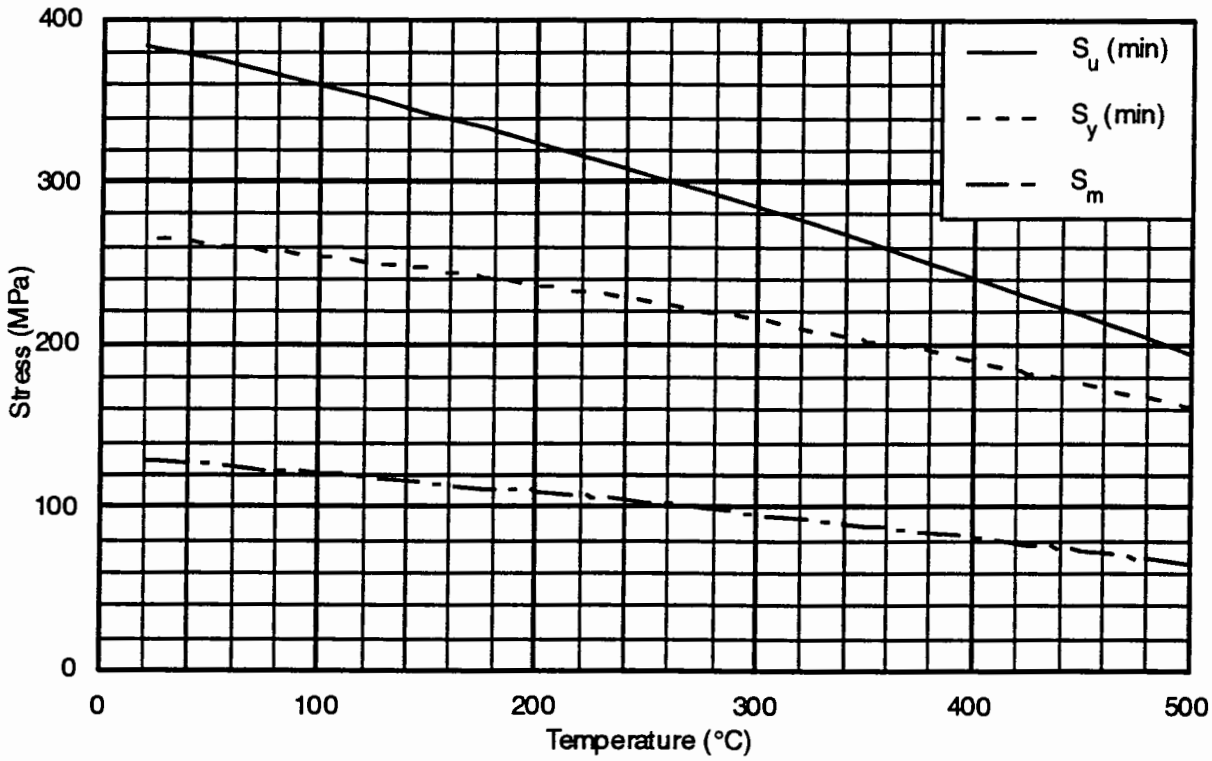

Variation of the Yield and Ultimate Tensile Stresses Versus Temperature for CuCrZr

ref [3], Figure A.S2.3.1-1:

APPENDIX 3

Bearing stresses in brackets

Let		
D =	0.75 inches	
R =	6,000 lbs	
t - channel	0.375 inches	
t - insert	0.75 inches	
t -bracket	0.5 inches	
l -bracket	1 inches	
brg stress	10667 psi	in channel
brg stress	10667 psi	in insert
brg stress	12000 psi	in bracket

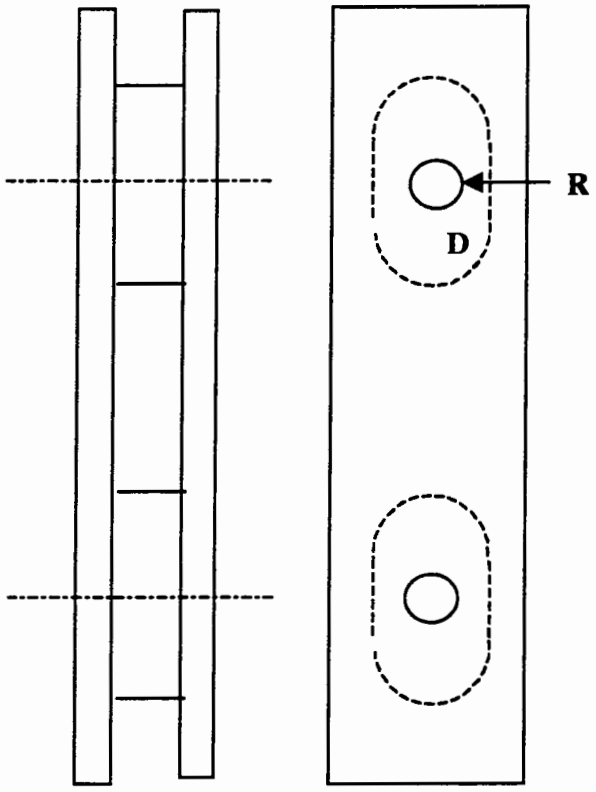

t

Section P, Primary Passive Plate stress results

P1 Disruption loading, single plate with simple boundary conditions
P2 - Disruption loading
P3 - Halo loading
P4 - Bakeout loading

Primary passive plate with disruption loads, displacement

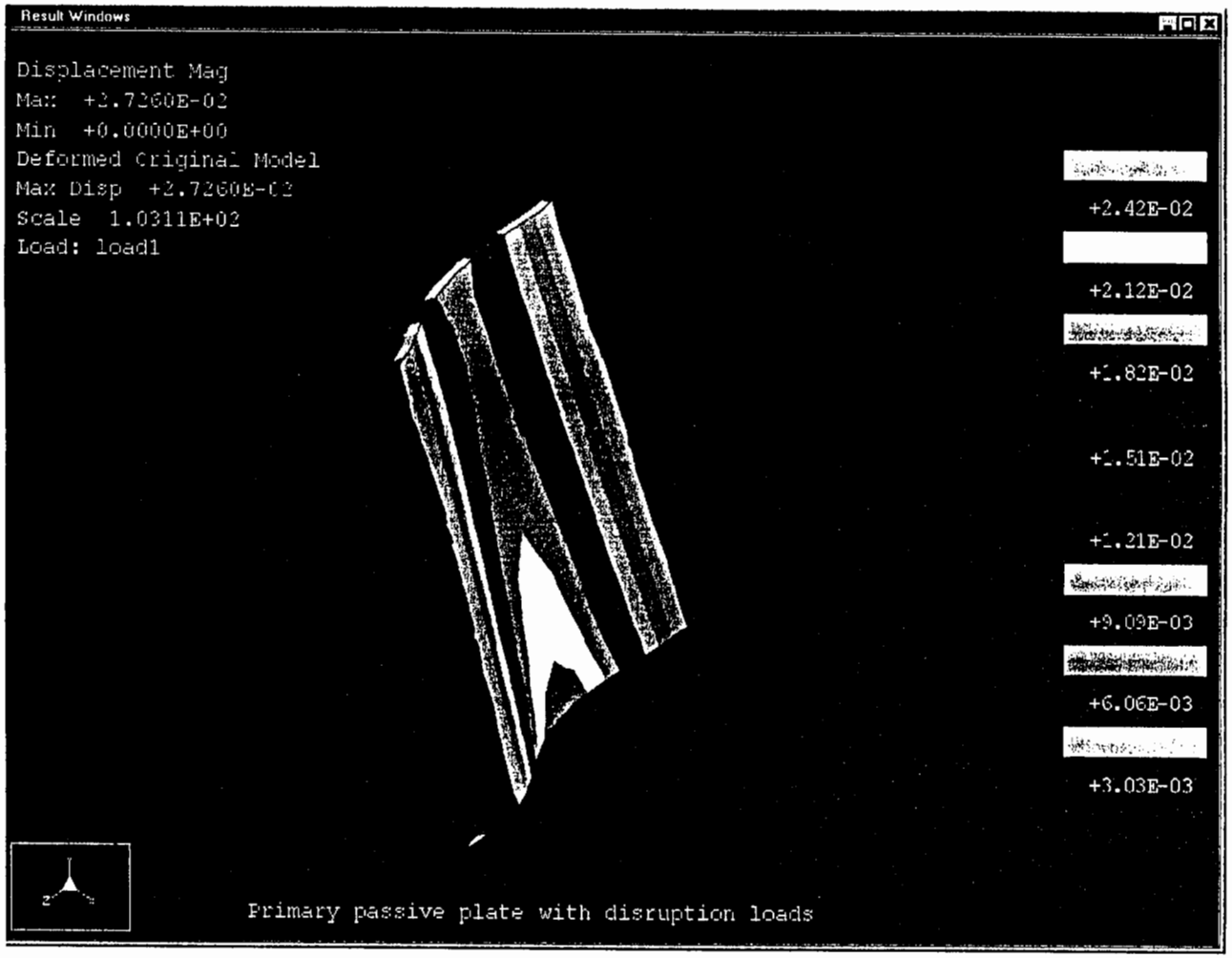

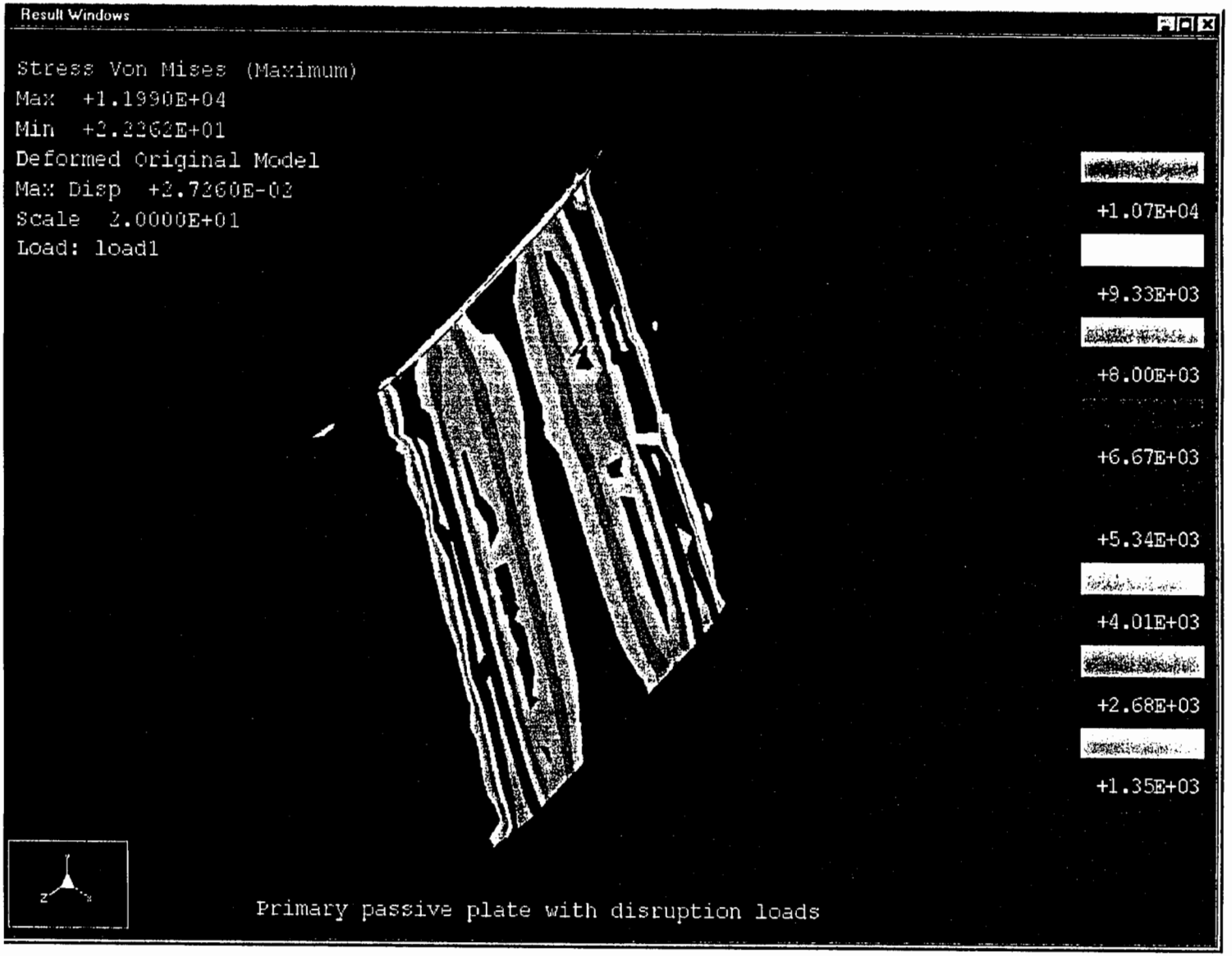
Result Windows
Stress Von Mises (Maximum)
Max +1.1990E+04
Min +2.2362E+01
Deformed Original Model
Max Disp +2.7260E-02
Scale 2.0000E+01
Load: load1
+1.07E+04
+9.33E+03
+8.00E+03
+6.67E+03
+5.34E+03
+4.01E+03
+2.68E+03
+1.35E+03
Primary passive plate with disruption loads

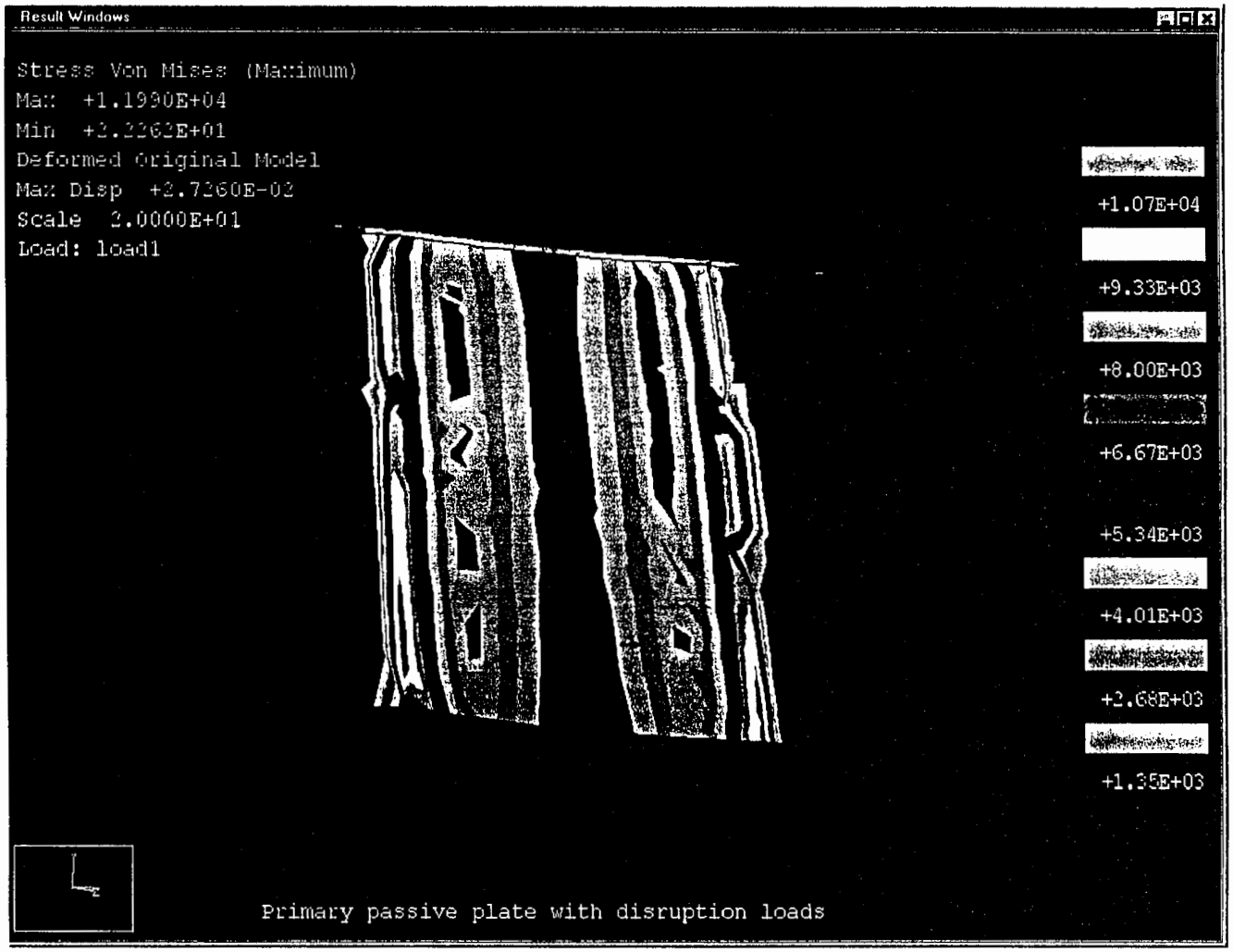
Result Windows
Stress Von Mises (Maximum)
Max +1.1990E+04
Min +3.2262E+01
Deformed Original Model
Max Disp +2.7260E-02
Scale 2.0000E+01
Load: load1
+1.07E+04
+9.33E+03
+8.00E+03
+6.67E+03
+5.34E+03
+4.01E+03
+2.68E+03
+1.35E+03
Primary passive plate with disruption loads

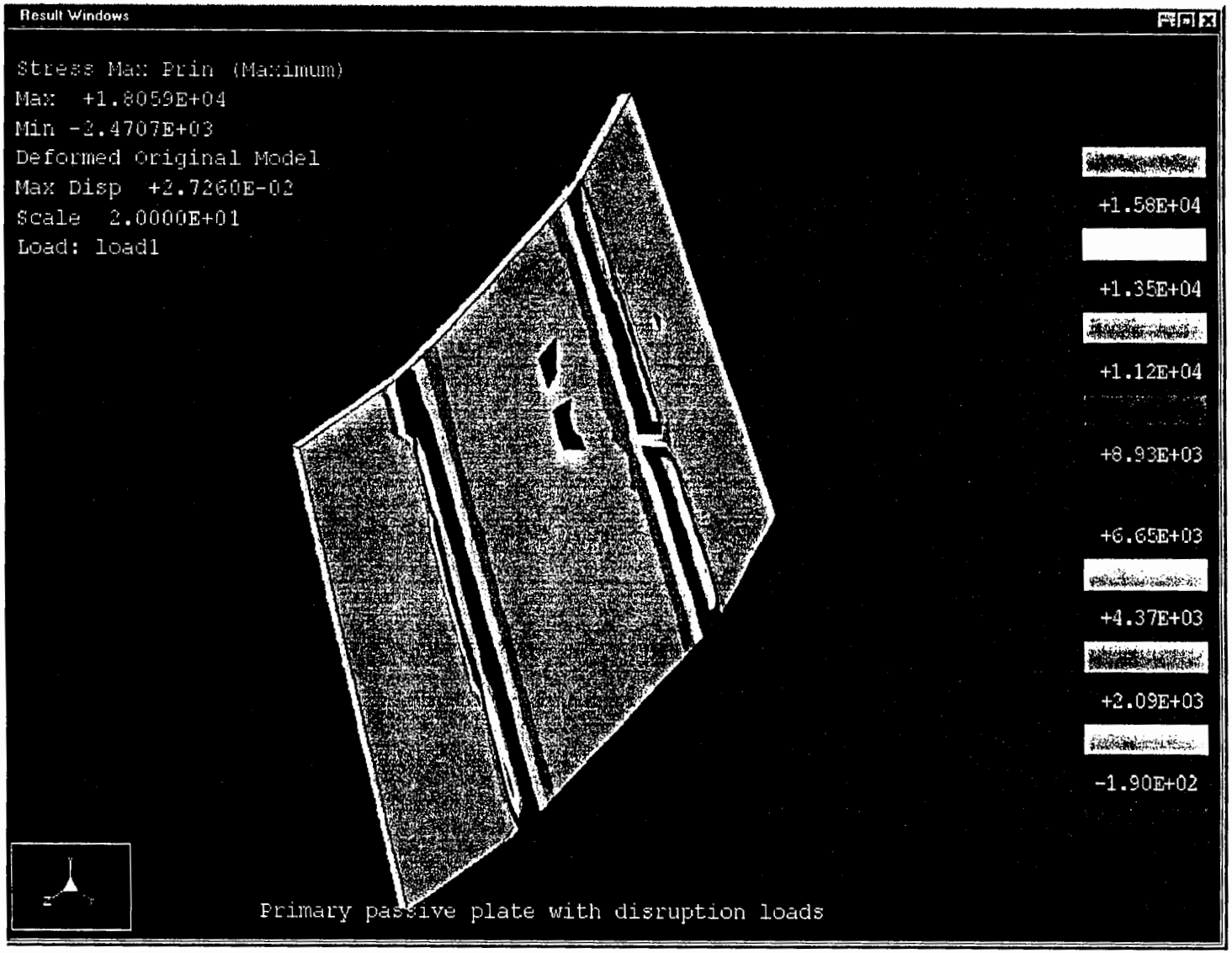
Result Windows
Stress Max Prin (Maximum)
Max +1.8059E+04
Min -2.4707E+03
Deformed Original Model
Max Disp +2.7260E-02
Scale 2.0000E+01
Load: load1
+1.58E+04
+1.35E+04
+1.12E+04
+8.93E+03
+6.65E+03
+4.37E+03
+2.09E+03
-1.90E+02
Primary passive plate with disruption loads


Result Windows
Displacement Mag
Max +5.4970E-02
Min +0.0000E+00
Deformed Original Model
Max Disp +5.4970E-02
Scale 1.0000E+01
Load: load1
+4.89E-02
+4.28E-02
+3.66E-02
+3.05E-02
+2.44E-02
+1.83E-02
+1.22E-02
+6.11E-03
Primary passive plates with disruption loads

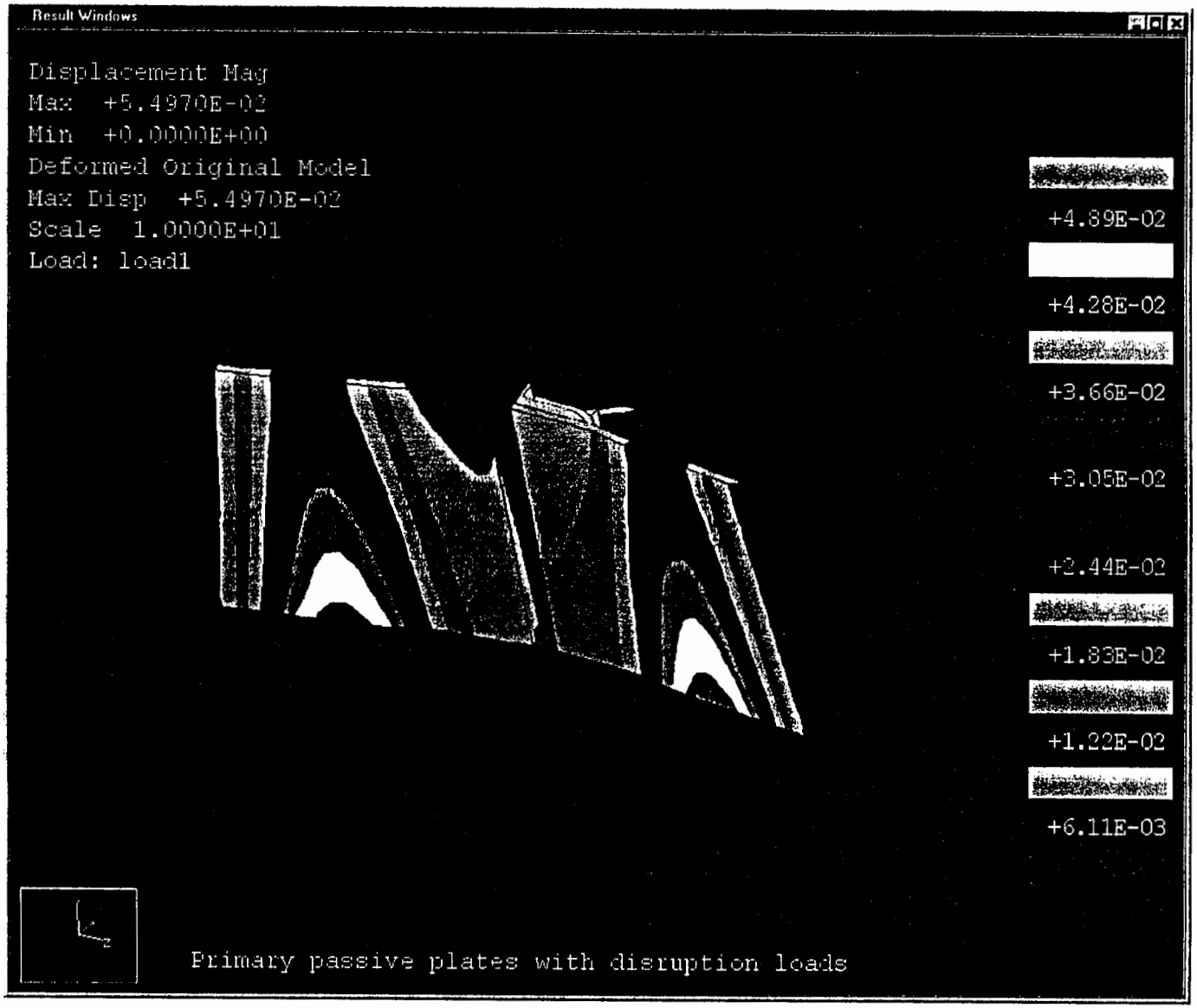
Result Windows
Displacement Mag
Max +5.4970E-02
Min +0.0000E+00
Deformed Original Model
Max Disp +5.4970E-02
Scale 1.0000E+01
Load: load1
+4.89E-02
+4.28E-02
+3.66E-02
+3.05E-02
+2.44E-02
+1.83E-02
+1.22E-02
+6.11E-03
Primary passive plates with disruption loads


Result Windows
Stress Von Mises (Maximum)
Max +6.1612E+04
Min +2.4132E+01
Deformed Original Model
Max Disp +5.4970E-02
Scale 1.0000E+01
Load: load1
+2.50E+04
+2.14E+04
+1.79E+04
+1.43E+04
+1.07E+04
+7.14E+03
+3.57E+03
+0.00E+00
Primary passive plates with disruption loads

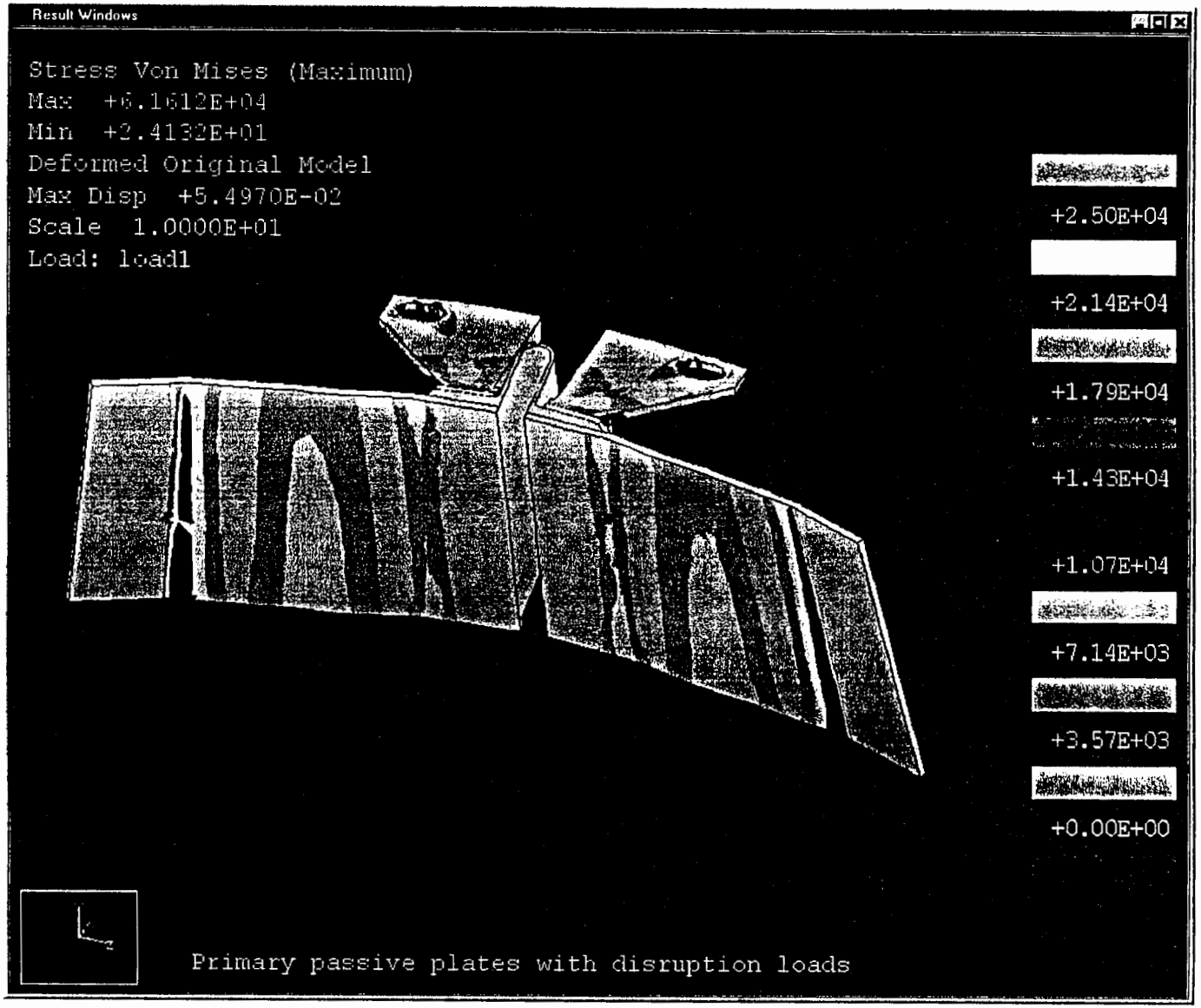
Result Windows
Stress Von Mises (Maximum)
Max +6.1612E+04
Min +2.4132E+01
Deformed Original Model
Max Disp +5.4970E-02
Scale 1.0000E+01
Load: load1
+2.50E+04
+2.14E+04
+1.79E+04
+1.43E+04
+1.07E+04
+7.14E+03
+3.57E+03
+0.00E+00
Primary passive plates with disruption loads

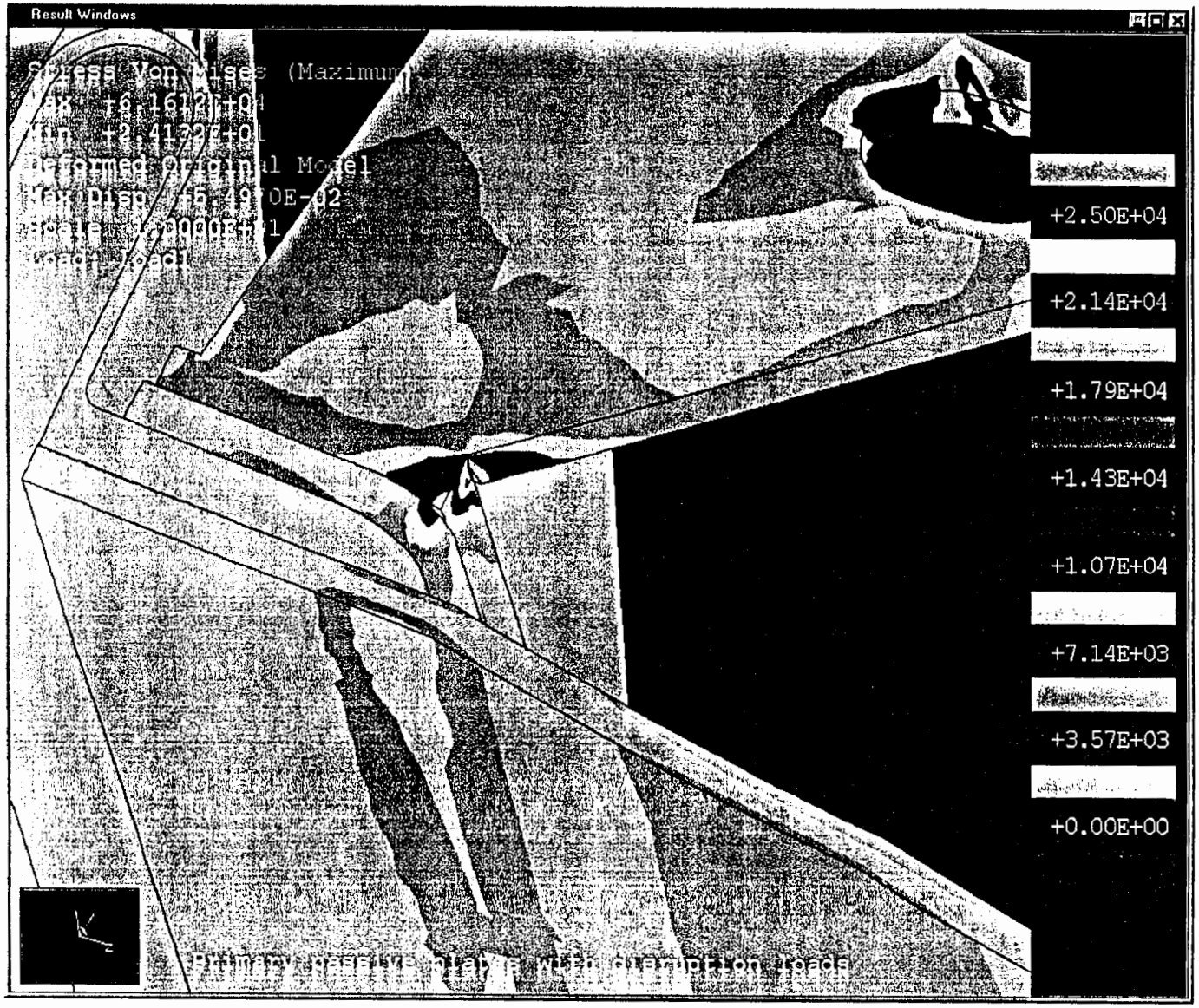
Result Windows
+2.50E+04
+2.14E+04
+1.79E+04
+1.43E+04
+1.07E+04
+7.14E+03
+3.57E+03
+0.00E+00

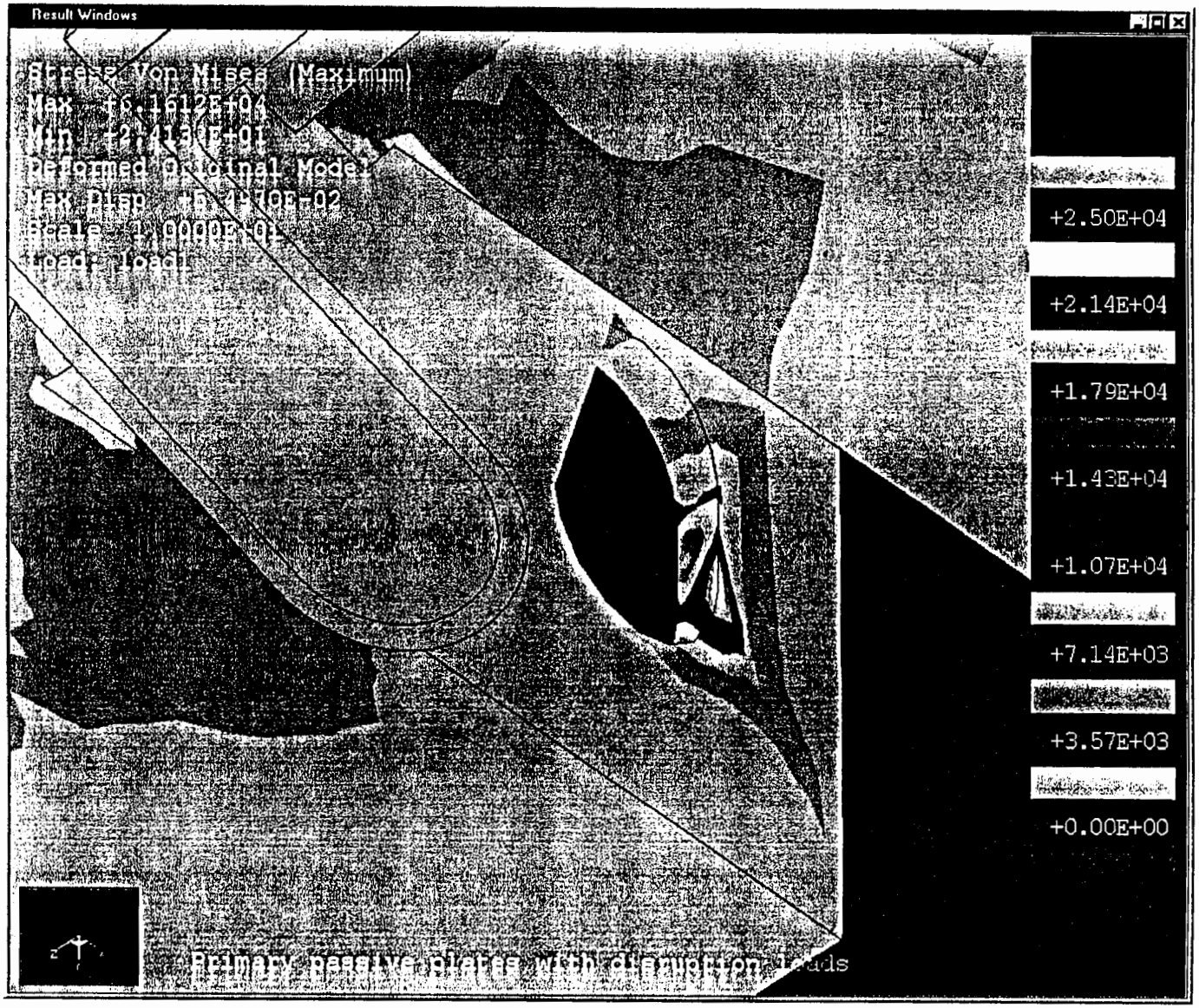
Result Windows
Stress Von Mises (Maximum)
+2.50E+04
+2.14E+04
+1.79E+04
+1.43E+04
+1.07E+04
+7.14E+03
+3.57E+03
+0.00E+00

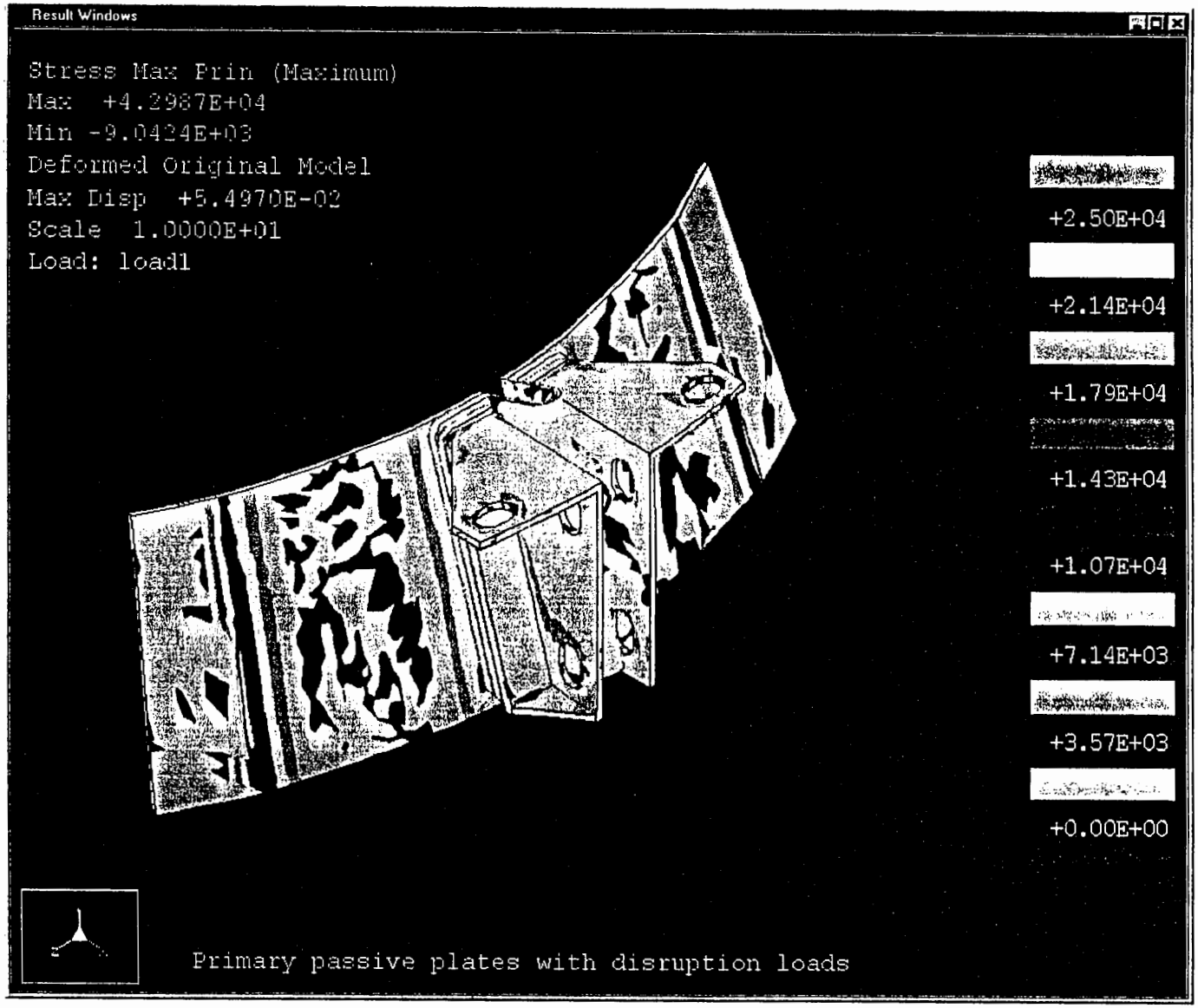
Result Windows
Stress Max Prin (Maximum)
Max +4.2987E+04
Min -9.0424E+03
Deformed Original Model
Max Disp +5.4970E-02
Scale 1.0000E+01
Load: load1
+2.50E+04
+2.14E+04
+1.79E+04
+1.43E+04
+1.07E+04
+7.14E+03
+3.57E+03
+0.00E+00
Primary passive plates with disruption loads

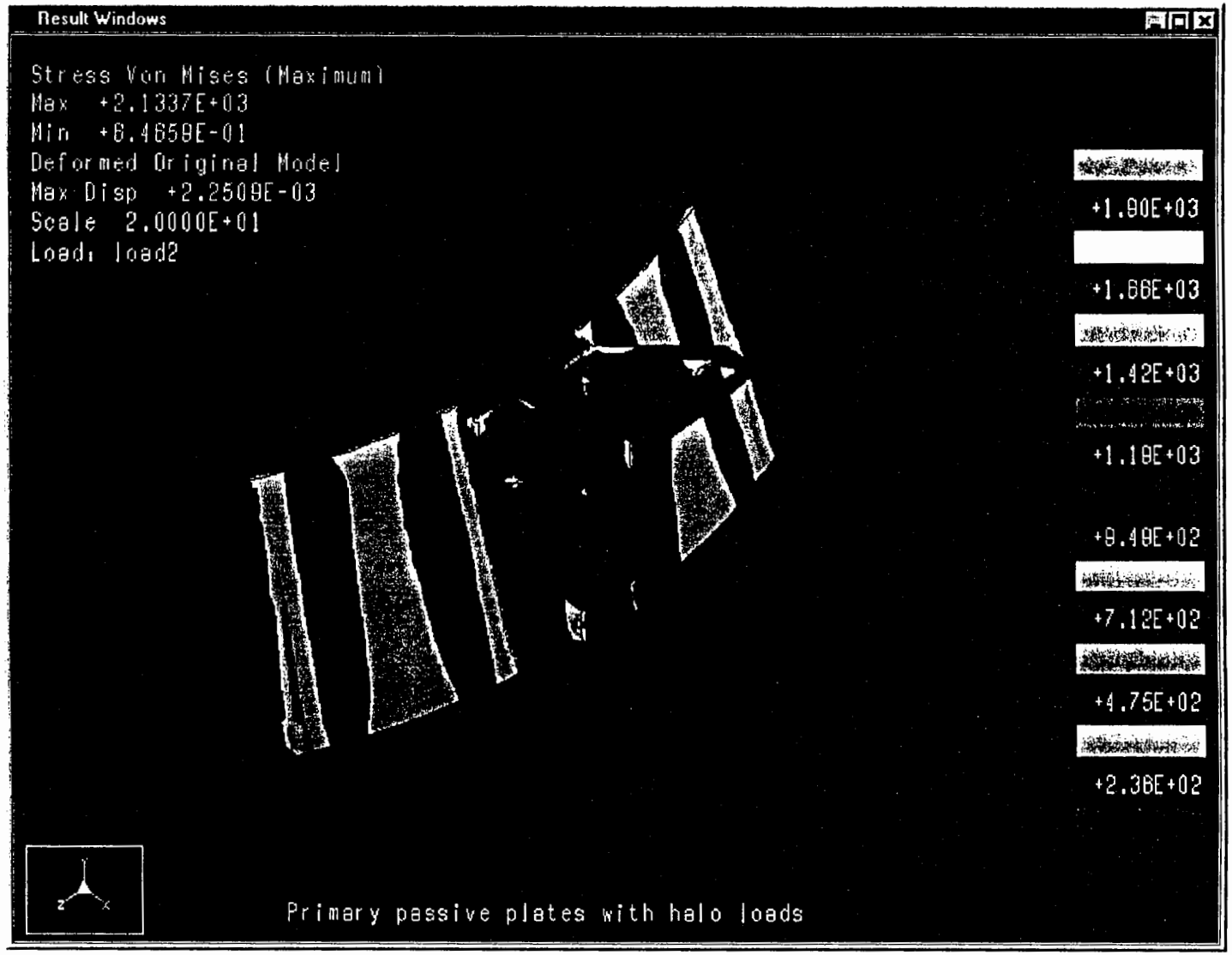
Result Windows
Stress Von Mises (Maximum)
Max +2.1337E+03
Min +8.4658E-01
Deformed Original Model
Max Disp +2.2509E-03
Scale 2.0000E+01
Load: load2
+1.90E+03
+1.66E+03
+1.42E+03
+1.18E+03
+9.49E+02
+7.12E+02
+4.75E+02
+2.36E+02
Primary passive plates with halo loads

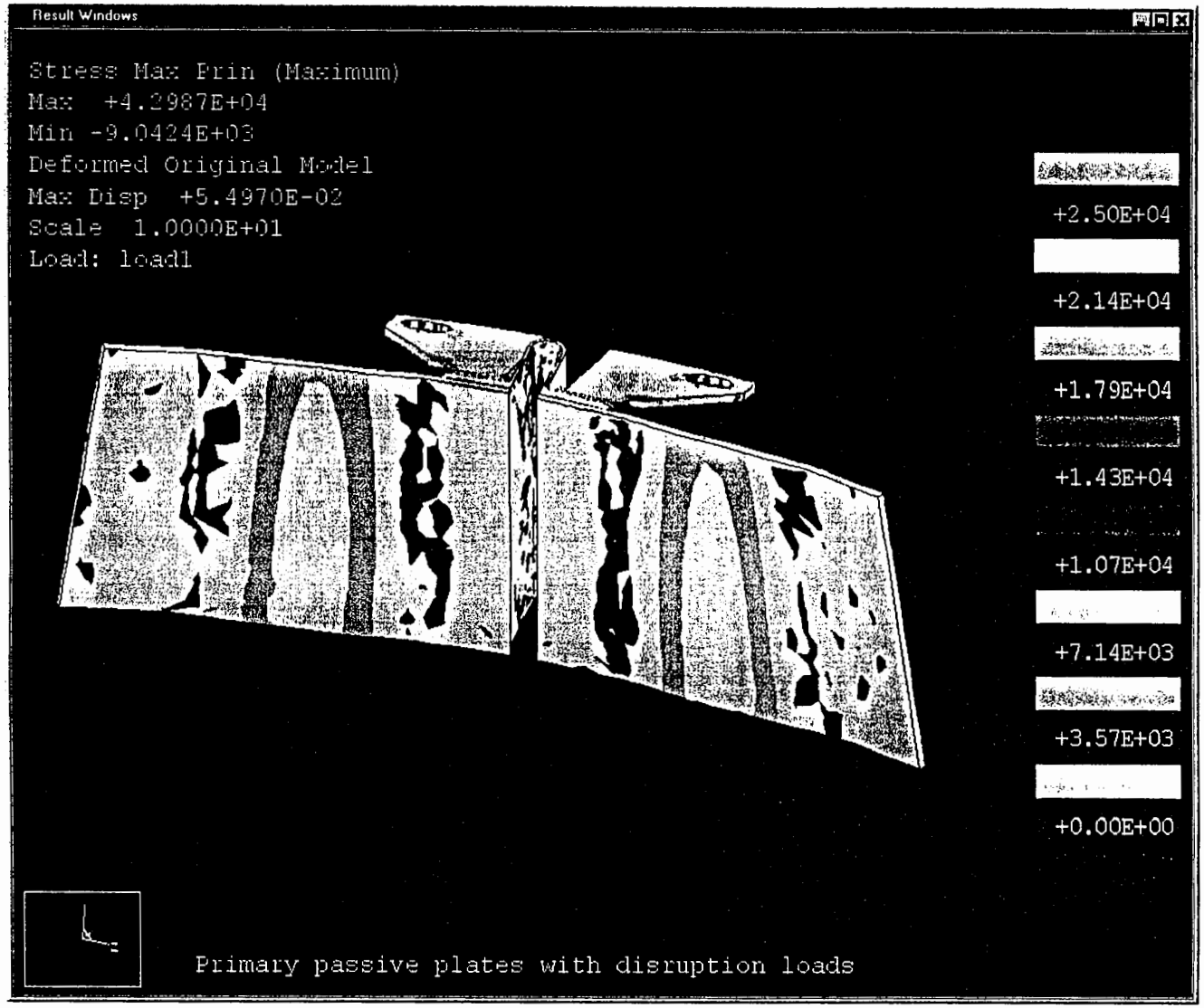
Result Windows
Stress Max Prin (Maximum)
Max +4.2987E+04
Min -9.0424E+03
Deformed Original Model
Max Disp +5.4970E-02
Scale 1.0000E+01
Load: load1
+2.50E+04
+2.14E+04
+1.79E+04
+1.43E+04
+1.07E+04
+7.14E+03
+3.57E+03
+0.00E+00
Primary passive plates with disruption loads

Primary passive plates, bakeout at 350C, vessel at 150C

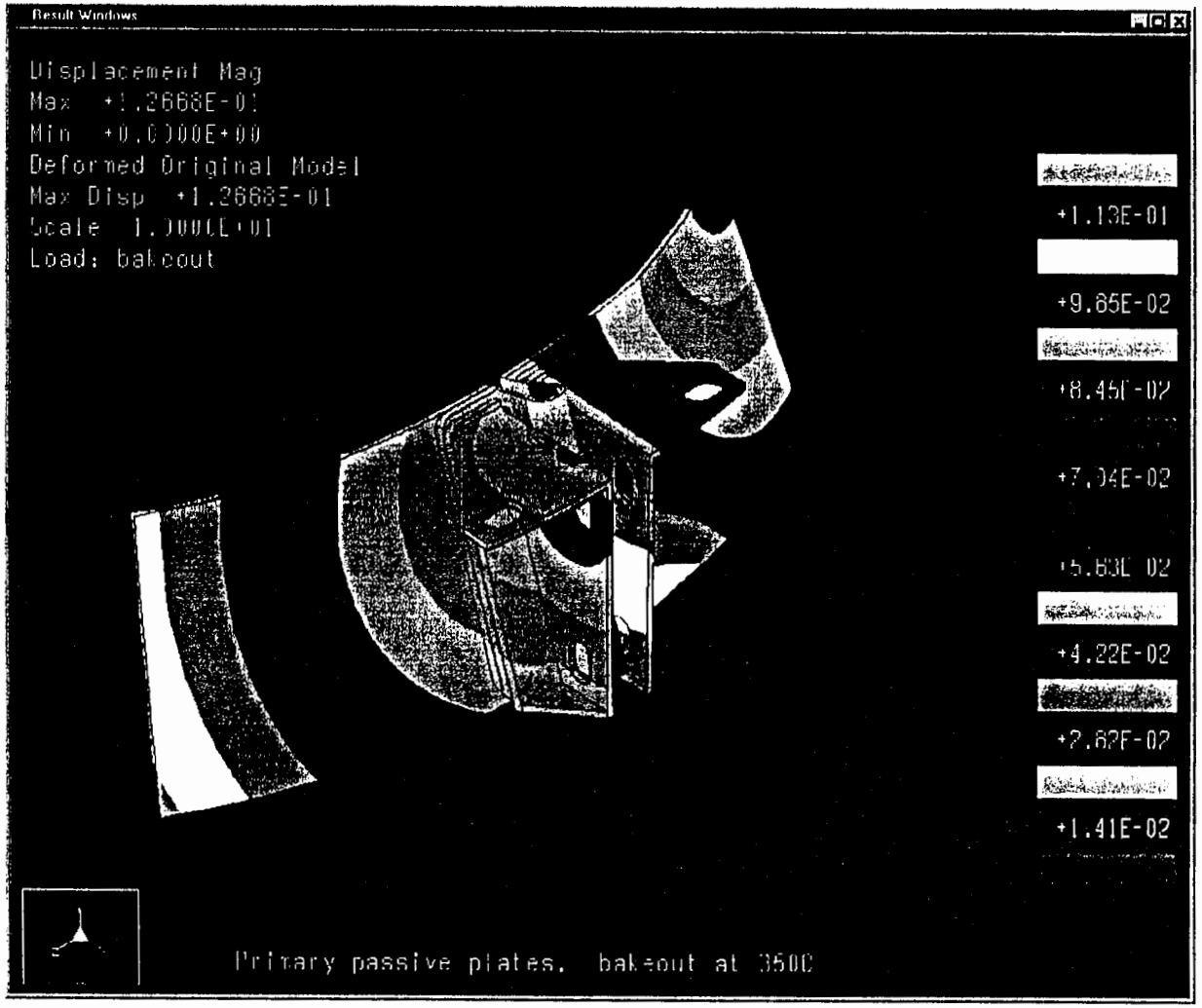

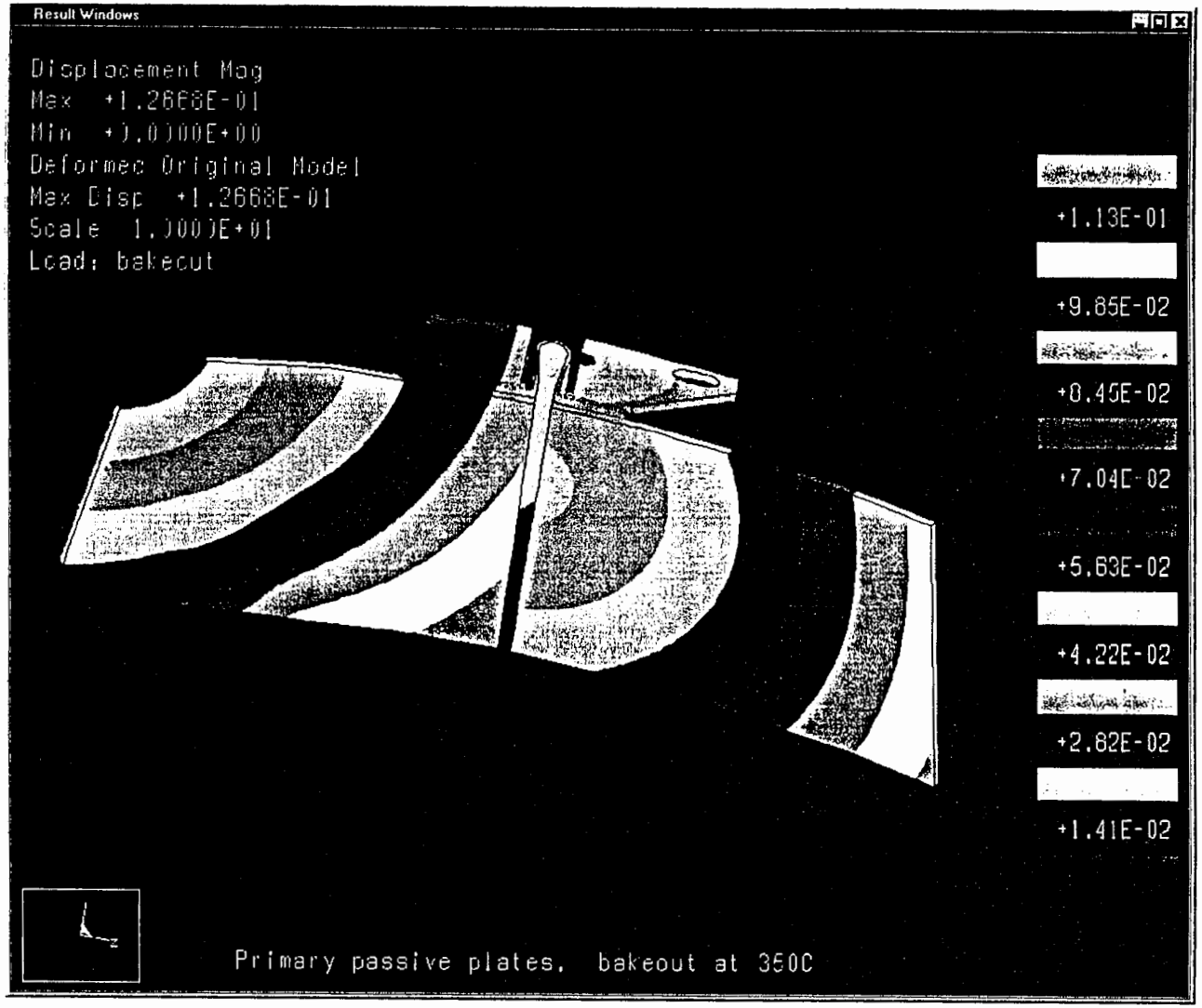
Result Windows
Displacement Mag
Max +1.2668E-01
Min +0.0000E+00
Deformed Original Model
Max Disp +1.2668E-01
Scale 1.0000E+01
Load: bakeout
+1.13E-01
+9.85E-02
+8.45E-02
+7.04E-02
+5.63E-02
+4.22E-02
+2.82E-02
+1.41E-02
Primary passive plates, bakeout at 350C

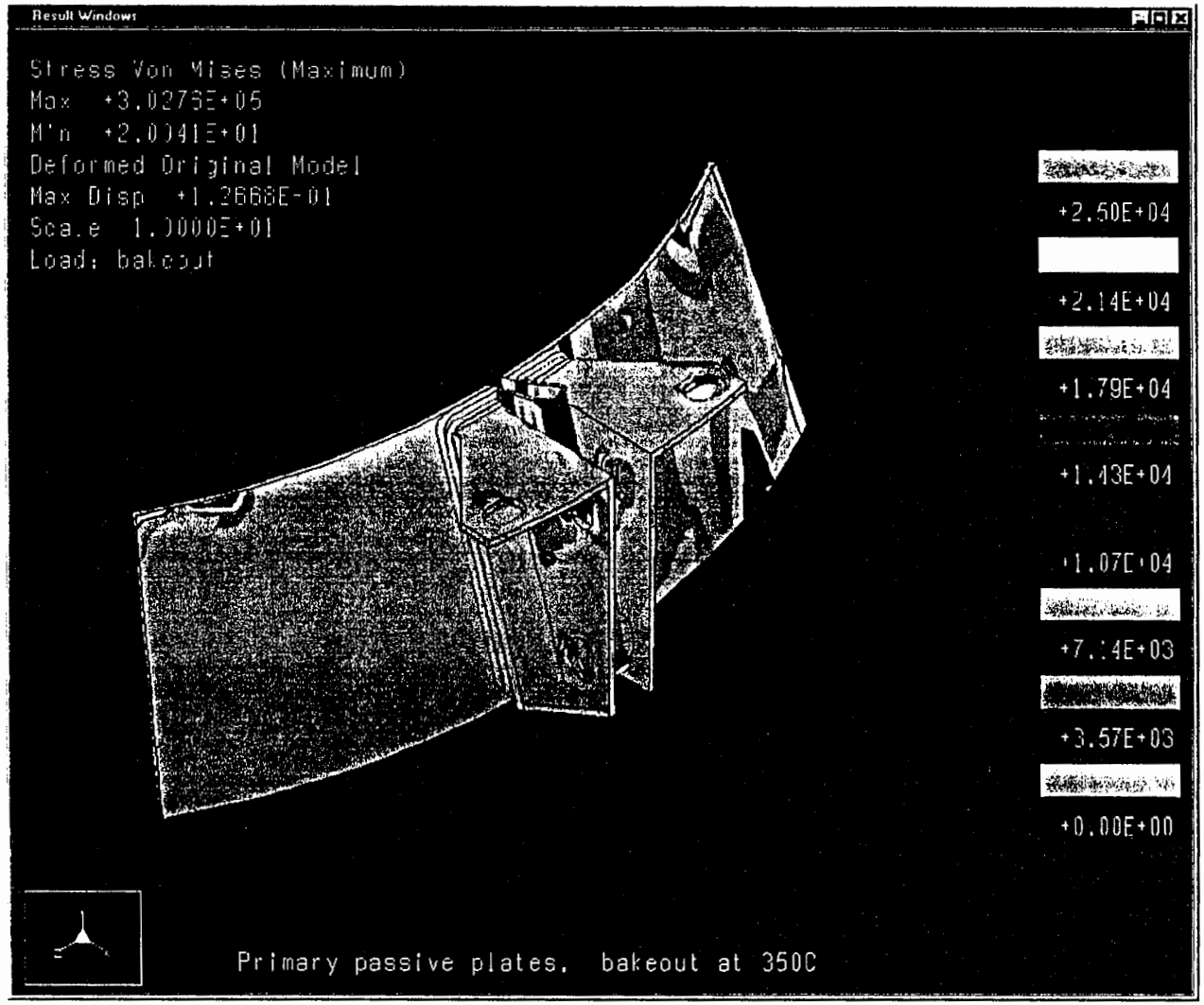
Result Windows
Stress Von Mises (Maximum)
Max +3.0278E+05
Min +2.0041E+01
Deformed Original Model
Max Disp +1.3668E-01
Scale 1.0000E+01
Load: bakeout
+2.50E+04
+2.14E+04
+1.79E+04
+1.43E+04
+1.07E+04
+7.14E+03
+3.57E+03
+0.00E+00
Primary passive plates, bakeout at 350C

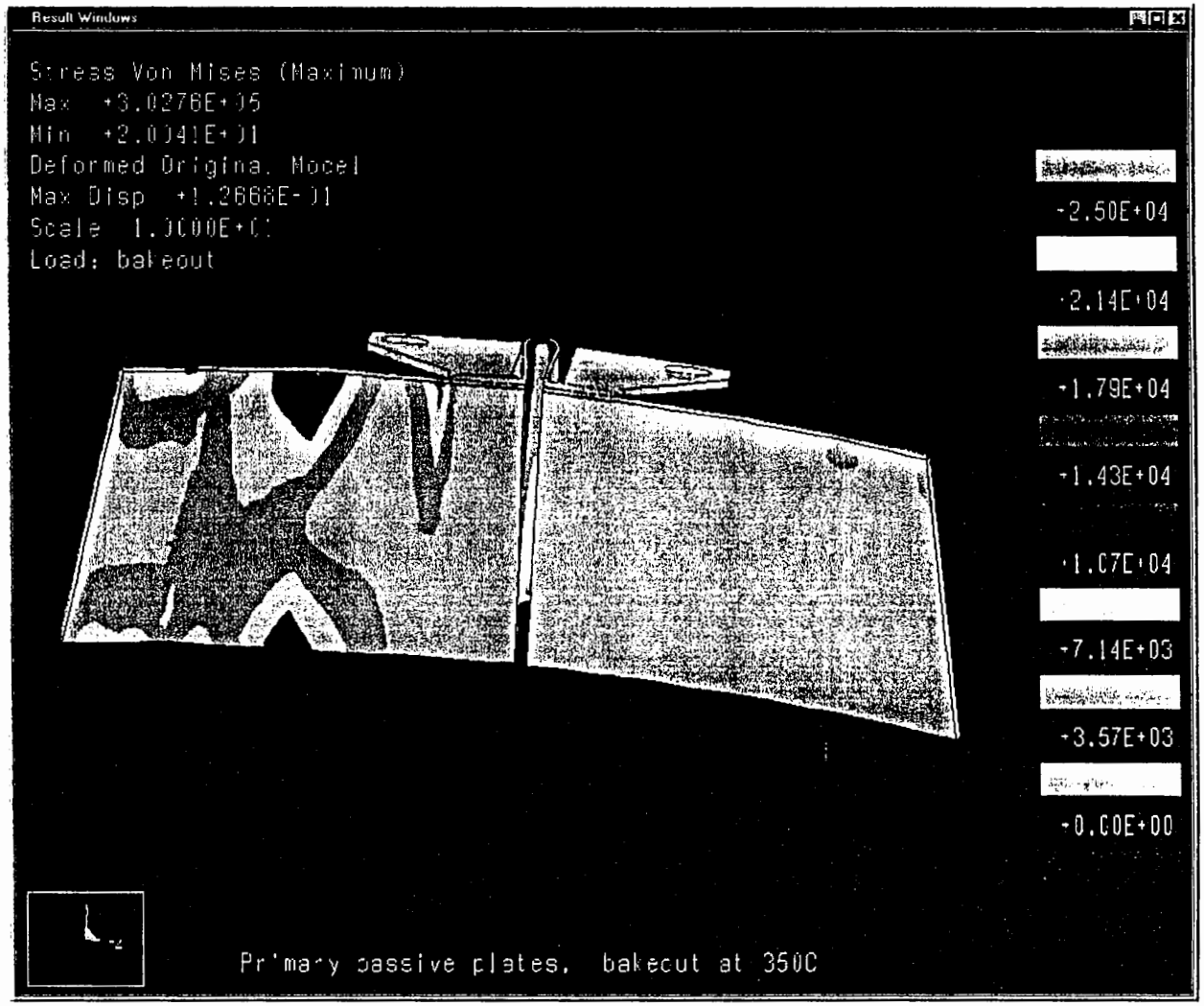
Result Windows
Stress Von Mises (Maximum)
Max +3.0276E+05
Min +2.0041E+01
Deformed Origina. Mocel
Max Disp +1.2666E-01
Scale 1.0000E+0
Load: bakeout
-2.50E+04
-2.14E+04
-1.79E+04
-1.43E+04
-1.07E+04
-7.14E+03
-3.57E+03
-0.00E+00
Pr'ma-y passive plates, bakecut at 350C

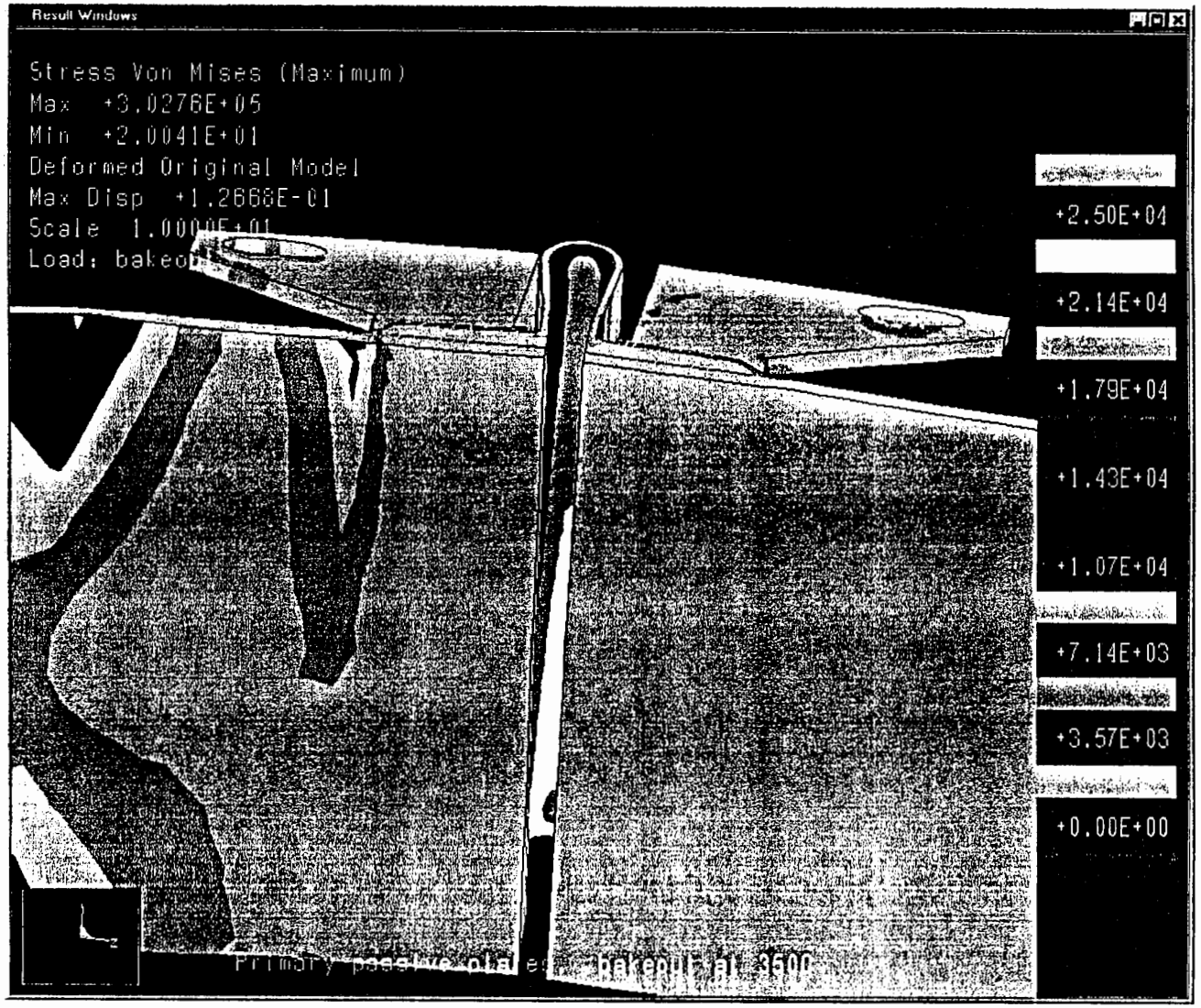
Result Windows
Stress Von Mises (Maximum)
Max +3.0276E+05
Min +2.0041E+01
Deformed Original Model
Max Disp +1.2668E-01
Scale 1.0000E+01
Load: bakeout
+2.50E+04
+2.14E+04
+1.79E+04
+1.43E+04
+1.07E+04
+7.14E+03
+3.57E+03
+0.00E+00

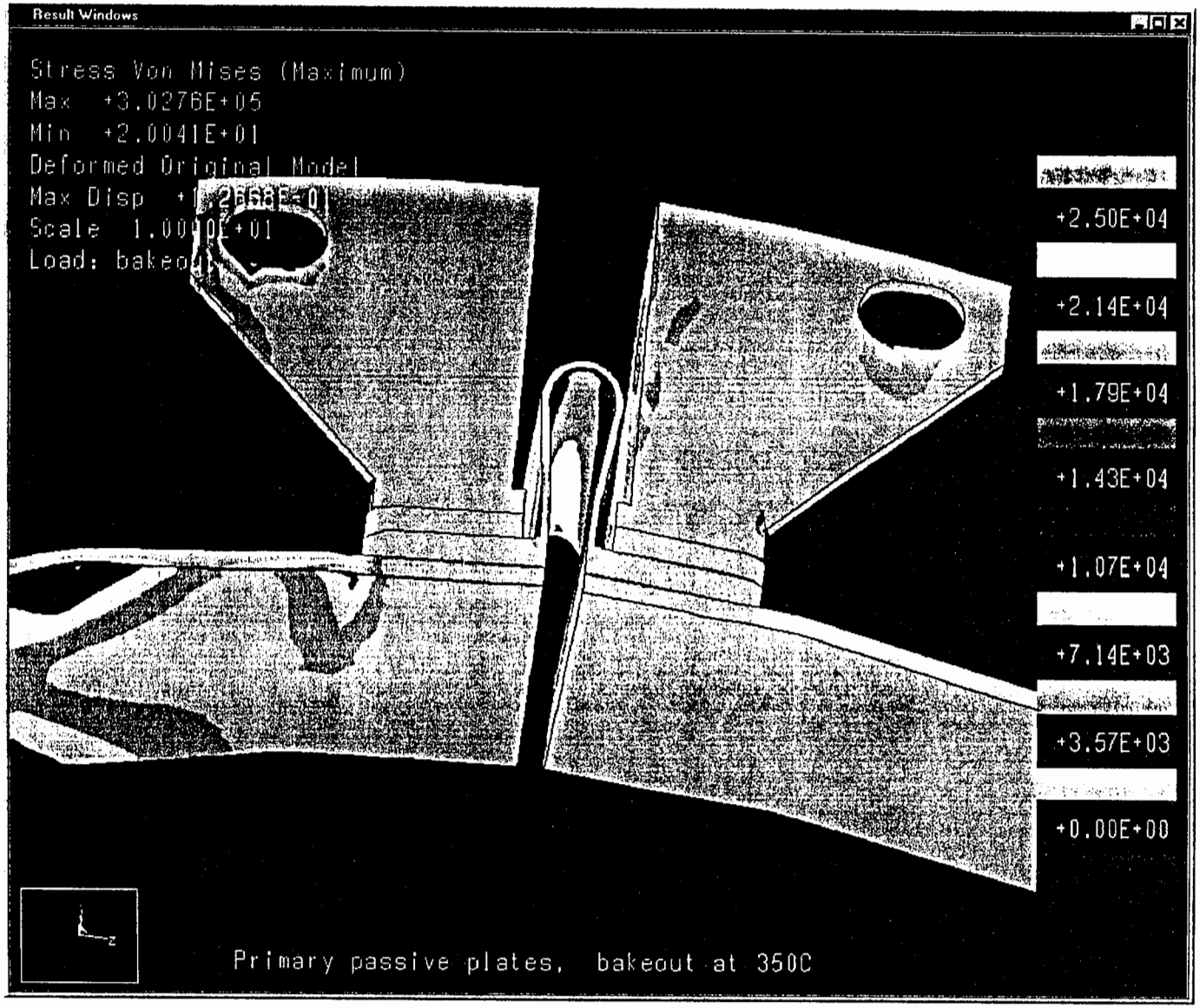
Result Windows
Stress Von Mises (Maximum)
Max +3.0276E+05
Min +2.0041E+01
Deformed Original Model
Max Disp
Scale 1.00
Load: bakeo
+2.50E+04
+2.14E+04
+1.79E+04
+1.43E+04
+1.07E+04
+7.14E+03
+3.57E+03
+0.00E+00
Primary passive plates, bakeout at 350C

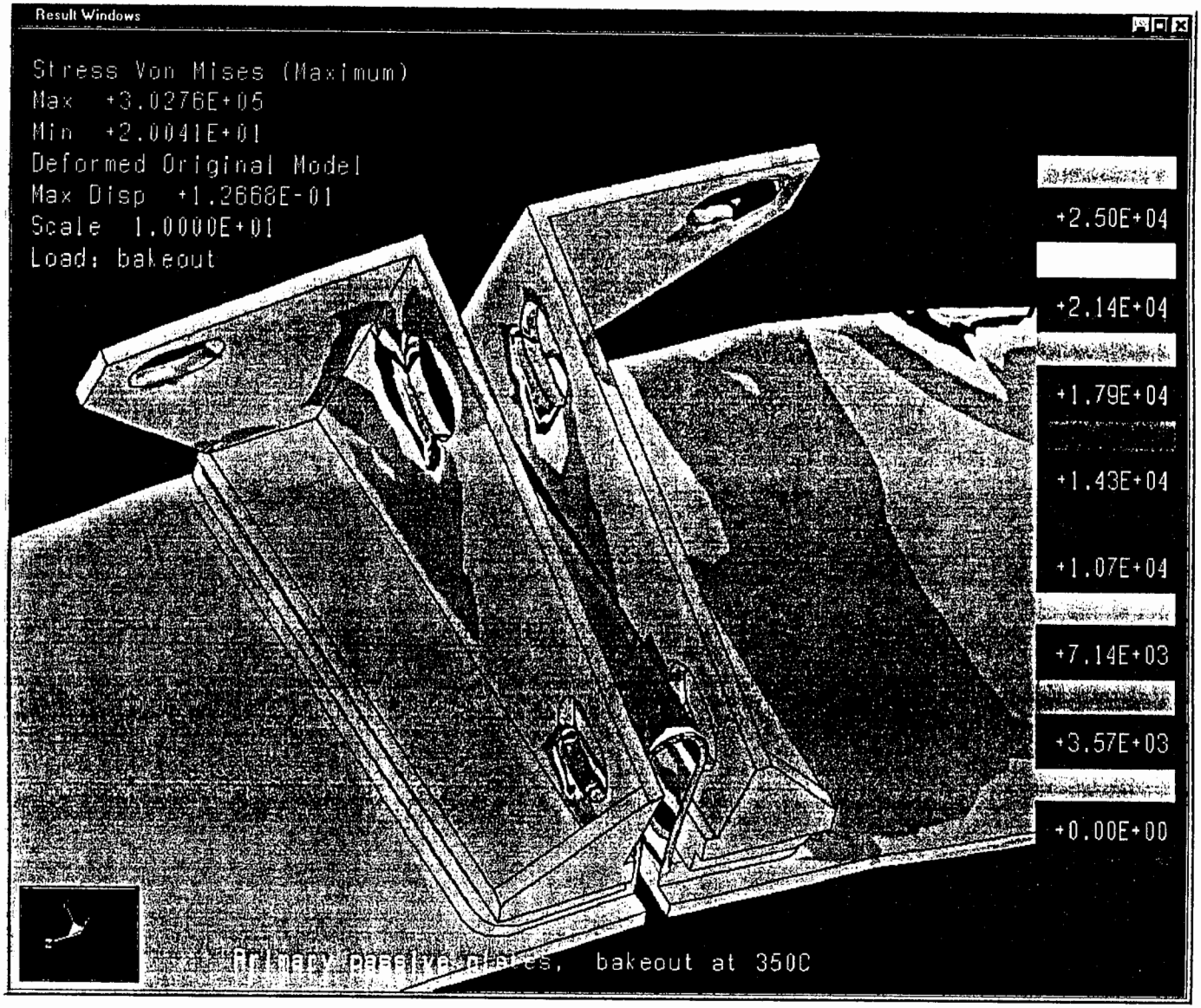
Result Windows
Stress Von Mises (Maximum)
Max +3.0276E+05
Min +2.0041E+01
Deformed Original Model
Max Disp +1.2668E-01
Scale 1.0000E+01
Load: bakeout
+2.50E+04
+2.14E+04
+1.79E+04
+1.43E+04
+1.07E+04
+7.14E+03
+3.57E+03
+0.00E+00
bakeout at 350C

Section S, Secondary Passive Plate stress results

S1 - Disruption loading
S2 - Halo loading
S3 - Bakeout loading

Secondary passive plates, disruption loads

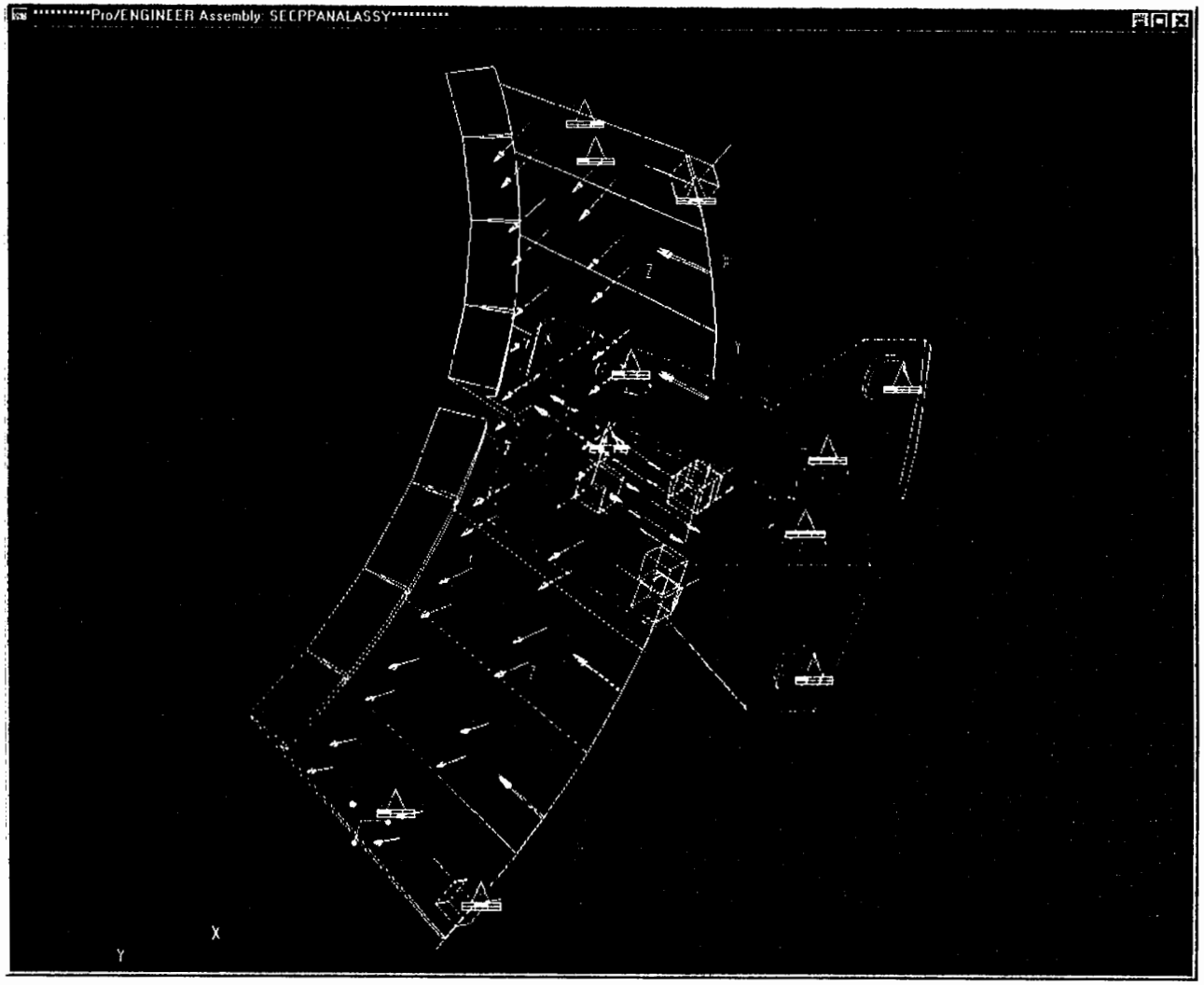

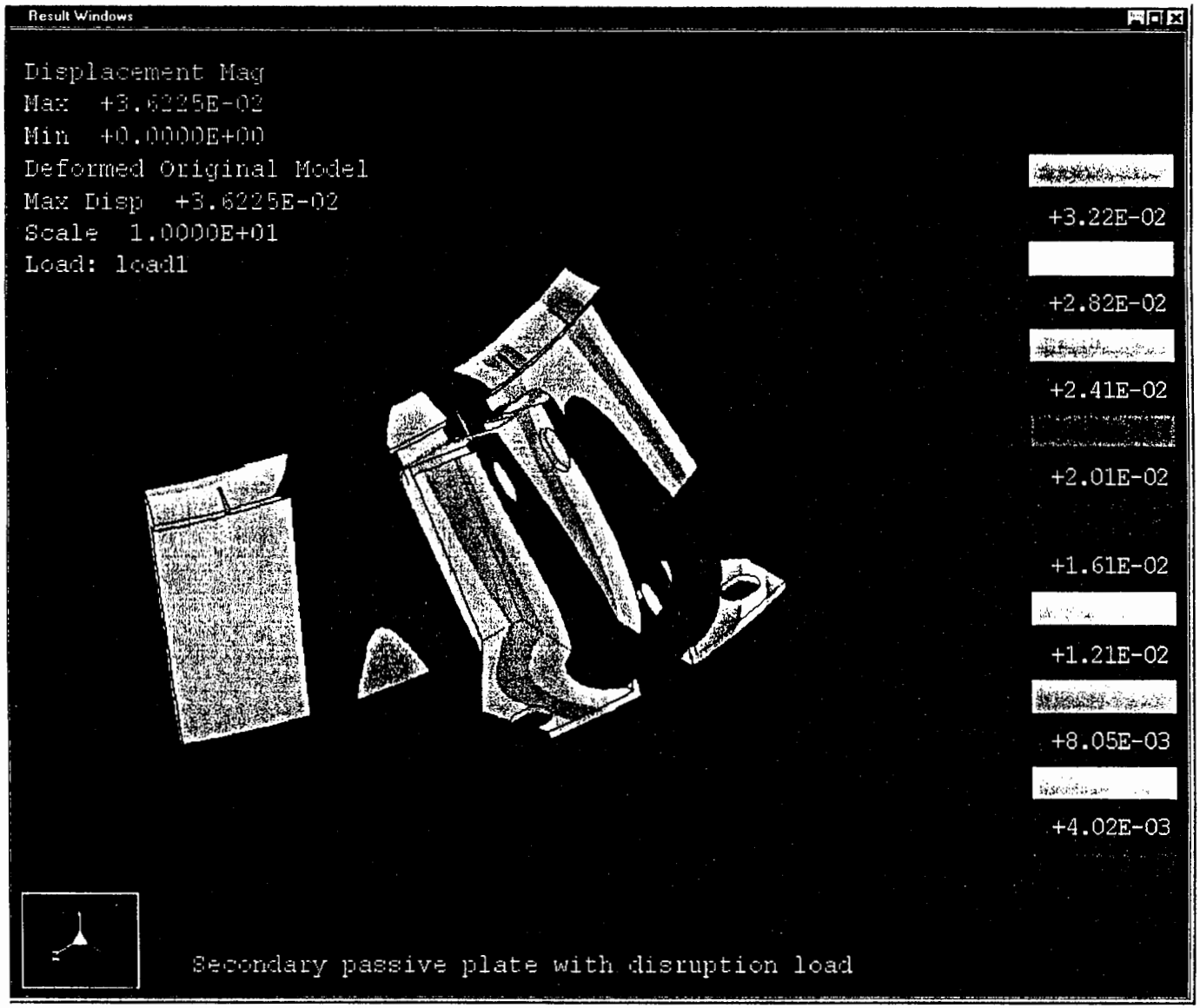
Result Windows
Displacement Mag
Max +3.6225E-02
Min +0.0000E+00
Deformed Original Model
Max Disp +3.6225E-02
Scale 1.0000E+01
Load: load1
+3.22E-02
+2.82E-02
+2.41E-02
+2.01E-02
+1.61E-02
+1.21E-02
+8.05E-03
+4.02E-03
Secondary passive plate with disruption load

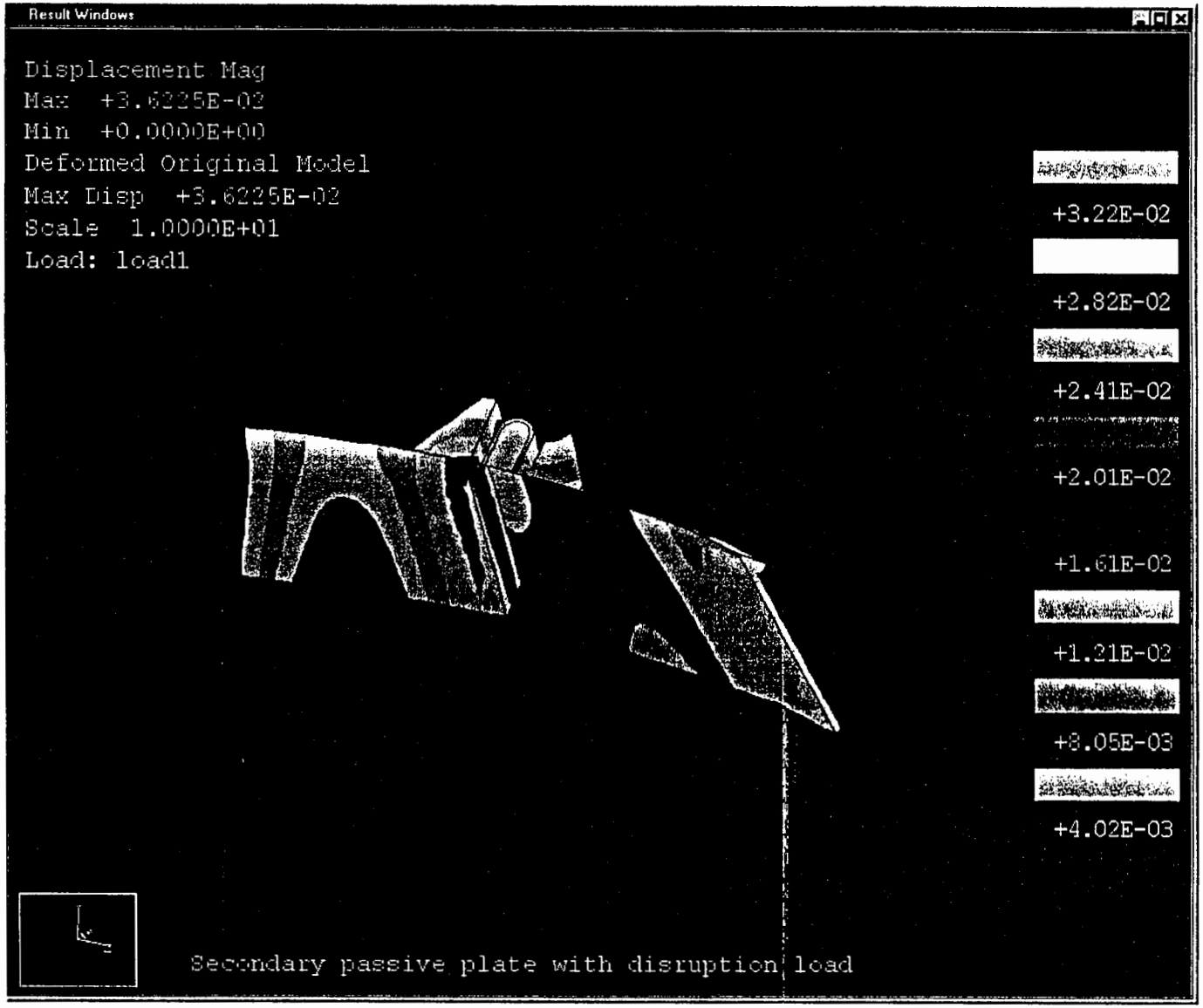
Result Windows
Displacement Mag
Max +3.6225E-02
Min +0.0000E+00
Deformed Original Model
Max Disp +3.6225E-02
Scale 1.0000E+01
Load: load1
+3.22E-02
+2.82E-02
+2.41E-02
+2.01E-02
+1.61E-02
+1.21E-02
+8.05E-03
+4.02E-03
Secondary passive plate with disruption load

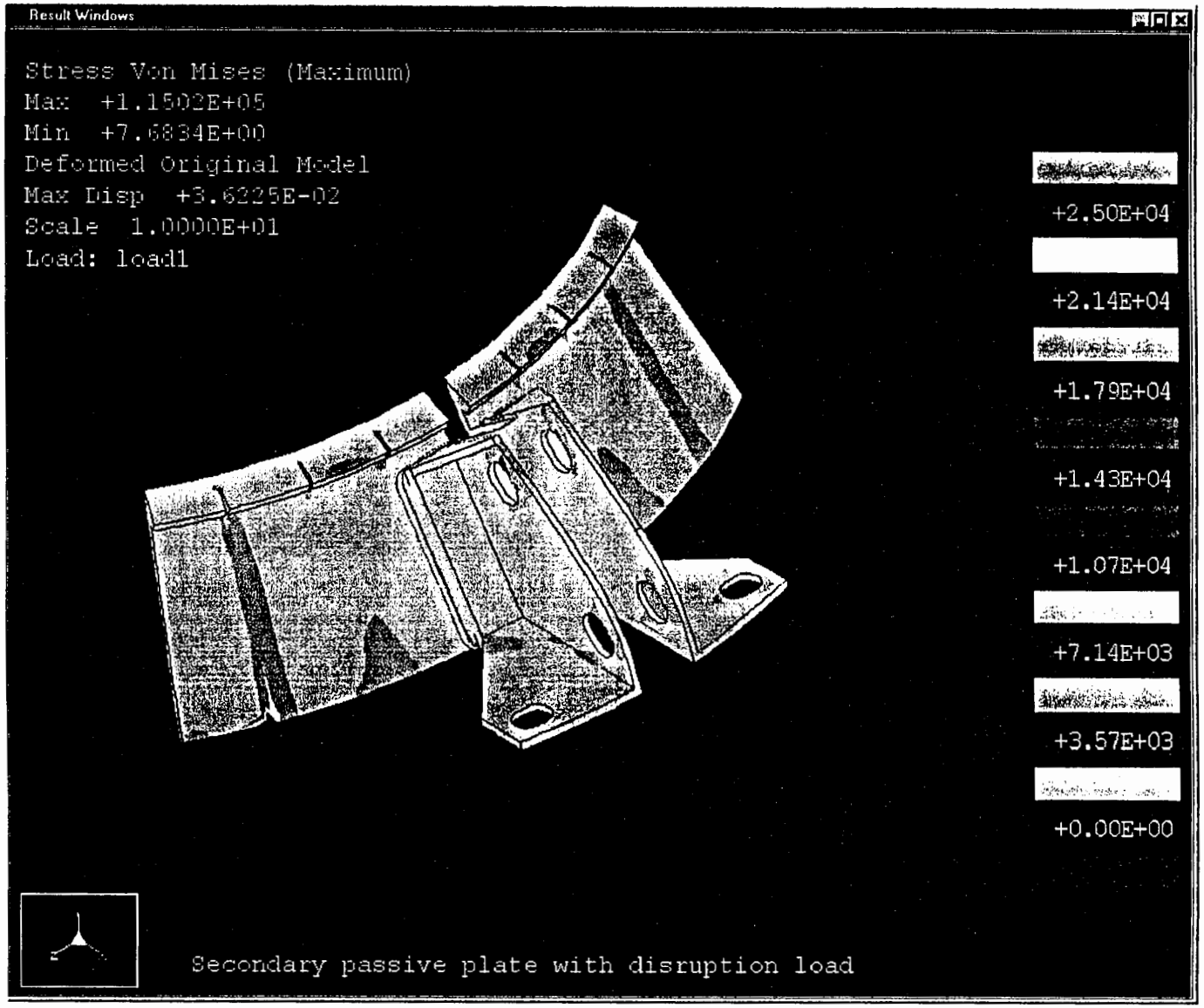
Result Windows
Stress Von Mises (Maximum)
Max +1.1502E+05
Min +7.6834E+00
Deformed Original Model
Max Disp +3.6225E-02
Scale 1.0000E+01
Load: load1
+2.50E+04
+2.14E+04
+1.79E+04
+1.43E+04
+1.07E+04
+7.14E+03
+3.57E+03
+0.00E+00
Secondary passive plate with disruption load

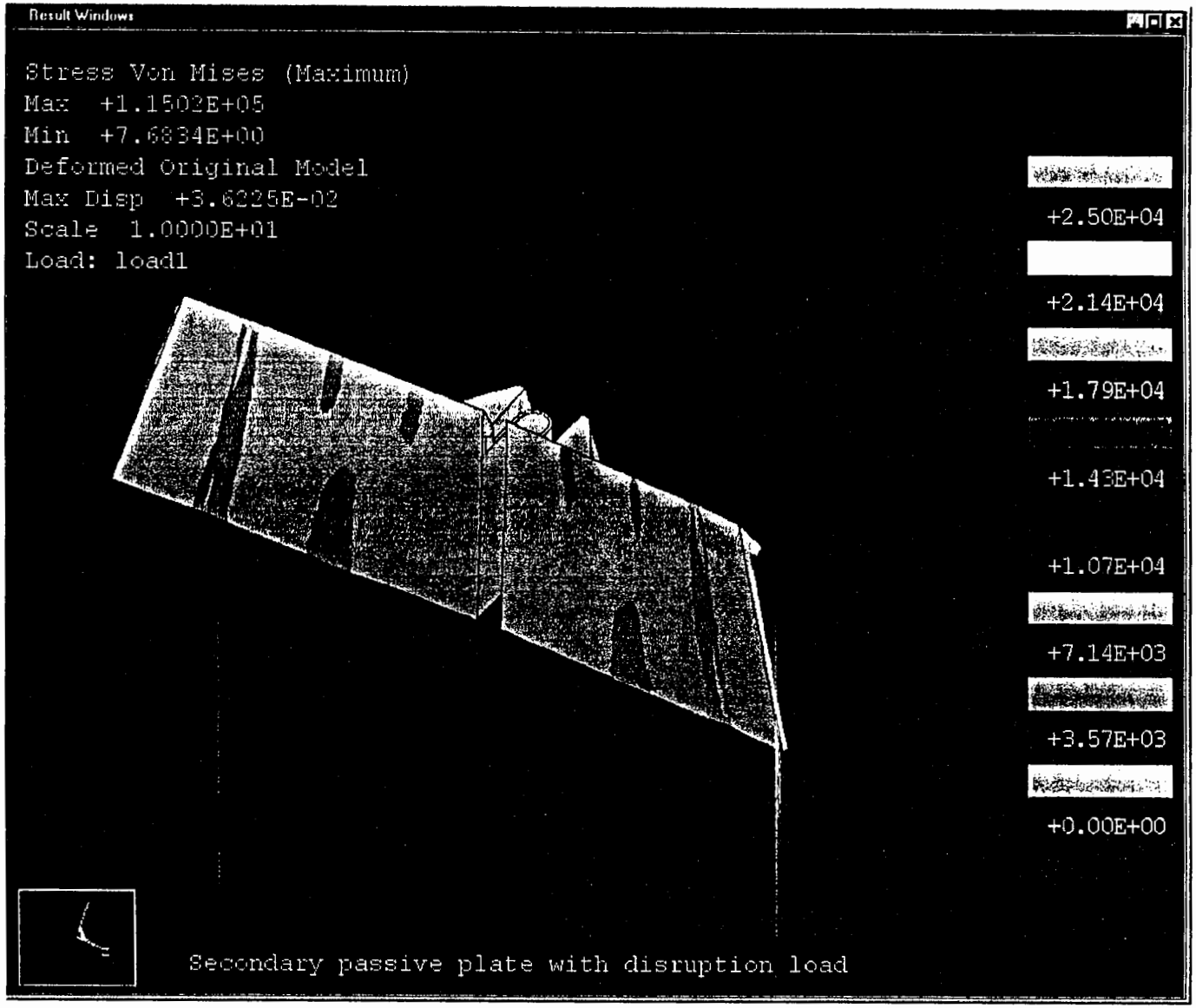
Result Windows
Stress Von Mises (Maximum)
Max +1.1502E+05
Min +7.6834E+00
Deformed Original Model
Max Disp +3.6225E-02
Scale 1.0000E+01
Load: load1
+2.50E+04
+2.14E+04
+1.79E+04
+1.43E+04
+1.07E+04
+7.14E+03
+3.57E+03
+0.00E+00
Secondary passive plate with disruption load


Result Windows
Stress Max Prin (Maximum)
Max +1.3123E+05
Min -4.4324E+04
Deformed Original Model
Max Disp +3.6225E-02
Scale 1.0000E+01
Load: load1
+2.50E+04
+2.14E+04
+1.79E+04
+1.43E+04
+1.07E+04
+7.14E+03
+3.57E+03
+0.00E+00
Secondary passive plate with disruption load

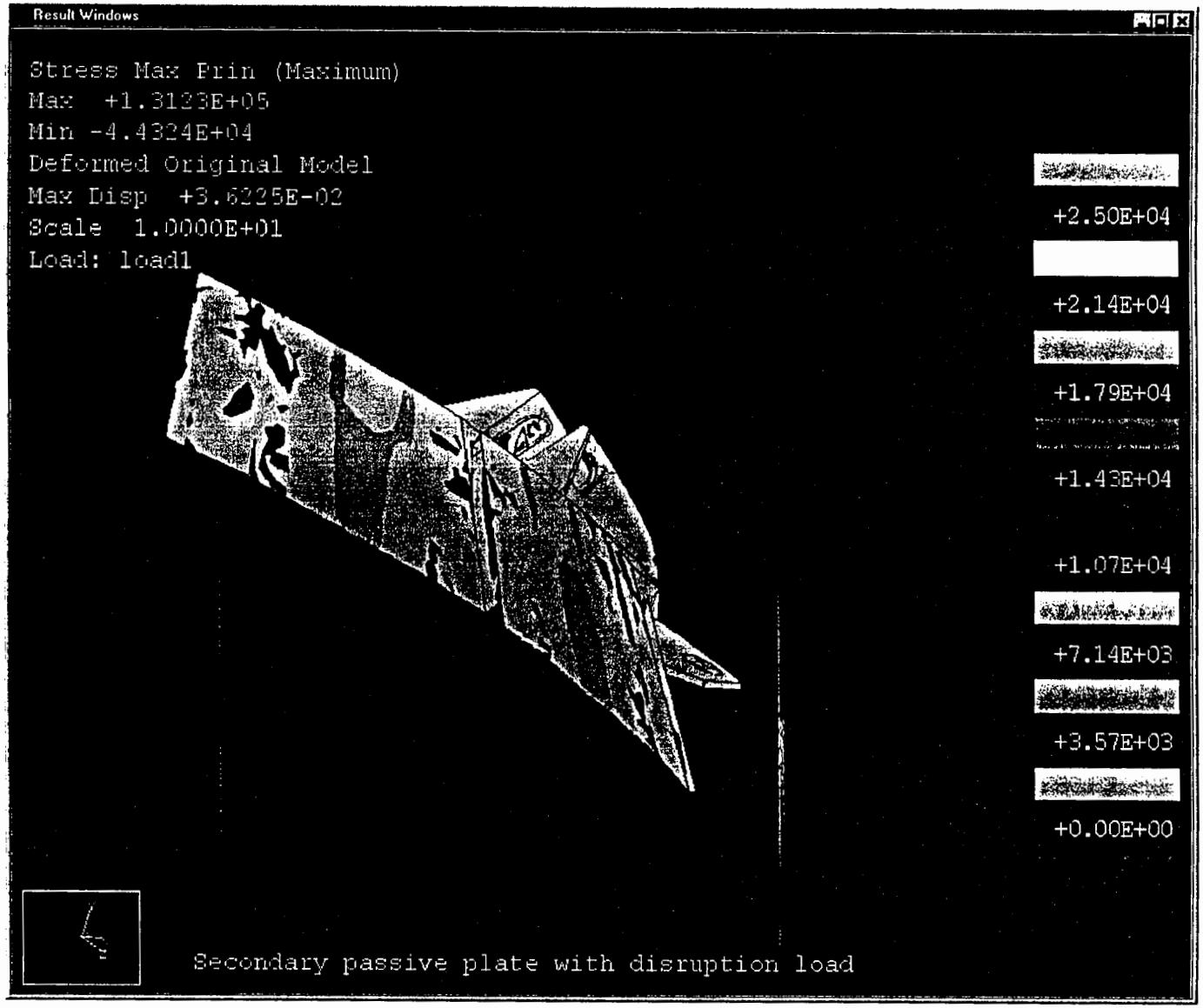
Result Windows
Stress Max Prin (Maximum)
Max +1.3123E+05
Min -4.4324E+04
Deformed Original Model
Max Disp +3.6225E-02
Scale 1.0000E+01
Load: load1
+2.50E+04
+2.14E+04
+1.79E+04
+1.43E+04
+1.07E+04
+7.14E+03
+3.57E+03
+0.00E+00
Secondary passive plate with disruption load

Secondary passive plates, halo loads

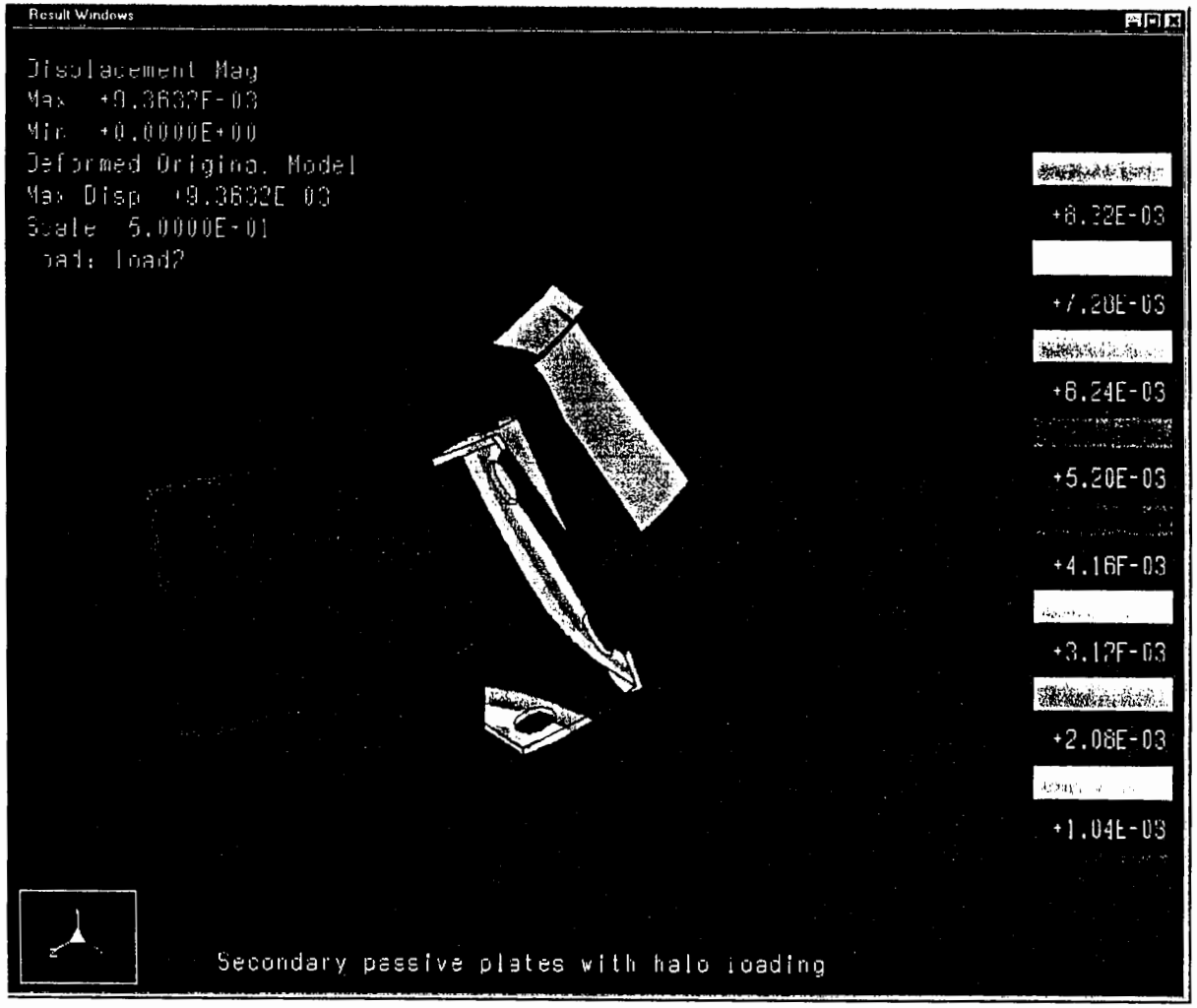

Secondary passive plates, halo loads

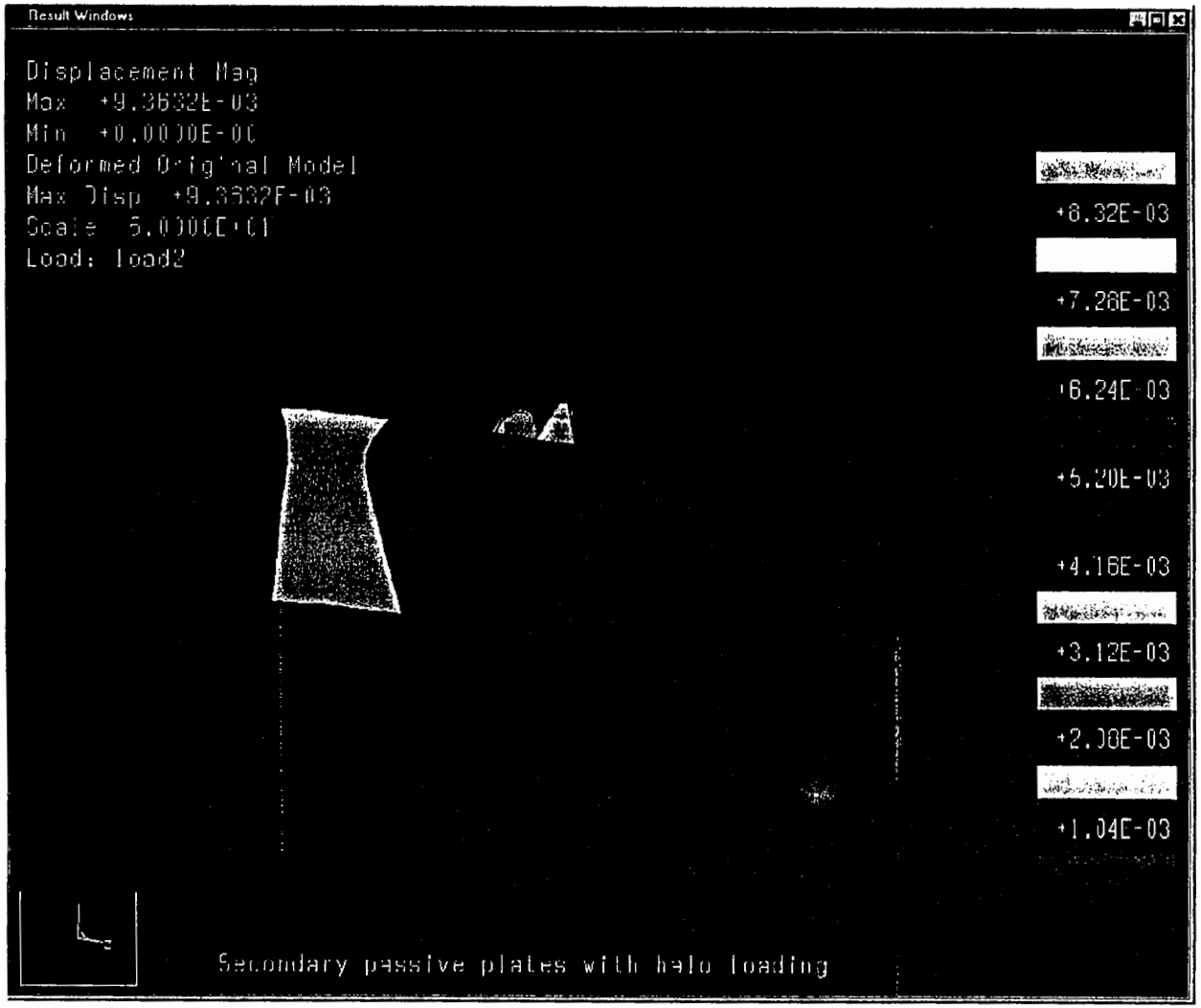

Secondary passive plates, halo loads

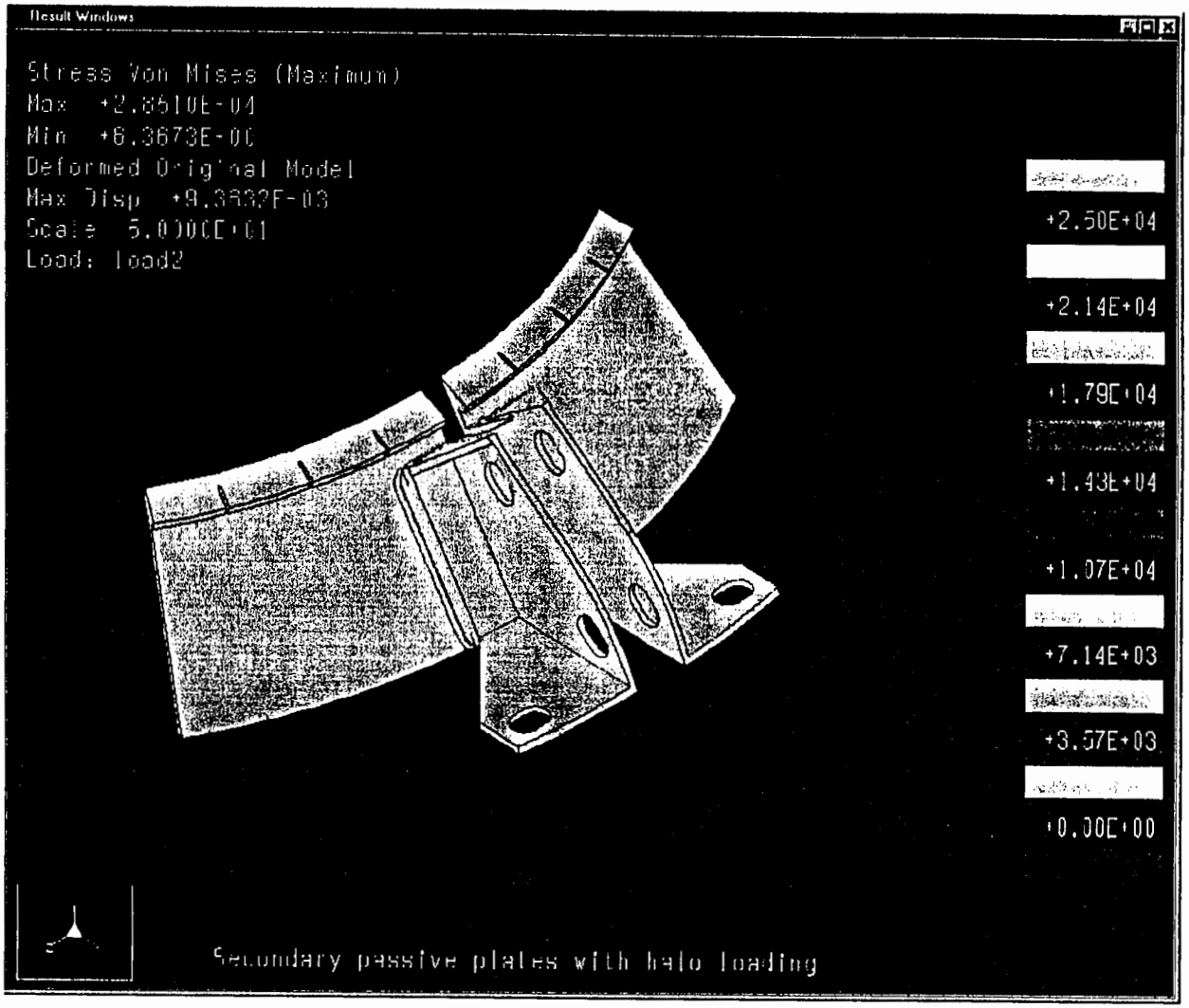

Secondary passive plates, halo loads

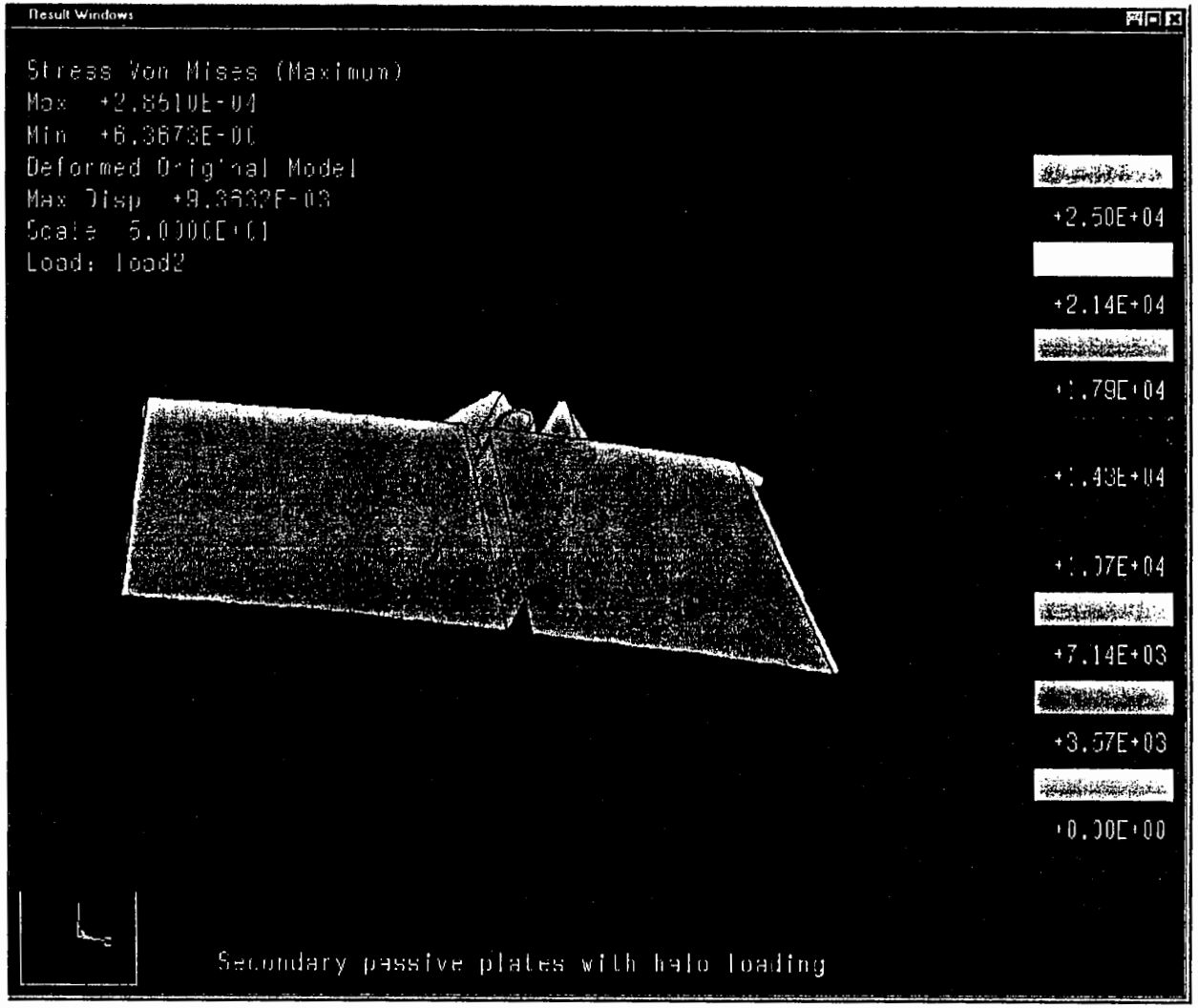

Secondary Passive plates during bakeout at 350C

Secondary Passive plates during bakeout at 350C

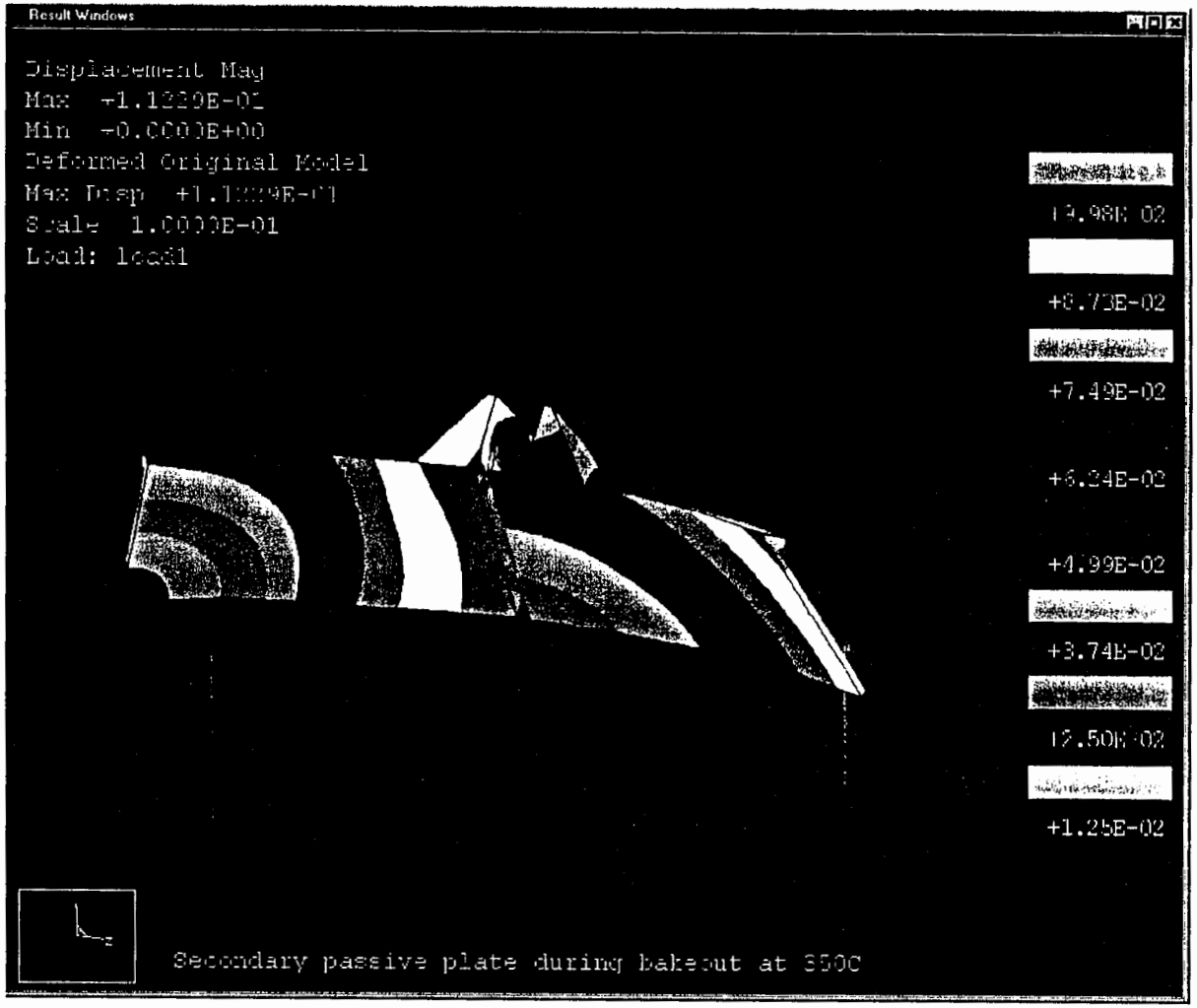

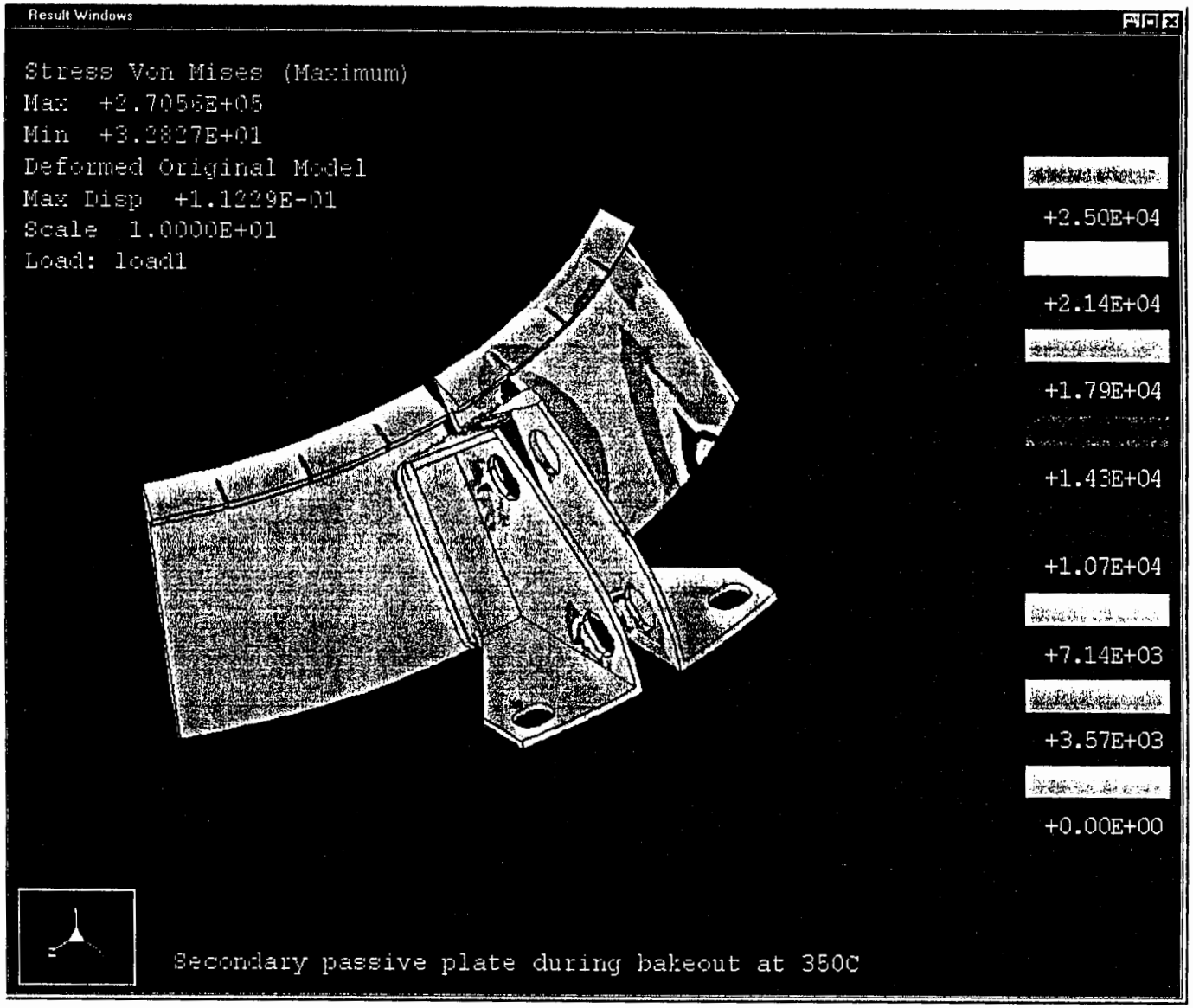
Result Windows
Stress Von Mises (Maximum)
Max +2.7056E+05
Min +3.2827E+01
Deformed Original Model
Max Disp +1.1229E-01
Scale 1.0000E+01
Load: load1
+2.50E+04
+2.14E+04
+1.79E+04
+1.43E+04
+1.07E+04
+7.14E+03
+3.57E+03
+0.00E+00
Secondary passive plate during bakeout at 350C

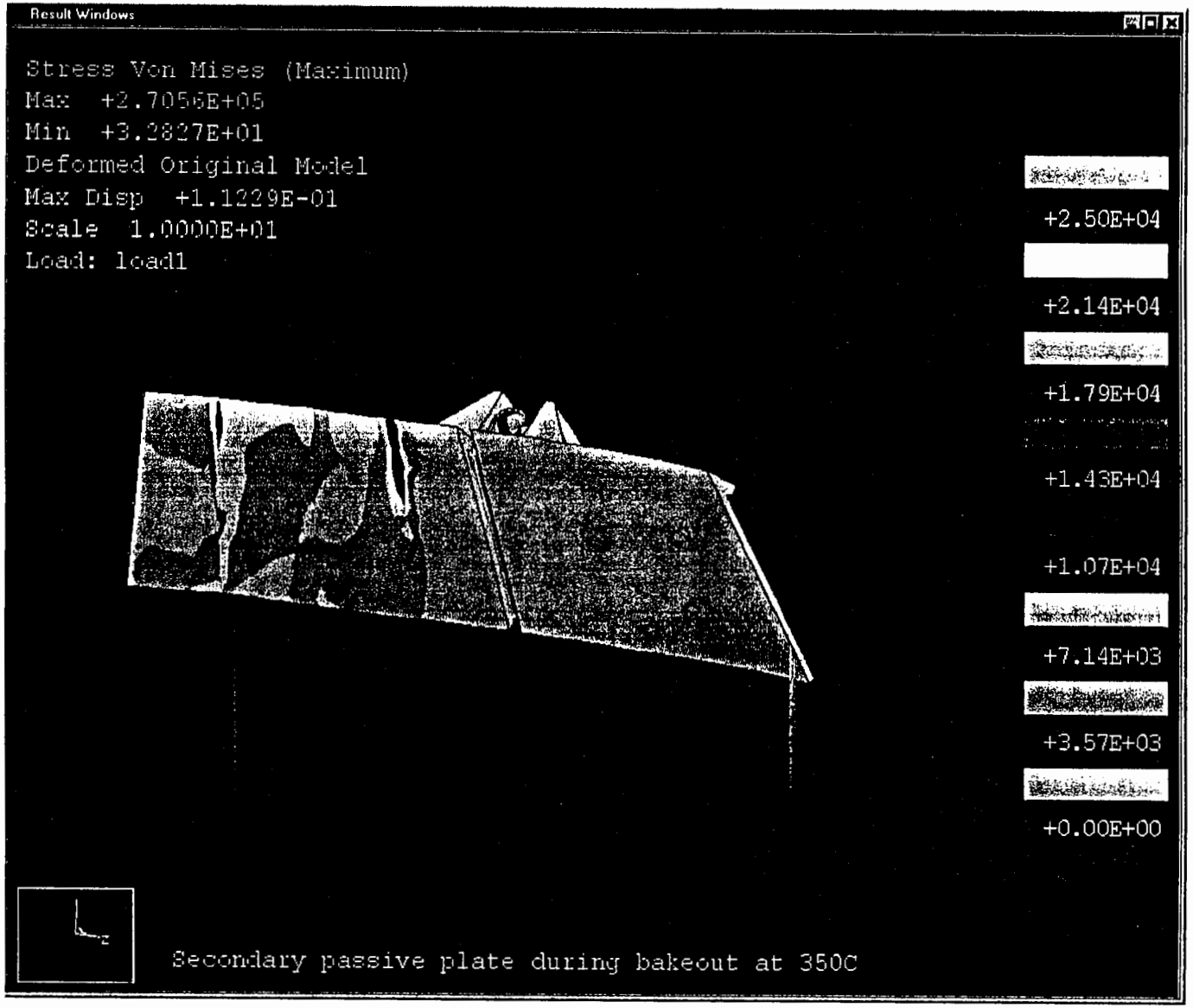
Result Windows
Stress Von Mises (Maximum)
Max +2.7056E+05
Min +3.2827E+01
Deformed Original Model
Max Disp +1.1229E-01
Scale 1.0000E+01
Load: load1
+2.50E+04
+2.14E+04
+1.79E+04
+1.43E+04
+1.07E+04
+7.14E+03
+3.57E+03
+0.00E+00
Secondary passive plate during bakeout at 350C

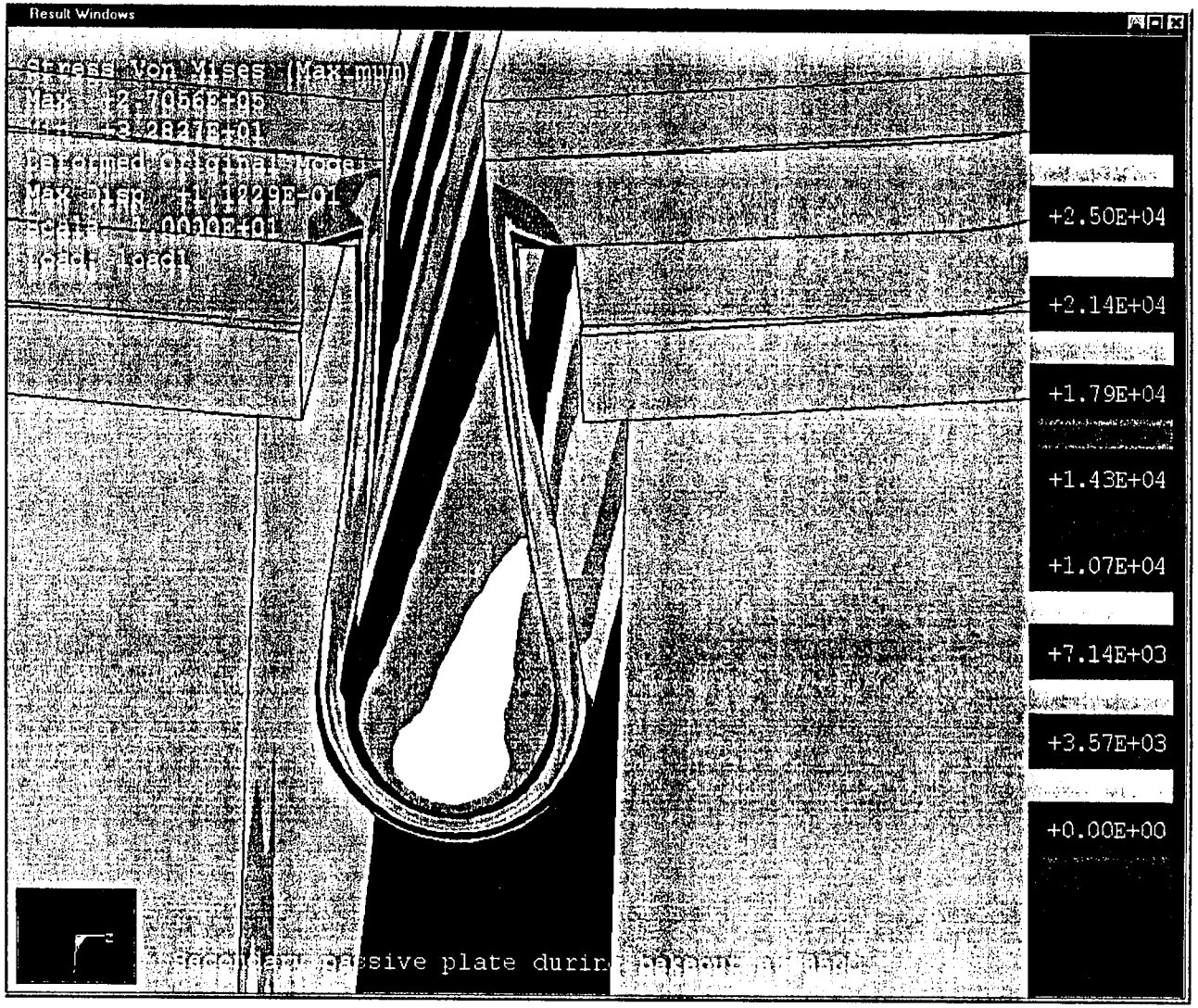
Result Windows
+2.50E+04
+2.14E+04
+1.79E+04
+1.43E+04
+1.07E+04
+7.14E+03
+3.57E+03
+0.00E+00

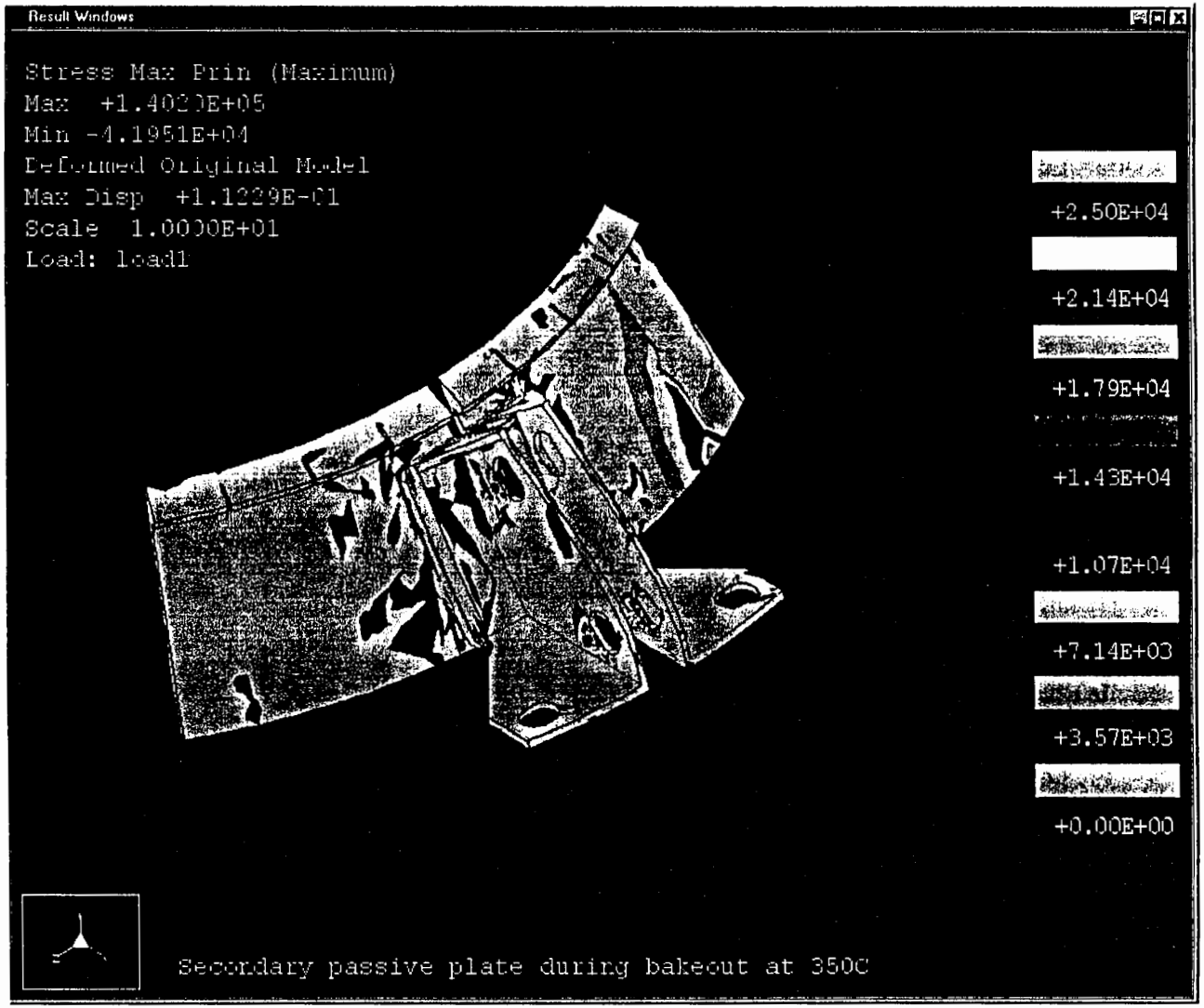
Result Windows
Stress Max Prin (Maximum)
Max +1.4020E+05
Min -4.1951E+04
Deformed Original Model
Max Disp +1.1229E-01
Scale 1.0000E+01
Load: load1
+2.50E+04
+2.14E+04
+1.79E+04
+1.43E+04
+1.07E+04
+7.14E+03
+3.57E+03
+0.00E+00
Secondary passive plate during bakeout at 350C

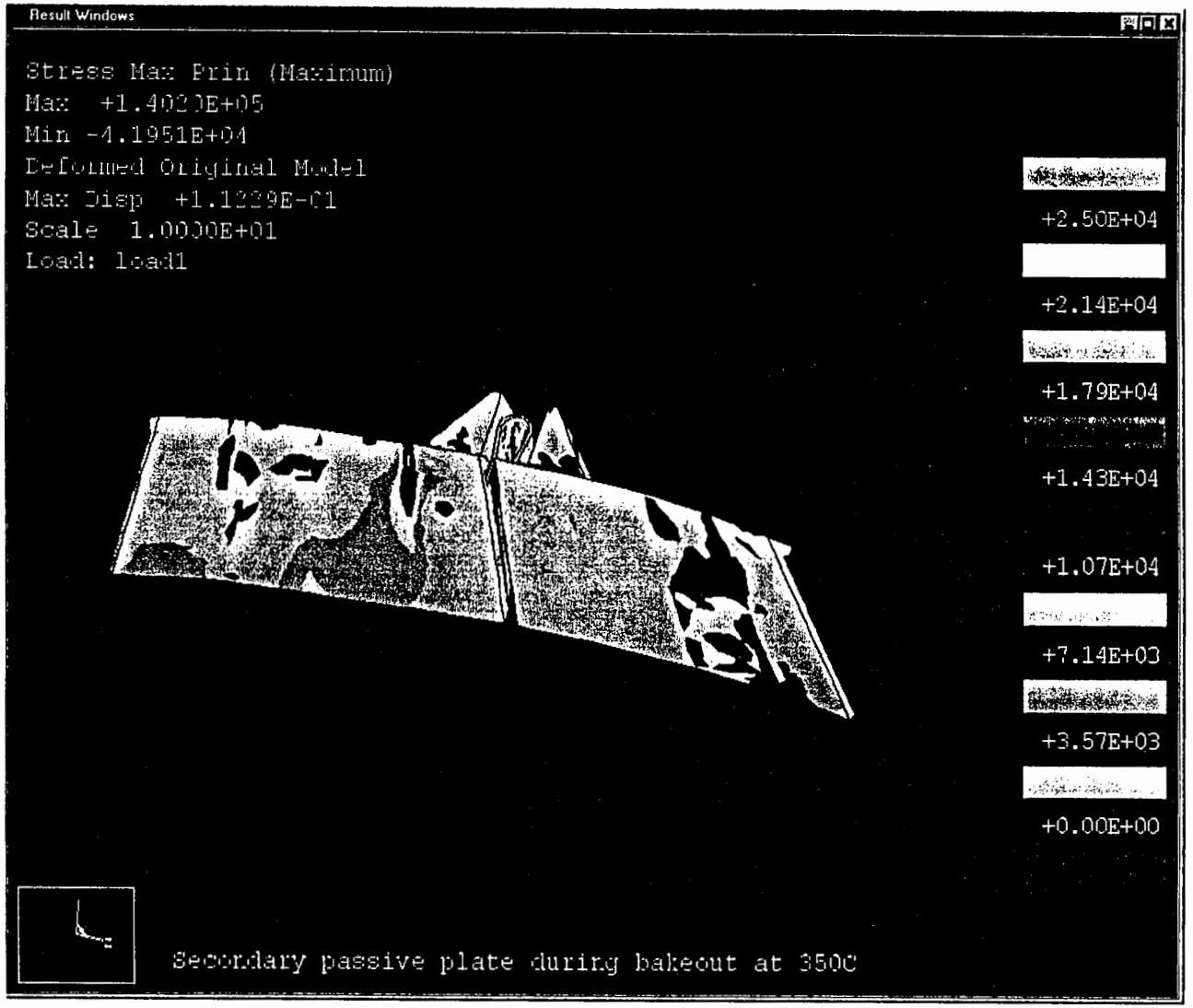
Result Windows
Stress Max Prin (Maximum)
Max +1.4020E+05
Min -4.1951E+04
Deformed Original Model
Max Disp +1.1229E-01
Scale 1.0000E+01
Load: load1
+2.50E+04
+2.14E+04
+1.79E+04
+1.43E+04
+1.07E+04
+7.14E+03
+3.57E+03
+0.00E+00
Secondary passive plate during bakeout at 350C

NSTX CALCULATION

TITLE OH Coil Thermal Behavior

CALC. NO. 13-3 DATE 3/31/00

ORIGINATOR C Neumeyer CHECKER Rev. 0

PURPOSE:

This calculation describes a simulation of the OH coil heating and cooling for three different repetition periods, 300, 450, and 600 seconds.

REFERENCES:

NSTX-CALC-13-1 gives the OH coil parameters and the derivation of the G function.

ASSUMPTIONS:

CALCULATION:

See attached FORTRAN code "cool.f", and i/o files for the 3 cases.

Note: all digital documents stored in NSTX File Share, Engineering Folder, Engineering Calculations Folder. Hard copies of all documents stored in NSTX project file.

CONCLUSION:

See memo 71_00302_CLN_01.doc

71-000302-CLN-01

TO: DISTRIBUTION
FROM: C NEUMEYER
SUBJECT: STUDY OF OH COIL COOLING vs. REP RATE

References:

[1] 71-000222-CLN-01, "OH Rep Rate Minimization, Minutes Of Meeting"
[2] NSTX-CALC-13-3, "OH Thermal Simulation"

A study has been performed [2] to determine the OH $\int i^2(t)dt$ allowables at repetition periods of 300, 450, and 600 seconds.

A FORTRAN program was used to simulate the heating and cooling of the OH coil during a sequence of pulses. This program divides the coil conductor length into small sections from which heat is transferred into slugs of water which move from section to section as time progresses.

Parameters were set to those corresponding to one of the two-in-hand conductors in the outermost layer of the coil, which amongst the 8 cooling paths has the longest length. The water flow was set equal to the trip setting of the water flow switch. Simulation parameters are summarized in Table 1.

Table 1 – Simulation Parameters

Parameter	Value	Units
Path length	362.2	feet
Conductor cross sectional area	0.2192	in^2
Cooling hole diameter	0.1880	in
Water inlet temperature	10	°C
Water flow rate	0.65	GPM

The temperature vs. time simulation at the end of the conductor (where the water exits the coil copper) was compared against an actual OH coil outlet water temperature strip chart recording taken during ISTP-001, and reasonably good agreement was obtained (Figure 1). It is noted that the temperature measurement was made using a thermocouple taped over a metal section of

pipe which is in the water stream after a section of plastic hose approximately 30 feet downstream of the actual outlet from the coil copper.

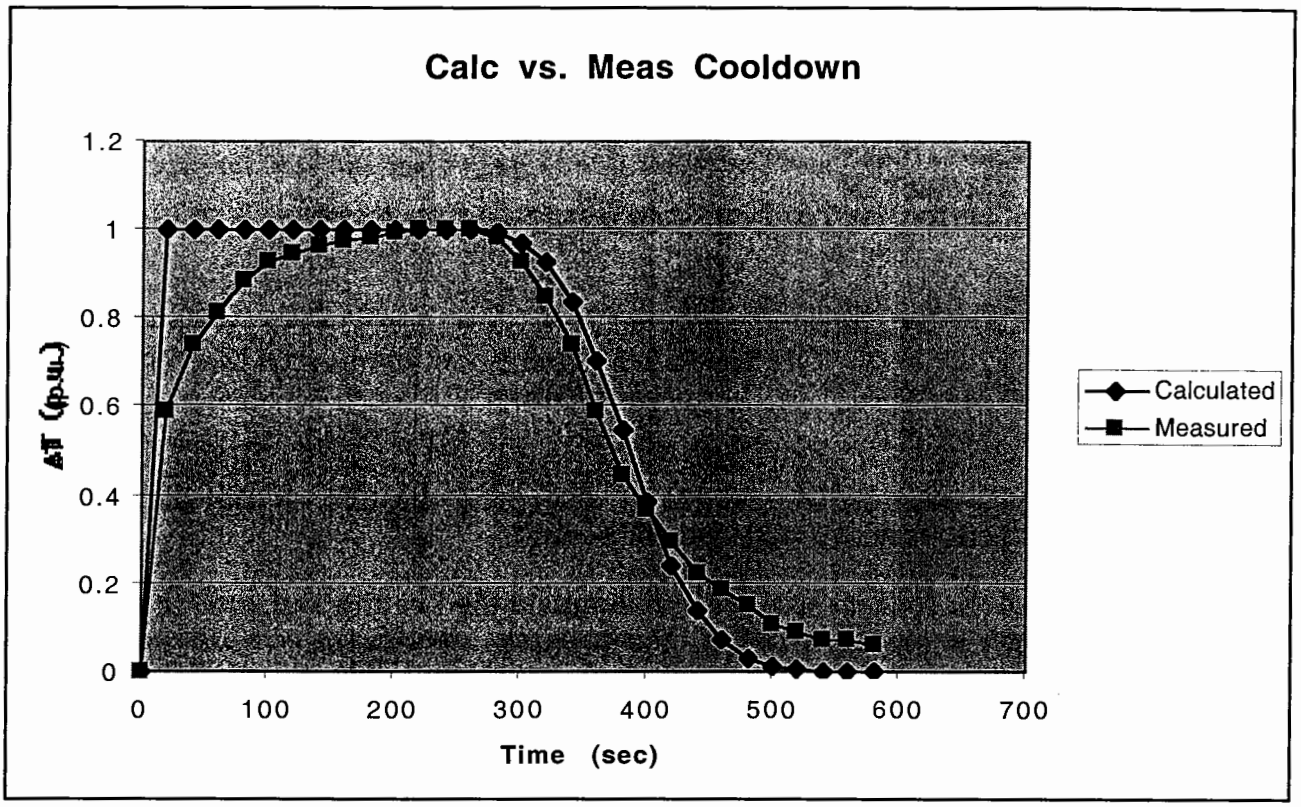

Figure 1: Calculated vs. Measured Cool Down

Simulation runs were made to determine the $\int i^2(t)dt$ allowables and ratched start of pulse (SOP) inlet water temperature at the three repetition periods with the constraint imposed that the maximum copper temperature at any time should not exceed 90 °C. This allows for the fact that, should a fault occur at I_{oh}=24kA and T_{oh} = 90 °C, the final temperature will not exceed 100 °C following an L/R decay of the current.

Table 2 summarizes the results obtained.

Table 2 – Simulation Results

Repetition Period	300 sec	450 sec	600 sec
Allowable $\int i^2(t)dt$	155.5 kA^2-sec	262.1 kA^2-sec	288.0 kA^2-sec
Allowable $\int i^2(t)dt$	54%	91%	100%
T_{sop}	43.4 °C	15.3 °C	10.0 °C

Figures 2 through 7 depict the copper temperature vs. time at the end (water outlet) of the winding for a series of 5 pulses, and the copper temperature vs.

time at the start (water inlet), middle, and end (water outlet) of the winding for the last of a series of 5 pulses (i.e. after ratcheting has taken place).

Note that, after the ratcheting stabilizes, the peak temperature at end of pulse is ≈ 90 °C, although this is not immediately evident on the curves (figures 2, 4, and 6) which depict the temperature evolution during the sequence of pulses because it occurs for a brief period only (until the entrained water and copper equilibrate a few seconds following the pulse) which is within the sampling interval of the graphics. Decay from the peak is visible, however, on figures 3, 5, and 7 which show the cooldown following the last pulse in the sequence, with 5 x smaller interval between plotted points.

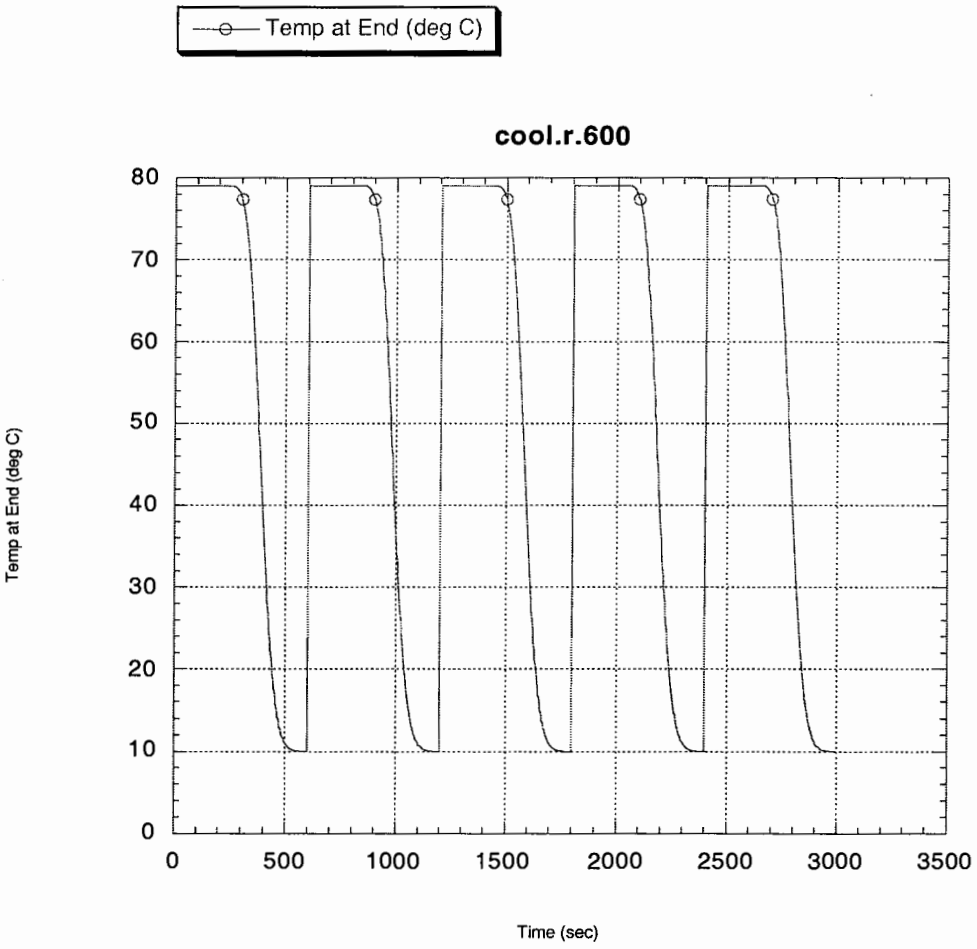

Figure 2: Temperature at End of Winding Due to Five Pulses in Sequence, 600 Second Repetition Period

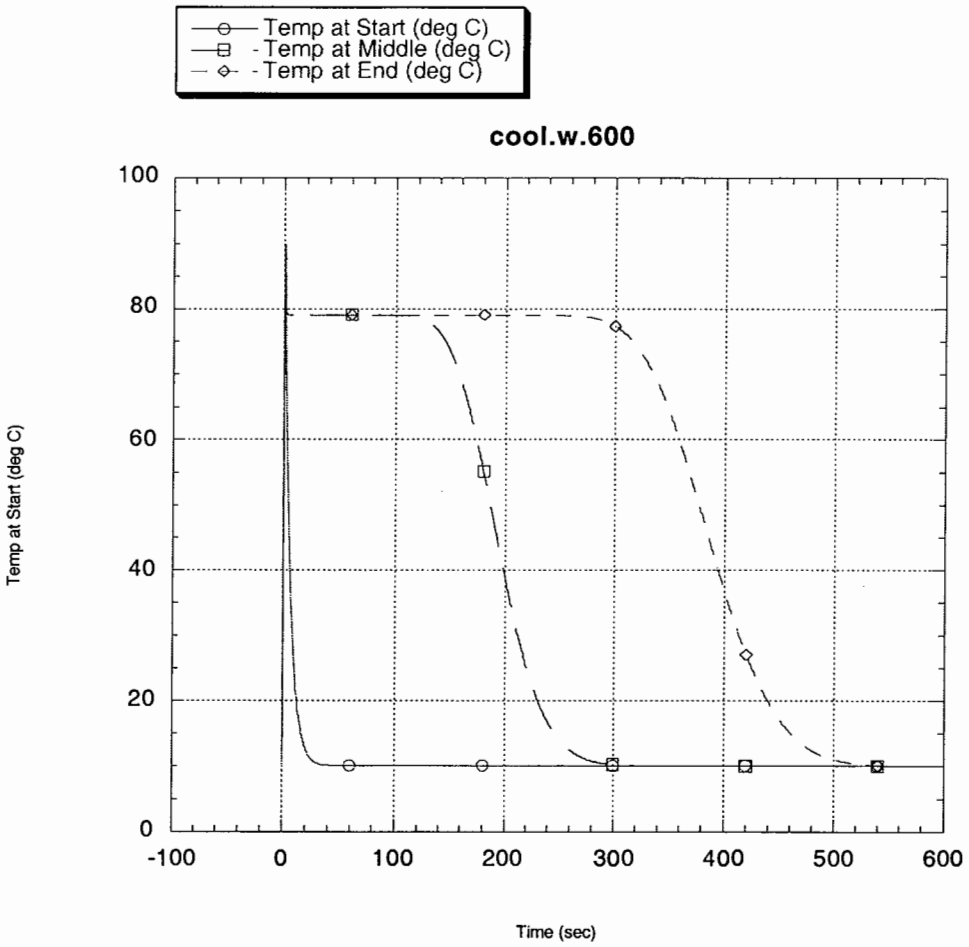

Figure 3: Temperature at Start, Middle, and End of Winding During and After Fifth Pulse, 600 Second Repetition Period

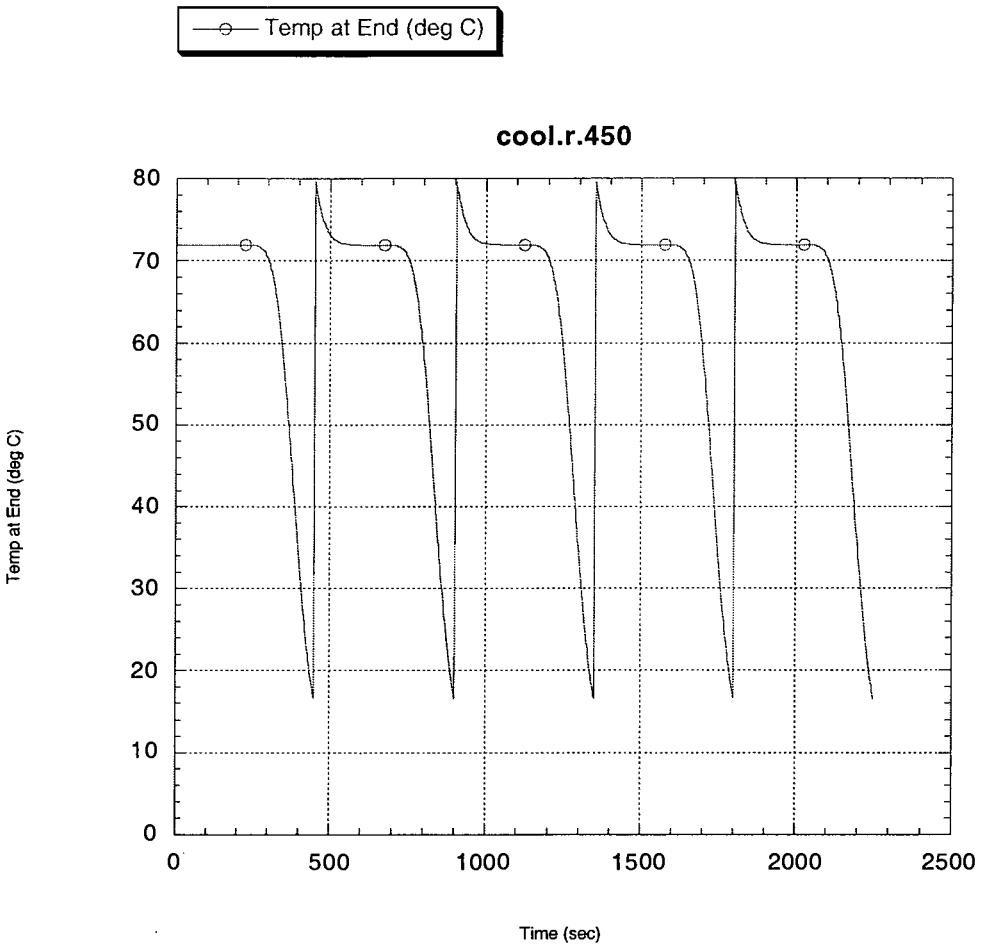

Figure 4: Temperature at End of Winding Due to Five Pulses in Sequence, 450 Second Repetition Period

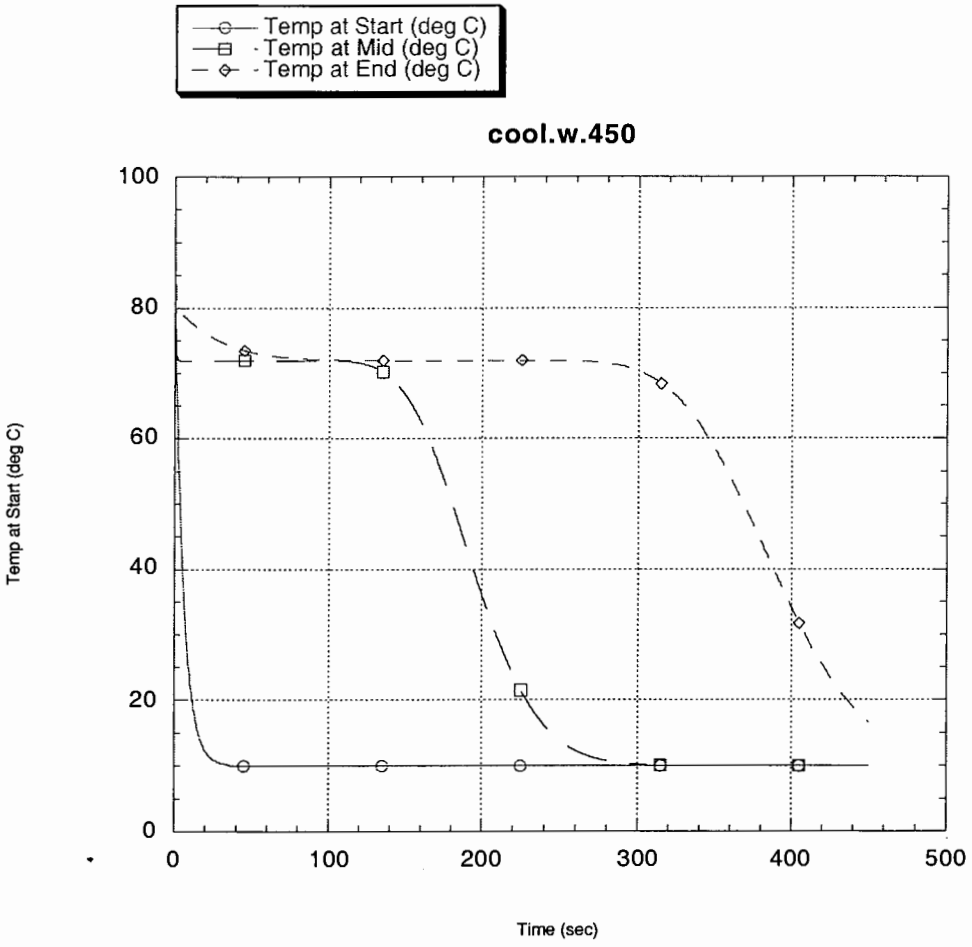

Figure 5: Temperature at Start, Middle, and End of Winding During and After Fifth Pulse, 450 Second Repetition Period

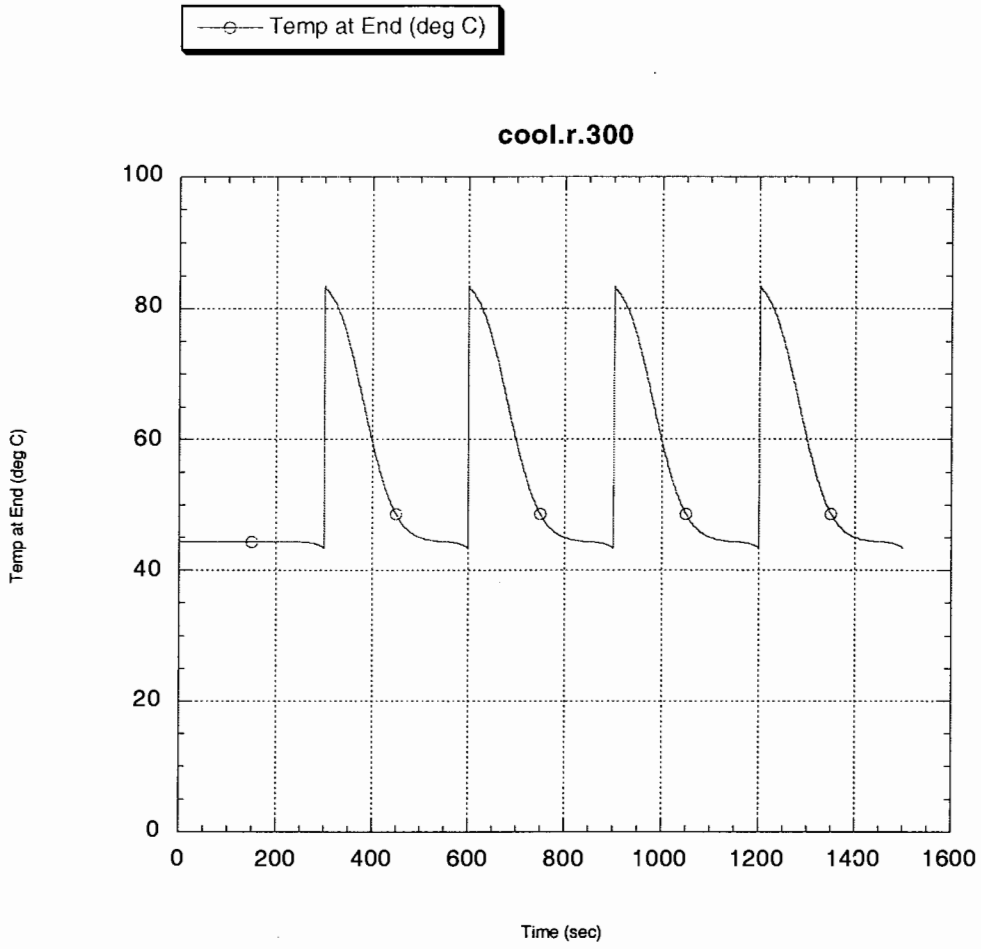

Figure 6: Temperature at End of Winding Due to Five Pulses in Sequence, 300 Second Repetition Period

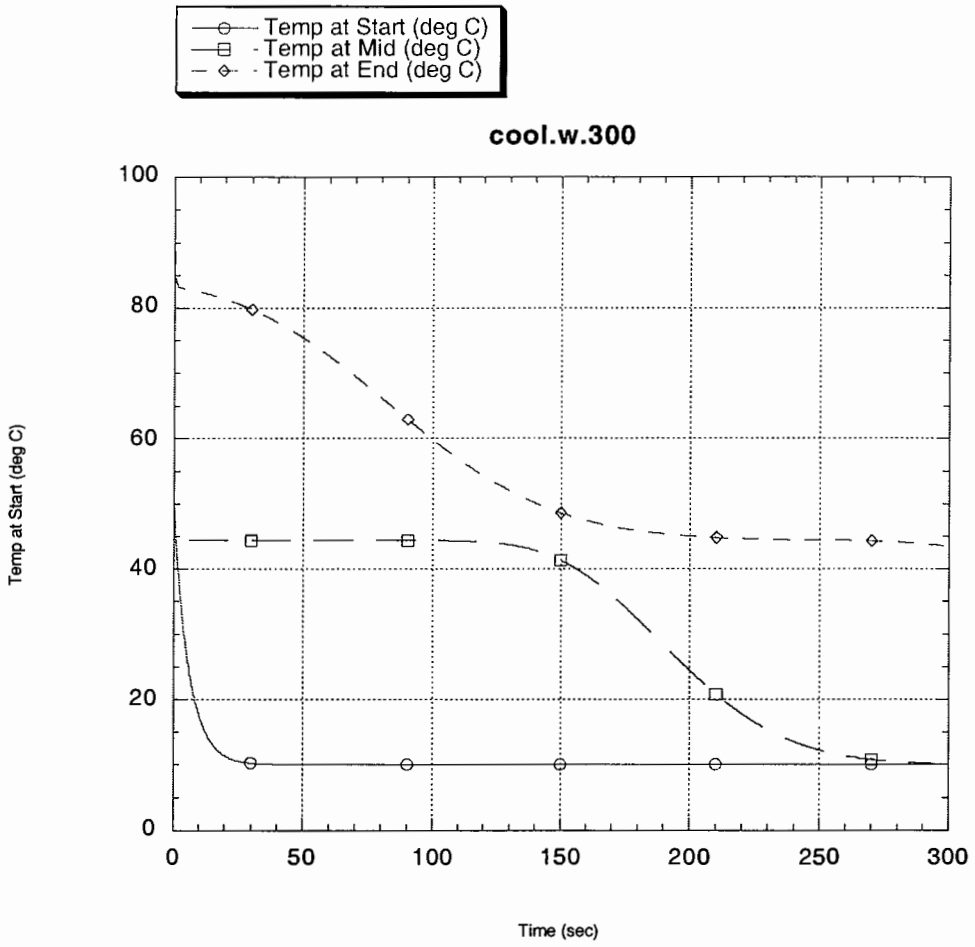

Figure 7: Temperature at Start, Middle, and End of Winding During and After Fifth Pulse, 300 Second Repetition Period

The Rochester Instrument Systems (RIS) protective device provides an $\int i^2(t)dt$ function along with a single time constant exponential decay. This simple model cannot effectively simulate the OH coil temperature vs. time because of the more complex behavior of the OH coil with its very long cooling paths and the attendant "cooling wave" effect. However, the RIS can still be used, in combination with the outlet water temperature interlock, to protect the coil. In this case the role of the RIS is to ensure that the $\int i^2(t)dt$ during a pulse is within the allowable, while the role of the water interlock is to ensure that sufficient

15. Appendix 3
Venturi Measurements and Calibration

P_{HP} = 480 PSI
P_{HPRTN} = 70 PSI
P_{RTN} = 15PSI

$P_{RF/TF}$ = 115 PSI
P_{RTN} = 15PSI

COIL	Venturi DP(" H2O)	Flow (GPM) ACTUAL / S.P.	Flow Sw. Setting (" H2O / GPM)	PLC Input
OH1X	~~135~~	.68 / .56	69/.51 95	10001
OH1Y	166	.75 / .72	69/.51 146	10005
OH2X	~~138~~	.69 / .64	84/.56 ~~120~~	10002
OH2Y	132	.68 / .64	84/.56 118	10006
OH3X	142	.70 / .65	100/.61 127	10003
OH3Y	132	.68 / .62	100/.61 112	10007
OH4X	142	.70 / .65	110/.65 126	10004
OH4Y	200	.82 / .79	110/.65 182	10008
TF1A	~~244~~	3.3 / 3.0	2.6/145 200	10010
TF1B	280	3.5 / 3.0	2.6/145 200	10014
TF1C	280	3.5 / 3.1	2.6/145 220	10011
TF2A	246	3.3 / 3.0	2.6/145 200	10015
TF2B	262	3.4 / 3.0	2.6/145 200	10012
TF2C	260	3.4 / 3.0	2.6/145 200	10016
TF3A	284	3.5 / 3.1	2.6/145 220	10017
TF3B	262	3.4 / 3.0	2.6/145 200	10021
TF3C	246	3.3 / 3.0	2.6/145 200	10018
TF4A	244	3.3 / 3.0	2.6/145 200	10022
TF4B	284	3.5 / 3.1	2.6/145 220	10019
TF4C	282	3.5 / 3.1	2.6/145 220	10023
TF5A	284	3.5 / 3.1	2.6/145 220	10020
TF5B	292	3.6 / 3.1	2.6/145 220	10025
TF5C	252	3.4 / 3.1	2.6/145 220	10024
TF6A	282	3.5 / 3.1	2.6/145 220	10029
TF6B	280	3.5 / 3.1	2.6/145 220	10026
TF6C	262	3.4 / 3.1	2.6/145 220	10030

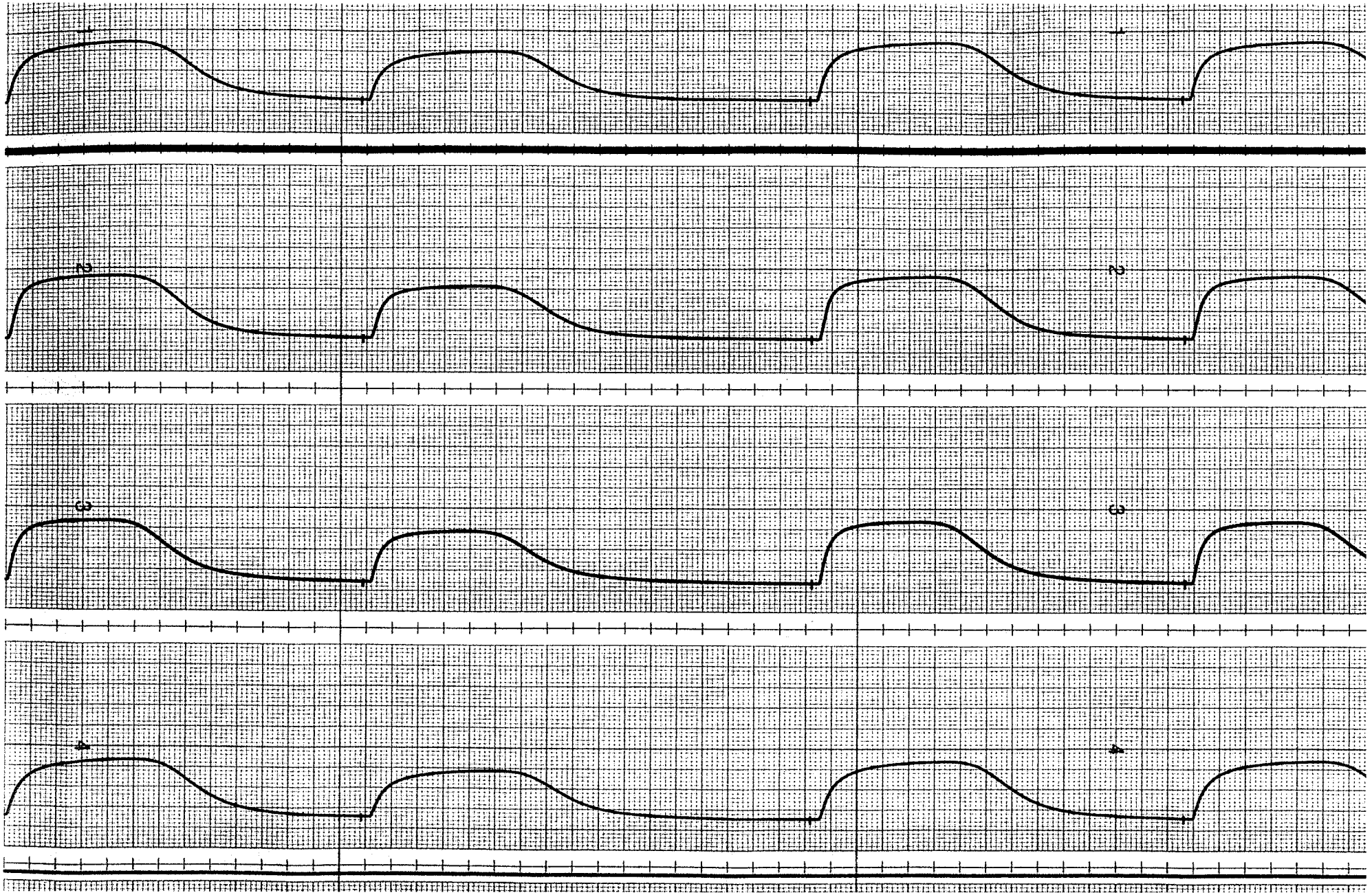

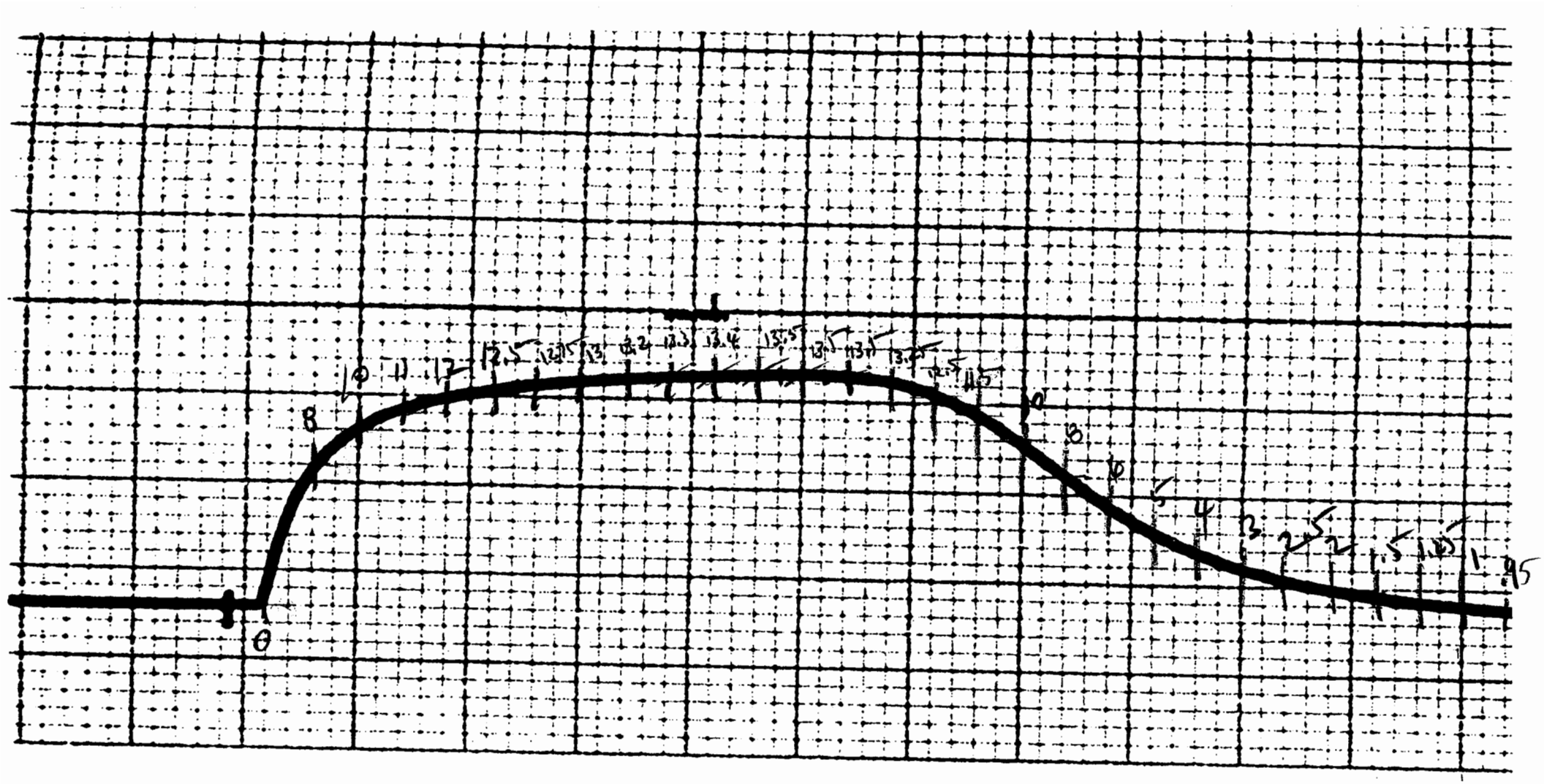
θ
B
C
D
E
11
12
12.5
13
13.2
13.3
13.4
13.5
13.5
13.5
13.25
12.5
11.5
10
9
8
7
6
5
4
3
2.5
2
1.5
1.05
1.05